National Library of Canada
Canadian Theses Service
Ottawa, Canada
K1A 0N4

Bibliothèque nationale du Canada
Services des thèses canadiennes

CANADIAN THESES

THÈSES CANADIENNES

NOTICE

The quality of this microfiche is heavily dependent upon the quality of the original thesis submitted for microfilming. Every effort has been made to ensure the highest quality of reproduction possible.

If pages are missing, contact the university which granted the degree.

Some pages may have indistinct print especially if the original pages were typed with a poor typewriter ribbon or if the university sent us an inferior photocopy.

Previously copyrighted materials (journal articles, published tests, etc.) are not filmed.

Reproduction in full or in part of this film is governed by the Canadian Copyright Act, R.S.C. 1970, c. C-30.

AVIS

La qualité de cette microfiche dépend grandement de la qualité de la thèse soumise au microfilmage. Nous avons tout fait pour assurer une qualité supérieure de reproduction.

S'il manque des pages, veuillez communiquer avec l'université qui a conféré le grade.

La qualité d'impression de certaines pages peut laisser à désirer, surtout si les pages originales ont été dactylographiées à l'aide d'un ruban usé ou si l'université nous a fait parvenir une photocopie de qualité inférieure.

Les documents qui font déjà l'objet d'un droit d'auteur (articles de revue, examens publiés, etc.) ne sont pas microfilmés.

La reproduction, même partielle, de ce microfilm est soumise à la Loi canadienne sur le droit d'auteur, SRC 1970, c. C-30.

THIS DISSERTATION
HAS BEEN MICROFILMED
EXACTLY AS RECEIVED

LA THÈSE A ÉTÉ
MICROFILMÉE TELLE QUE
NOUS L'AVONS REÇUE

NL-339 (r.86/06)

Canada

THE UNIVERSITY OF ALBERTA

Multiple-Source Excitation of Acoustic Resonances of Damped Small-Room Enclosures

by

Cornelius Jan Buma

A THESIS

SUBMITTED TO THE FACULTY OF GRADUATE STUDIES AND RESEARCH

IN PARTIAL FULFILMENT OF THE REQUIREMENTS FOR THE DEGREE

OF Master of Science

Department of Mechanical Engineering

EDMONTON, ALBERTA

Spring 1986

Permission has been granted to the National Library of Canada to microfilm this thesis and to lend or sell copies of the film.

The author (copyright owner) has reserved other publication rights, and neither the thesis nor extensive extracts from it may be printed or otherwise reproduced without his/her written permission.

L'autorisation a été accordée à la Bibliothèque nationale du Canada de microfilmer cette thèse et de prêter ou de vendre des exemplaires du film.

L'auteur (titulaire du droit d'auteur) se réserve les autres droits de publication; ni la thèse ni de longs extraits de celle-ci ne doivent être imprimés ou autrement reproduits sans son autorisation écrite.

ISBN 0-315-30145-7

THE UNIVERSITY OF ALBERTA

RELEASE FORM

NAME OF AUTHOR

Cornelius Jan Buma

TITLE OF THESIS

Multiple-Source Excitation of Acoustic Resonances of Damped Small-Room Enclosures

DEGREE FOR WHICH THESIS WAS PRESENTED Master of Science

YEAR THIS DEGREE GRANTED Spring 1986

Permission is hereby granted to THE UNIVERSITY OF ALBERTA LIBRARY to reproduce single copies of this thesis and to lend or sell such copies for private, scholarly or scientific research purposes only.

The author reserves other publication rights, and neither the thesis nor extensive extracts from it may be printed or otherwise reproduced without the author's written permission.

(SIGNED) .....C. J. Buma.....

PERMANENT ADDRESS:

.....10408-36 Avenue.....

.....Edmonton, Alberta.....

.....Canada, T6J 2H4.....

DATED .....25 February 1986.....

THE UNIVERSITY OF ALBERTA

FACULTY OF GRADUATE STUDIES AND RESEARCH

The undersigned certify that they have read, and recommend to the Faculty of Graduate Studies and Research, for acceptance, a thesis entitled **Multiple-Source Excitation of Acoustic Resonances of Damped Small-Room Enclosures** submitted by **Cornelius Jan Buma** in partial fulfilment of the requirements for the degree of **Master of Science**.

A. Cuzzi

.....

Supervisor

Gary Faulkner

.....

F.W. Anderson

.....

Date.... FEBRUARY 20/86

soli Deo gloria

Abstract

Prompted by the common problem of noise inside motor vehicles, this study investigates the dependence of the acoustic response of form-wise accurate models of vehicle passenger compartments on variation of an internal absorbent lining. While gradually increasing the extent of area coverage of the lining (varying the combination of fully-lined panels), progressions of damping factor and frequency shift have been noted. Consideration, based upon seven fundamental acoustic resonances, is given to both averaged data (to observe overall progressions of the dependent variables) and progressions of individual modes (to discern the specific influence of lining location on different resonances). Dissimilarity of the (two) enclosures allows comparison of (i) enclosure volume, (ii) enclosure shape and (iii) wall material as to their influence on resonant (acoustic) response. Results indicate that damping and shift are, effectively, linearly dependent on area coverage, that averaging of modal data reduces the effect of extrema caused by lining location, that dissipation of acoustic energy is greatest when lining is located in a mode's antinodal regions, and that enclosure characteristics are of some (though relatively small) influence on acoustic response.

Multiple-source excitation, because of the inherent flexibility of discrete interdependent sources, allowed very effective generation of individual cavity resonances. Source

network layout, relative to lining configuration, is of discernible influence in causing extrema of modal damping and shift.

Acknowledgements

The author wishes to express his gratitude to the following individuals and groups for their assistance during this project:

- Dr. A. Craggs for making this project available initially (Summer 1982) as a research project and presently as an M.Sc. study, for insight and advice offered and for providing the stimulus to presenting this study at the CANCAM '85 Conference in London, Ontario;
- General Motors Corporation and NSERC for providing (via grants to Dr. Craggs) funding for this project;
- Fellow graduate student Glen Stevenson for the numerical simulation of the car-model response and for permitting inclusion of several diagrams in this thesis;
- The students of Mec.E. 401/403 during the winter session 1984-85 for some most-practical instruction on "getting one's message across" by means of a report;
- Len Steele for initial entry of the thesis-text into computer memory; and
- The author's parents, Hans and Julie Buma, for "keeping a way clear" to complete this study.

Table of Contents

Chapter — Page

PART I -- BACKGROUND

1. INTRODUCTION 1
   1.1 Highway Vehicles 1
   1.2 Small-Room Enclosure 2
   1.3 Resonance Excitation 3
   1.4 Dissipation of Acoustic Energy 4
   1.5 Previous Investigations 5
   1.6 Background Work (Local) 6
   1.7 Goals of Present Study 8
2. THEORY 10
   2.1 General 10
   2.2 Frequency and Mode Shape 12
   2.3 Sound Absorption 17
   2.4 Resonant Damping 20
   2.5 Forced Resonant Response 21

PART II -- INVESTIGATION

3. EQUIPMENT 24
   3.1 Vehicle Models 24
   3.2 Porous Lining 28
   3.3 Resonance Excitation 30
   3.4 Resonance Measurement 32
4. METHOD 35
   4.1 Truck-Cab Model 35
   4.2 Car-Model 40

4.2.1 Unlined 40

4.2.2 Lined 44

4.3 Lining Configurations 49

4.3.1 Truck-cab model 49

4.3.2 Car-model 50

PART III -- EVALUATION

5. DISCUSSION OF RESULTS 53

5.1 Truck-Cab Model 54

5.1.1 Damping factor 54

5.1.2 Frequency shift 63

5.2 Car Model 71

5.2.1 Damping factor 71

5.2.2 Frequency shift 80

5.3 Comparison of Models 86

5.4 A Proposition 92

6. CONCLUSION 97

BIBLIOGRAPHY 104

APPENDIX A1 -- ESTIMATION OF CAVITY RESONANCES OF TRUCK-CAB MODEL 108

APPENDIX A2 -- ESTIMATION OF FLOW RESISTIVITY OF POROUS MATERIALS 116

APPENDIX A3 -- BROADBAND RESPONSES AND MOST-USED LAYOUTS OF EQUIPMENT 119

APPENDIX A4 -- TABLES OF MEASURED DATA 126

List of Tables

Table		Page
4.1	Car-Model: Measured and Computed Frequencies.	43
4.2	Lining Configurations Tested.	51
5.1	Relocation of Nodal Surface (Mode 010).	85
5.2	Comparison of Acoustic Response of Truck-Cab and Car Models.	87
A4.1	Truck-Cab Model -- Damping Factor ($x10^3$).	127
A4.2	Truck-Cab Model -- Frequency Shift (%).	128
A4.3	Truck-Cab Model -- Resonant Amplitude (mV).	129
A4.4	Car-Model -- Damping Factor ($x10^3$).	130
A4.5	Car-Model -- Frequency Shift (%).	131
A4.6	Car-Model -- Resonant Amplitude (mV).	132

List of Figures

Figure		Page
2.1	Random Acoustic Signal (Measured in Fixed Location).	10
2.2	32-Node Acoustic Finite Element.	16
2.3	Grid and Node Numbering Scheme of Complex Shaped Enclosure.	16
2.4	Mode Shapes of Complex Shaped Enclosure.	18
2.5	Determination of Damping Factor.	20
3.1	Experimental Enclosure: Truck-Cab Model (Perfectly Rectangular).	25
3.2	Experimental Enclosure: Car-Model (Complex Shaped).	27
3.3	Acoustic Absorption Coefficient of Polyfoam J39.	29
3.4	Schematic Diagram of Equipment Used.	34
4.1	Sample Traces Containing a "Split Peak".	38
4.2	Single Source Excitation of Resonant Spectrum of Car-Model.	41
4.3	Variation of Measured Response (Car-Model: Mode 100).	45
4.4	Variation of Measured Response (Car-Model: Mode 011).	46
4.5	Supplementary Layout of Source Network.	48
5.1	Resonant Damping in Unlined Enclosures.	55
5.2	Overall Damping: Lined Truck-Cab Model.	57
5.3	Modal-Group Damping: Lined Truck-Cab Model.	58
5.4	Axial Damping: Lined Truck-Cab Model.	62
5.5	Tangential Damping: Lined Truck-Cab Model.	64

Figure Page

5.6 Overall Frequency Shift: Lined Truck-Cab Model. 66

5.7 Modal-Group Frequency Shift: Lined Truck-Cab Model. 68

5.8 Overall Damping: Lined Car-Model. 73

5.9 Modal-Group Damping: Lined Car-Model. 74

5.10 Axial Damping: Lined Car-Model. 77

5.11 Tangential Damping: Lined Car-Model. 78

5.12 Overall Frequency Shift: Lined Car-Model. 81

5.13 Modal-Group Frequency Shift: Lined Car-Model. 82

5.14 Revised Axial Frequency Shift (Car-Model). 94

A2.1 Estimation of Flow Resistivity 117

A3.1 Typical Response of Sources to Broadband Noise. 120

A3.2 Response of Individual Sources (0-1,000 Hz). 121

A3.3 Most-Used Network Layouts: Truck-cab Model 122

A3.4 Most-Used Network Layouts: Car-Model (Fund. Modes) 123

A3.5 Most-Used Network Layouts: Car-Model (Non-Fund. Modes) 124

PART I -- BACKGROUND

1. INTRODUCTION

1.1 Highway Vehicles

Noise in highway vehicles[1] has in many ways gained acceptance as a modern "fact of life". Yet, neither vehicle-user nor vehicle-designer voluntarily resigns himself to this "fact". In keeping with the drive to "fill the earth and subdue it", vehicle noise is perceived as a phenomenon that must first be understood and can then be manipulated. Since, from a vehicle occupant's perspective, ergonomic and safety considerations are high priorities, psycho-acoustic comfort is viewed as a secondary concern. Often, more attention is devoted to the effect of vehicle noise on the environment than to its effect on users. Vehicle occupants are confronted with two problems: (1) the proximity of noise sources and (2) reinforcement of noise as the passenger compartment may act as an acoustic resonator. The major sources of noise are:

- engine and drive train -- vibration transmitted as either air-borne or structure-borne noise;
- road noise -- arising from the dynamic contact between tires and road and therefore transmitted predominantly as structural noise;
- wind noise -- from air penetrating the enclosure

---

[1] The "highway vehicles" considered in this study are trucks with a separate box-like operator cab and automobiles.

through improperly-sealed doors and windows; and

- structural resonance -- where enclosure panels, driven by mechanical vibrations, contribute additional components of internal noise.

Noise originating from these sources may be reinforced if the natural acoustic resonances of the passenger compartment are excited. The present study deals with the excitation and control (through acoustic absorption) of these resonances.

1.2 Small-Room Enclosure

The passenger compartments of most highway vechicles (in fact, of all but buses and large delivery trucks where cab and payload bay are joined) are an example of what is known, in terms of acoustic properties, as a small-room enclosure. Characteristics of such spaces are:

- a modal density which is low in the low frequency[2] region and
- a limited reverberant field such that acoustic energy is dissipated quickly.

Low-frequency resonances ("boom" frequencies) often attain very large amplitudes and are therefore a primary source of irritation to vehicle occupants. Irritation can be both conscious (the occupant perceives, for example, a high-level background noise or one or more single-frequency pitches) and subconscious (where an unrecognized high-intensity noise of very low frequency may result in operator fatigue). Low

---

[2] Low-frequency in this study refers to frequencies less than 300 Hz.

modal density in this region permits a mode-by-mode approach to studying acoustic resonance: the effect of altering one or more variables can be observed on individual resonant modes. (For large enclosures, where low-frequency modal density is high, statistical techniques are employed which provide data for resonances in selected frequency ranges). The rapid dissipation of resonant acoustic energy (due to limited size of the reverberant field) necessitates continuous excitation in order to study the enclosure's acoustic properties.

1.3 Resonance Excitation

Excitation of a vehicle's acoustic resonances during normal operation occurs in a random manner. Modes may be excited separately or simultaneously and may be driven by any of various sources. In addition, noise of random frequency content may impinge on the enclosure. In modelling such "real world" occurrences it is always desired to be able to account for any random excitation. Yet, it is often necessary (and beneficial) to impose known constraints on the response.

The major constraint employed in the present study is the excitation of resonances individually. A degree of realism is retained, however, by exciting the resonances with white noise (random generation, with equal amplitude, of all frequencies between 20 and 20,000 Hz). The advantage of excitation of individual modes is that greater accuracy

can be achieved in estimating the frequency, mode shape and damping factor of each resonance. (Although pure-tone and sweep-frequency excitation could be employed, the end result, identical for all three methods, requires considerably more experimental work if the latter are used).

1.4 Dissipation of Acoustic Energy

Origin and maintenance of cavity resonance form the first consideration in the study of vehicle interior noise. Of equal importance is the phenomenon of sound absorption. Though some acoustic energy is naturally dissipated (due to the finite viscosity of air), to noticeably decrease overall noise level it is necessary to increase the damping. The traditional and simplest means to achieve this is to install a high-porosity boundary lining. In large vehicles, where there is often an excess of space, lining thickness and/or the proportion of surface area covered can be increased freely. In smaller vehicles, since space is usually limited, the lining must be optimized. Lining configuration then remains the only variable: after chosing a maximum lining thickness the location and extent-of-area-coverage must be decided. The effects of these two variables are to be considered in what follows.

1.5 Previous Investigations

The interior acoustics of highway vehicles is known to be a very complex problem. The irregular shape of typical passenger compartments, the presence of seats and occupants and the properties of any boundary-lining components usually lead to considerable distortion of resonant mode shapes. In addition, neither the phenomenon of sound absorption nor the interaction of a vibrating enclosure shell with the enclosed air-space are yet fully understood. The relatively limited number of studies (spanning three-and-one-half decades) described in the literature have dealt with various aspects of interior acoustics though detailed information on the lining-resonance interaction remains scanty.

The earliest studies of vehicle interior acoustics are very general in their approach (for example, Bristow, 1952). This is seen especially in the use of one-third octave band-width for analysis of the sound field. In the majority of subsequent investigations discrete resonances are considered though never in terms of the unbroken series (Jennequin, 1971; Raff, 1973). Several studies, on the premise that only the first and second longitudinal modes are of importance, make use of two-dimensional models (length-by-height) (Nakamura, 1961; Shuku, 1972). Occasionally, scale models of vehicles are used (mostly for verification of numerical models; Petyt, 1975); note that extreme scaling is not applicable for study of low-frequency resonances. The interaction of the shell and the enclosed air volume has received

considerable attention (Craggs, 1971, 1973; Le Salver, 1972; Nefske, 1985). Concerning experimental work, enclosure resonances in these studies are excited by means of: (a) vibration excitation of the shell (Shuku, 1972); (b) a vehicle driving test (recorded on magnetic tape; Nefske, 1985); or (c) a single point-source (loudspeaker; Raff, 1973; Petyt, 1975). Regarding sound absorption, the overall influence of porous linings has been considered (Raff, 1973; West, 1966; Aspinall, 1972) as well as, to some extent, that of lining configuration (Shuku, 1972). The latter acknowledges shift of frequency though none consider in detail the progression of damping factor (neither as a statistical or a discrete quantity). Considerable effort has gone into numerical modelling (finite elements) of undamped resonances (Shuku, 1972; Craggs, 1972; Nefske, 1978; etc.) though simulation of damped resonances is relatively unknown.

Excellent references on the subject of interior acoustics are Gladwell (1964) (historical development) and Howell (1980) (development and bibliography).

1.6 Background Work (Local)

An overview of the "groundwork" carried out at the University of Alberta and of direct relevance to the present study is useful. Initially (summer 1982) a fully-rectangular wooden enclosure was constructed to model the operator cab of a typical freight-transport truck (detailed description

in Section 3.1). A porous lining, the thickness of which was subsequently increased, completely covered one wall of the enclosure. A single source and condensor microphone, both fixed in location, enabled excitation and measurement of the reverberant field. The multiple-resonance spectra obtained from such tests become less useful as lining thickness increases since the resonant regions of different modes overlap. Identification of modes and accurate determination of modal damping factor then become difficult.

It was therefore decided to isolate the fundamental resonances by means of a multiple-source network. Choosing a specific mode, sources would be located in its antinodal regions and, the entire array being supplied from a single white-noise generator, the phase of each source would be (remotely) set according to the assumed mode shape. Experiments repeated in the model truck-cab (variable: lining thickness) provided much better estimates of damping factor (as well as of damped modal frequency) and a workable method for multiple-source excitation.

After this, multiple-source excitation was used to study the acoustic characteristics of in-use highway vehicles. The vehicles used (all North American-built) were a 1974 subcompact sedan and two 1977 passenger vans emptied of their additional bench seats. Data derived from these vehicles were of mixed value: representative fundamental resonances could be generated and their damping factors determined. However, because of structural and lining

characteristics, it was not possible to generate the complete spectrum of fundamental resonances in either type of vehicle. Also, of the modes generated, some could not be used to provide data because of poor repeatability.

In summary, "in-house" work led to partial development of the multiple-source excitation technique as well as to reference data on a model enclosure and several current vehicles. (The single-source tests were done by S. Lorimer and the multiple-source tests by the present author, both, at that time, research assistants to Professor A. Craggs.)

1.7 Goals of Present Study

Recognizing some of the gaps left by previous studies, the course charted for the present investigation can be outlined as follows.

Particular attention is given to the behaviour of the seven fundamental acoustic resonances of enclosures (three axial, three tangential, and one oblique). The primary objective is to determine the dependence of modal damping and resonant frequency on the following variables:

- lining configuration -- determine an analytical relationship between resonant damping and area of lining coverage (obtain a similar relationship for frequency shift);
- enclosure shape -- observe how resonant behaviour differs between regular (perfectly rectangular) and irregularly shaped (e.g. automobiles) enclosures; and

- enclosure wall material -- observe the different effect (if any) of using wood or steel for the enclosing shell.

Further, it is desired to evaluate the use of multiple-source excitation in an acoustic application.

Information generated by this study can, in due course, be used as a means to two ends. First, regarding the "acoustics" of highway vehicles, the design of new vehicles and the application of palliative treatments to existing vehicles will be facilitated if their overall acoustic behaviour is better understood. Study of some of the mechanisms of energy dissipation and indentification of practical limitations on enhancement of damping will contribute to this understanding. Second, concerning acoustics as a science, information presented and discussed in the following chapters will contribute towards a more complete understanding of the resonant behaviour of small-room enclosures (especially those of irregular geometry) as well as of the phenomenon of sound absorption.

2. THEORY

2.1 General

In order to study analytically the behaviour of noise in vehicular passenger compartments, the science of acoustics must be applied to small-room enclosures. In the context of audible sound, an acoustic signal can be qualitatively described as a fluctuation of air pressure about a mean (atmospheric) value (see Figure 2.1).

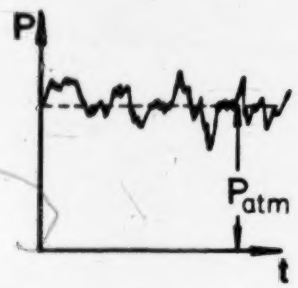

Figure 2.1 Random Acoustic Signal (Measured in Fixed Location).

This diagram represents the instantaneous air pressure at a particular location in a random noise field. If a pure tone impinges on the microphone, the fluctuating signal takes the form of a sine wave; if the ambient sounds are related (for example, a fundamental frequency with several harmonics), the signal displays a pressure-time pattern which is repeated (termed "periodic"). The acoustic pressure of a signal refers to the average deviation of the pressure fluctuation from the atmospheric mean value and is measured as a root-mean-square (RMS) quantity. (By way of comparison,

whereas atmospheric presure at sea level is 101.3 kPa, a sound pressure level of 100 dB corresponds to an acoustic pressure of 2 Pa - reference 20 x 10^{-6} Pa).

Since air is a highly elastic medium, having both mass and stiffness, it can sustain continuous oscillations of pressure. In free space these oscillations propagate in all directions away from their source (progressive waves) and in partially- or fully-enclosed spaces may form resonances (standing waves) as acoustic energy from the source interferes with that reflected by the enclosure. Standing waves display regions of constant (atmospheric) and fluctuating pressure (nodes and antinodes, respectively) which are fixed in location within the enclosure. In antinodal regions air pressure alternates between compression and rarefaction at a rate ("frequency") determined by physical parameters such as enclosure size and density of the medium. The patterns of nodal-antinodal regions for each standing wave are known as the mode shape.

Mathematical models exist which accurately describe standing wave behaviour in perfectly-rectangular enclosures. Using numerical methods (finite elements) these models can be extended to complex-shaped enclosures.

Dissipation of acoustic energy in an enclosure occurs as the result, usually, of two mechanisms: natural and artificial damping. Natural damping, resulting from the finite viscosity of air, is significant only for high frequencies. Artificial damping is usually achieved by means

of a porous lining in which acoustic energy is converted to other forms of energy (mainly heat). Thus, if the lining is effective, acoustic energy is reflected at a level well below that at which it impinges on the lining and overall noise level in the enclosure will be reduced. The effect of artificial damping is expressed by means of two quantities:

1. the sound absorption coefficient which expresses the effectiveness of the lining in absorbing acoustic energy; and
2. the damping factor to express the dissipative effect in terms of single resonances.

The mathematical (and numerical) models which describe acoustic damping are as yet incomplete. One of the purposes of this study is to provide experimental data to be able to further develop these models.

2.2 Frequency and Mode Shape

A single fundamental equation is used to describe the resonant behaviour of any enclosure, though enclosure geometry determines how the equation is applied.

The equation describing the propagation of waves in fluid media (Morse, page 389) is:

$$\nabla^2 p - (1/c^2)\, \partial^2 p/\partial t^2 = 0 \qquad (2.1)$$

where:

∇^2 is an operator indicating the spatial second derivative (for a one-dimensional problem, ∇^2 is replaced by $\partial^2/\partial x^2$);

p is the acoustic pressure; and

c is sonic speed.

(The derivation of this equation assumes isentropic compression of an ideal gas medium.)

The solution of Eq. (2.1) for a one-dimensional enclosure (consider, as an example, a rigid-walled tube of length L, with a rigid termination at either end, that is where x=0 and x=L) expresses dependence on both time and location:

$$p = A[\cos(\omega_n/c)x]\{\exp(j\omega_n t)\} \qquad (2.2)$$

Here A is the maximum pressure amplitude, ω indicates the normal modes of the enclosure and n is an integer-valued index corresponding to successive harmonics of the fundamental normal mode. The time-dependent term $\{\exp(j\omega t)\}$ has unit magnitude and indicates the phase of the pressure signal at any instant of time. Since acoustic pressure reaches its maximum value at a termination ($\partial p/\partial x=0$ at x=0 and x=L), by taking the derivative of Eq. (2.2) and solving for the ω_n, the frequncies of the normal modes of the enclosure are given by:

$$\omega_n = n\pi c / L \qquad (2.3a)$$

or

$$f_n = nc / 2L \qquad (2.3b)$$

Extending this to three dimensions (in terms of a perfectly rectangular enclosure of dimensions AxBxD), Eq. (2.2) becomes (Morse, Eq. (32.11)):

$$p = \hat{p}[\cos(l\pi x/A)\cos(m\pi y/B)\cos(n\pi z/D)]\{\exp(j\omega_{lmn}t)\} \qquad (2.4)$$

with, as natural frequencies,

$$f_{lmn} = c/2\ [l^2/A^2 + m^2/B^2 + n^2/D^2]^{1/2} \qquad (2.5)$$

The indices l, m and n (associated with the A, B and D dimensions, respectively) assume integer-values only. Normal modes of an enclosure are termed axial (one index non-zero), tangential (two indices non-zero) or oblique. The pressure distribution associated with a particular resonance, given by Eq. (2.4), is known as the mode shape.

Application of the above model to estimate the seven fundamental resonances of the perfectly-rectangular enclosure used in this study is given, along with a numerical simulation, in Appendix A1.

The conditions for application of the above model are, in summary:

- a perfectly-rectangular enclosure with
- rigid walls and
- no damping occurring.

If the first of these conditions is relaxed such that one or more enclosure dimensions are not rectangular, Eq. (2.2) to (2.5) are no longer applicable. Equation 2.1 however, appropriately modified, can still be applied to a discretized model of the enclosure.

For the discretization, the entire enclosure is considered to be an assembly of smaller elements ("air volumes"), each containing a common number of nodes[3] (point locations) at which acoustic pressure is estimated. Nodes of

---

[3] Not to be confused with the nodes of resonant pressure distributions.

neighboring elements which coincide are given the same "address" in the global (assembled) system such that the pressure wave can be modelled as a continuous function.

Modification of Eq. (2.1) entails a discretization so as to accommodate the global matrix of discrete pressures. Equation (2.1) then becomes (a very succinct presentation of the theory underlying this reformulation is given in Craggs, 1982):

$$([S] - (\omega/c)^2[P])\{p\} = \{0\} \tag{2.6}$$

where the [S] and [P] matrices are acoustic kinetic and potential energy matrices, respectively, which are derived from geometric considerations. {p} is a column vector containing the nodal pressure distribution. The non-trivial solution of Eq. (2.6) requires

$$(\omega/c)^2\underline{X} = [P]^{-1}[S]\underline{X} \tag{2.7}$$

This provides a series of eigenvalues from which resonant frequencies can be determined. Backsubstitution of individual eigenvalues into Eq. (2.6) provides an eigenvector (normalized pressure distribution) from which pressure mode shape can be found. This numerical modelling technique proved crucial to understanding the resonant behaviour of the irregularly-shaped enclosure used in this study.

The numerical simulation made use of a 32-node element (Figure 2.2) which models air pressure as a cubic distribution. The element is isoparametric such that distortions of the pressure distribution are of the same order as geometric distortions. The fully-assembled model of

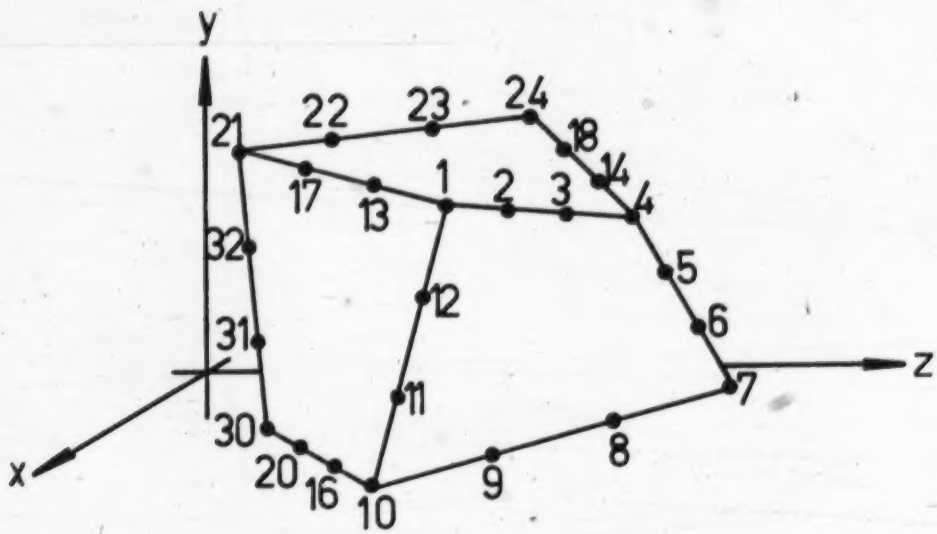

Figure 2.2 32-Node Acoustic Finite Element.

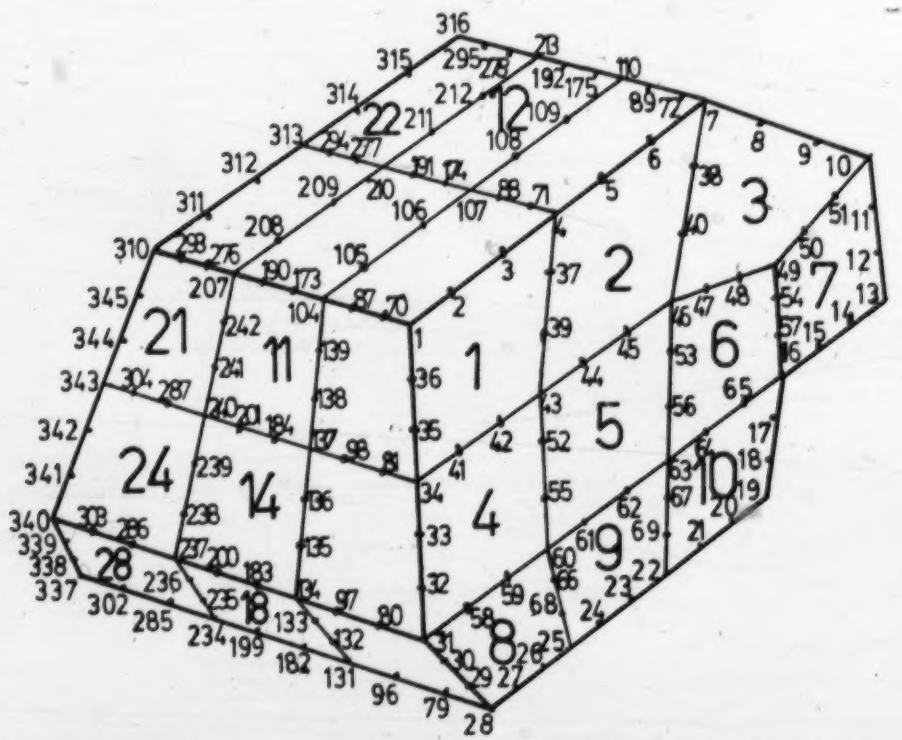

Figure 2.3 Grid and Node Numbering Scheme of Complex Shaped Enclosure.

the complex-shaped enclosure consisted of 378 nodes[4] distributed over 30 elements (see Figure 2.3). In this way estimates were obtained of the lowest fifteen resonant frequencies and their mode shapes (see Figure 2.4).

(The perfectly-rectangular enclosure (Section 3.1) was modelled with an 8-node element as a means of model verification. See Appendix A1.)

The "mode labels" used in Figure 2.4 (110, 020, etc.) originate in the classification of modes in perfectly-rectangular enclosures; recall the indices of Eq. (2.4) and (2.5). Since these equations are not directly applicable to complex-shaped enclosures, the mode-label digits no longer represent the indices of the equations but provide only an indication of the number of phase changes (+ to -, - to +) in each direction. Where, for higher modes, distortion becomes severe, alternate labelling schemes would have to be devised.

2.3 Sound Absorption

Though detailed analysis of the mechanism of sound absorption is not presently necessary, some qualitative observations are useful.

Sound absorption is here defined as the dissipation of the acoustic energy present in one medium (air) in a neighboring medium usually of higher density (in this case a

---

[4] The enormous global matrix this represents, 378x378 entries, required six-and-one-half hours of computing time to solve using an Amdahl 5860 and an AP-190L array processor.

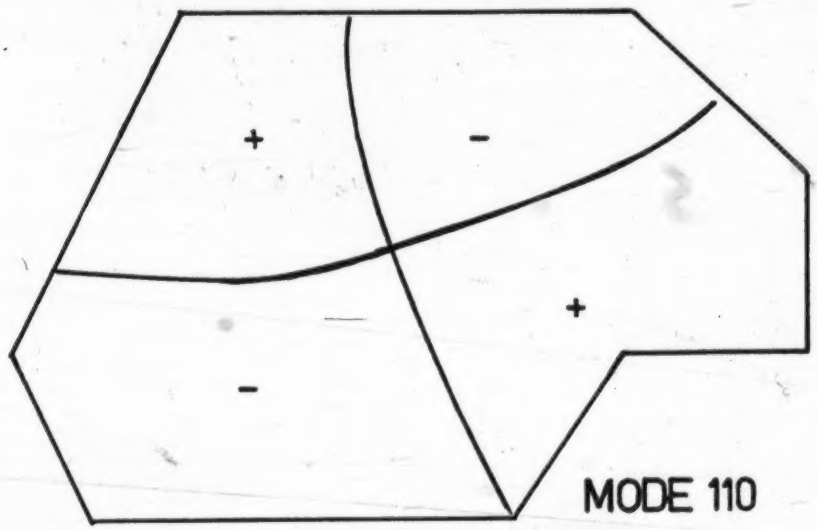

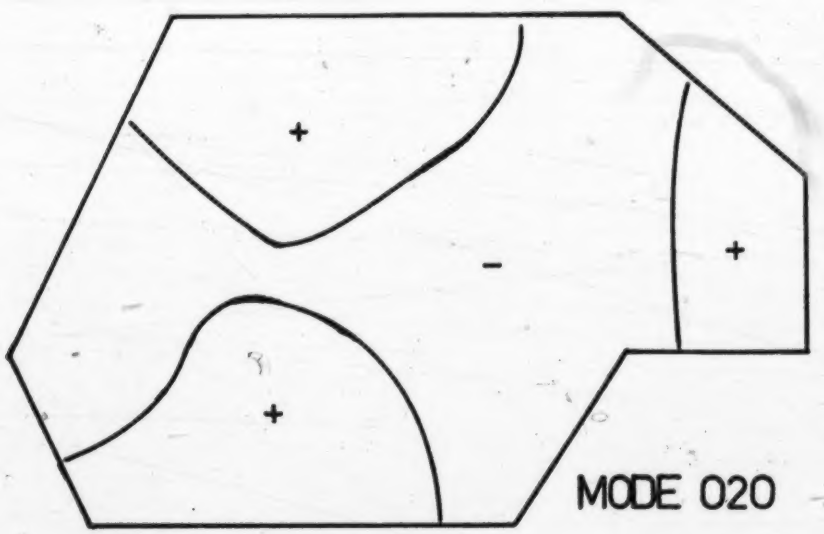

Figure 2.4 Mode Shapes of Complex Shaped Enclosure.

high-porosity lining). The amount of acoustic energy which a lining will absorb at any frequency is given by its absorption coefficient. The porous lining dissipates part of the acoustic energy impinging on it (by increasing the viscous boundary layer enclosing the sound field) and reflects the remainder (due to the higher effective density of the air contained in the lining pores).

The porous lining used for this study (described in Section 3.2) can be considered in terms of the Rayleigh model (Kuttruff, page 144):

> "The Rayleigh-model consists of a great number of similar equally spaced parallel channels which traverse a skeleton material considered to be completely rigid."

Since the channels of the model are very narrow

> "the profile of the air stream [within a channel] is determined almost completely by the viscosity of the air and not by any inertial forces."

The effect of the lining is to increase tremendously the viscous boundary layer surrounding the reverberant field. It is in the boundary layer, where viscosity is high, that most of the acoustic energy is dissipated.

The thickness of the boundary layer within the pore space is frequency-dependent. At low frequencies the velocity profile of the air-stream in a pore is parabolic (as in the case of non-oscillating flow) and the boundary layer is relatively thick. At high frequencies, flow is approximately uniform across the section of the pore (Helmholtz flow condition) and the boundary layer is much narrower. If the boundary layer is thick (implying that the

effect of viscosity is greater), the impedance of the air in a pore is high and, from the perspective of incident acoustic energy, the effective density of the lining is also high. Effective density is thus also frequency-dependent. This dependence is expressed by means of the following relationship (Craggs, 1984):

$$\rho_e = \rho_o (1 + 0.46\sqrt{(R_s/\omega)}) \qquad (2.8)$$

where ρ_o is the density of the ambient air, R_s the static flow resistivity (see Section 3.2 and Appendix A2), and ω the driving frequency.

The preceding can be used to explain the behaviour of the absorption coefficient: at low frequencies effective density of the lining is high (thick boundary layer) and more acoustic energy is reflected, while at high frequencies effective density is nearer the actual density of air and more energy will be absorbed.

2.4 Resonant Damping

The acoustic absorption coefficient expresses quantitatively the acoustic energy absorbed by a medium at a given frequency. To quantify the effect of an absorbent lining on individual resonances, the damping factor is normally used. Damping factor (ζ) is the ratio of the width of a resonant peak (measured at $1/\sqrt{2}$ of its maximum amplitude) to twice its center frequency (see Figure 2.5; note that both amplitude and frequency scales are linear).

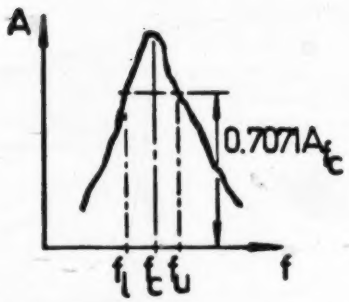

$$\zeta = (f_u - f_l) / 2f_c$$

Figure 2.5. Determination of damping factor.

(The factor 2 in the denominator arises in the derivation of damping factor.)

Damping factor is used in this study as defined above. Other investigators (e.g. Jha, 1972) make use of a Q-factor which is related to damping factor as follows: $Q = 1/2\zeta$.

Damping factor provides a measure of how strongly a resonance is single-valued in terms of frequency. As the damping factor of a resonance increases, the specific frequency which will be reinforced becomes increasingly random. The effect, in terms of a vehicle occupant, is that the resonance takes on more the character of noise (random frequency content) rather than a single penetrant frequency. In addition, as energy is dissipated, occupants benefit from reduced reverberant amplitudes.

2.5 Forced Resonant Response

Having seen the free response of enclosures in Section 2.2 it is necessary to discuss, briefly, the important features of forced resonant response. This is usually

expressed in terms of a series of the normal modes. The equation describing the response of a room to a given volume source distribution is (Morse, page 313):

$$\nabla^2 p - (1/c^2)\, \partial^2 p/\partial t^2 = -j\rho\omega Q(x,y,z) \qquad (2.9)$$

where ρ is the density of air, and ω is the driving frequency of the volume source strength distribution, $Q(x,y,z)$. The solution of this equation for an enclosure is written in terms of a series of the normal modes:

$$p = \Sigma_o^{\infty} \Phi_N(x,y,z) q \qquad (2.10)$$

For a rectangular room

$$\Phi_N(x,y,z) = [\cos(l\pi x/A)\, \cos(m\pi y/B)\, \cos(n\pi z/D)] \qquad (2.11)$$

Here the single integer N is adapted for convenience only. Substitution of the series (2.10) into the governing equation gives (note: V is enclosure volume)

$$p = - \Sigma_o^{\infty} \frac{\rho\omega c^2 \int_V \Phi_N(x,y,z) Q \, dV}{(\omega_N^2 - \omega^2)} \qquad (2.12)$$

Obviously, if the source frequency $\omega = \omega_N$ one of the modes, the resonant mode, will dominate the total response.

The response is limited only by the damping in the system. Usually, for convenience the damping is assumed to be viscous in nature and the response of each mode is likened to a simple damped oscillator so that the term $(\omega_N^2 - \omega^2)$ in the denominator is replaced by the term $(\omega_N^2 - \omega^2 + 2j\omega\zeta)$, the series then becomes

$$p = - \Sigma_o^{\infty} \frac{j\rho\omega c^2 \int_V \Phi_N(x,y,z) Q \, dV}{(\omega_N^2 - \omega^2 + 2j\omega\zeta_N)} \qquad (2.13)$$

where ζ is the modal damping factor. While in deriving the

expression viscous damping has been assumed, this number is commonly used as a measure of the most general forms of damping, and can be found by experimental means (Section 2.4).

In what follows it is desired to find the effects of the amount of absorption material on the damping of the individual modes. Using a finite number of sources (loudspeakers) whose phases can be set independently, the integral $\int \Phi_N(x,y,z) Q \, dV$ appearing in the numerator for each mode can be adjusted to enhance the response of one mode and attenuate that of others. Steady-state resonant response is then given by

$$p = \frac{j\rho\omega c^2 \int_V \Phi_N(x,y,z) Q \, dV}{(\omega_N^2 - \omega^2 + 2j\omega\zeta_N)} \tag{2.14}$$

and the mean square pressure (p^2) by

$$p^2 = \frac{\rho^2\omega^2 c^4 (\int_V \Phi_N(x,y,z) Q \, dV)^2}{((\omega_N^2 - \omega^2)^2 + 4\omega^2\zeta_N^2)} \tag{2.15}$$

The effects of damping are twofold (i) response (pressure amplitude) at resonance is reduced and (ii) the frequency at which the maximum response takes place is reduced according to the relationship $\omega_m^2 = \omega_N^2(1-\zeta^2)$. An additional consequence, associated with the decrease of frequency, is an increase of resonant wavelength. This results in shifting of node planes (where incoming and reflected acoustic energies cancel) away from more reflective panels.

PART II -- INVESTIGATION

3. EQUIPMENT

In this chapter an explanation is provided of the equipment used in this study. The two passenger compartment models are described, the acoustical properties of the porous lining are discussed and descriptions are included of the equipment used to excite and measure enclosure resonances.

3.1 Vehicle Models

The damped-resonance data required for this study were generated in two form-wise accurate models rather than in actual vehicle passenger compartments. This choice, based on the experience of earlier work (see Section 1.6), allowed concentration upon such overriding variables as enclosure shape, wall material and lining location. Assumptions did not have to be made about the influences of structural irregularities (usually for enclosure strength) and multi-component linings normally found in vehicle bodies.

The first enclosure, a rectangular parallelepiped of wood on which some testing had been done previously (Section 1.6), represented the operator cab of a typical freight-transport truck (see Figure 3.1). Internal dimensions of the model were (L:H:W) 1.52 m x 1.42 m x 1.22 m providing an enclosure volume and total internal surface area, respectively, of 2.63 m^3 and 11.5 m^2. Enclosure walls,

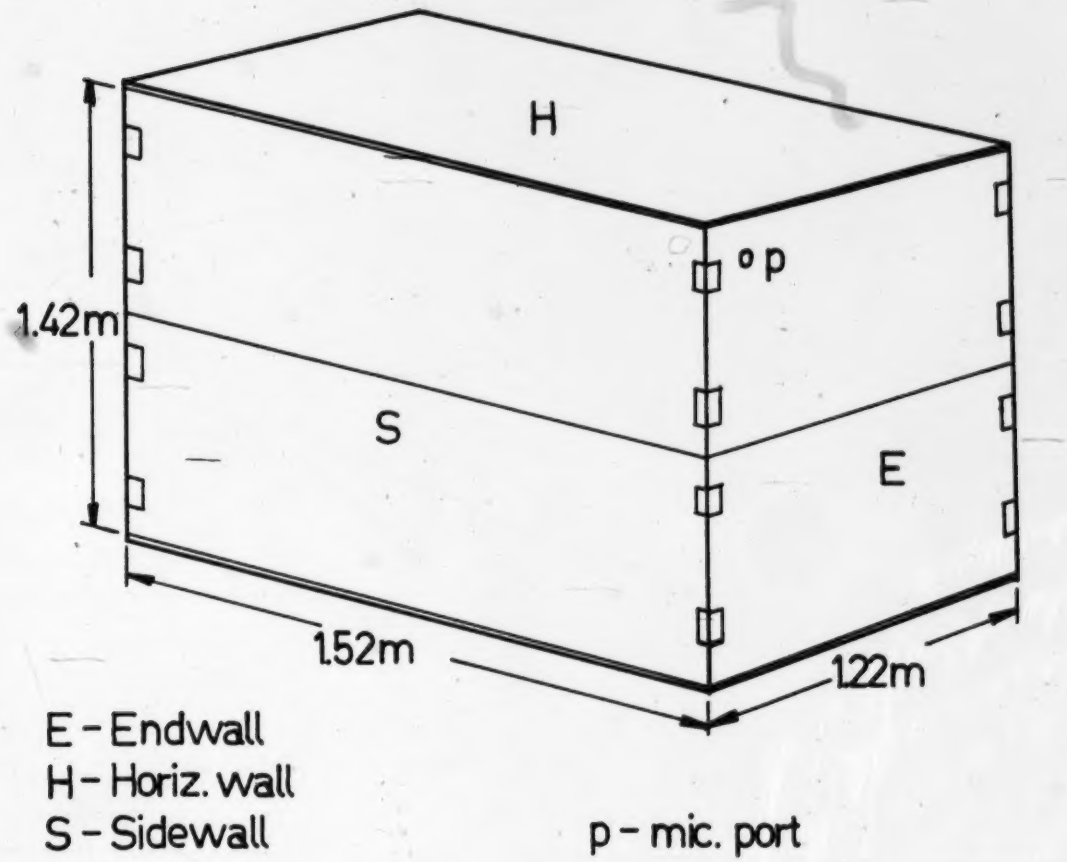

Figure 3.1 Experimental Enclosure: Truck-Cab Model (Perfectly Rectangular).

double sheets of 7/16-inch plywood (total thickness: 22 mm), were held together at (vertical) corners by external screw-mounted brackets, and coated with a high-gloss varnish. Vertical walls had a continuous seam at midheight to allow the model to be moved easily to and from the anechoic testroom and for access during testing. Two box-like halves were thus obtained which would be "stacked" atop the floor-panel and covered with the roof-panel. Horizontal seams in the model were left untreated, overlap of the wood panels assuring airtightness adequate for resonance testing.

Since the truck-cab model is perfectly rectangular, equations (2.4) and (2.5) are applicable to it. The indices l, m and n of these equations are thus also the digits of the mode labels for the truck-cab model corresponding to, respectively, the length, height and width dimensions.

The second model, chosen for its complex geometry (see Figure 3.2), was between one-half and two-thirds the size of a standard automobile enclosure. Constructed of sheet steel (thickness: 0.9 mm), it had no braces or ridges for reinforcement. All overlapping seams were riveted and sealed with silicon gel. The "lid", the only removable panel, rested on flatbar provided with rubber stripping and could be held in place with a series of wingnuts (not used). Additional sheet material was left at the front of the car-model for eventual vibration-excitation tests (the rear can be used similarly). The sheet steel used for this enclosure has a smooth, glossy appearance and was therefore

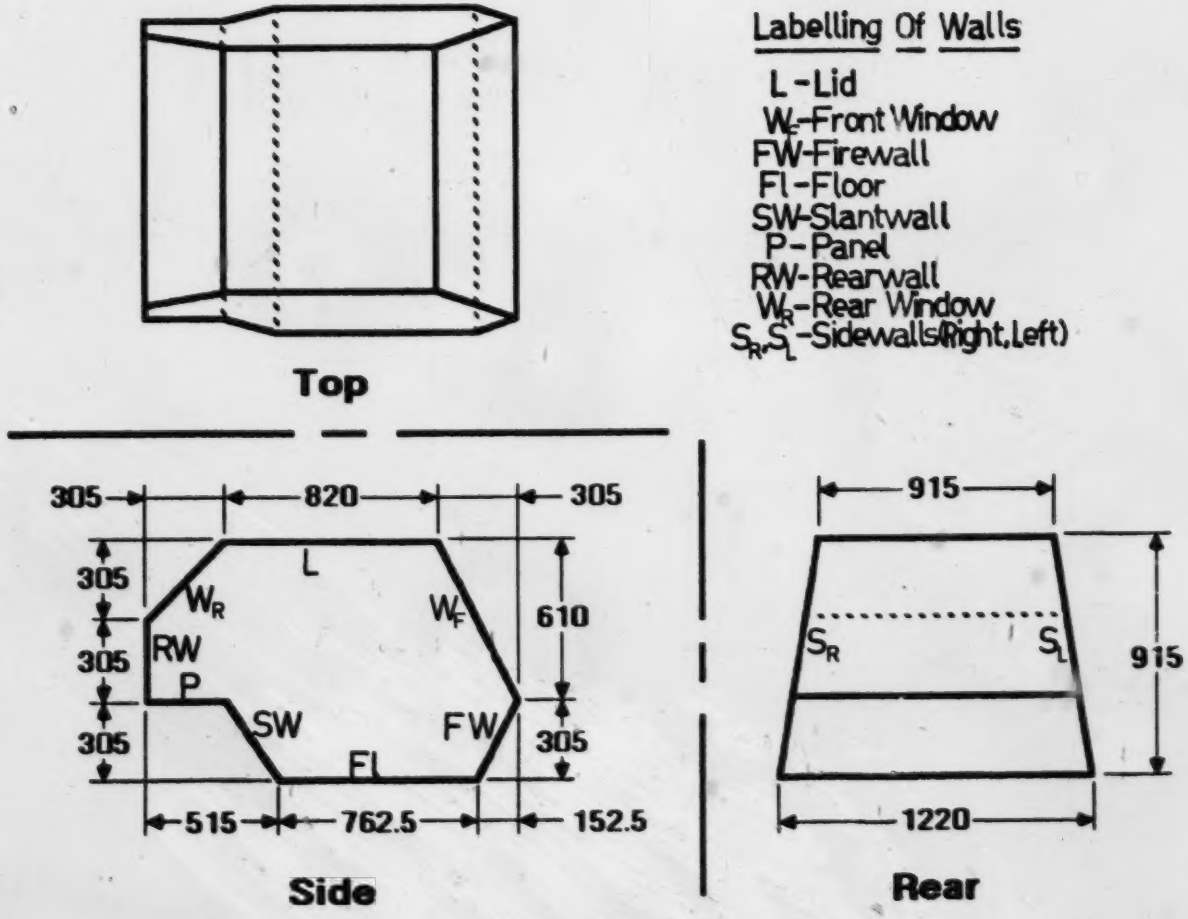

Figure 3.2 Experimental Enclosure: Car-Model (Complex Shaped).

not painted. Total enclosed volume and internal surface area of the model were 1.1 m^3 and 5.7 m^2, respectively.

Note that although the ratio of shell stiffness to acoustic stiffness of the enclosed volume is greater in actual vehicles than in the models used (due to scaling down and absence of any panel reinforcement) the influence of the (more flexible) model enclosures on acoustic resonances was still relatively small.

3.2 Porous Lining

The porous lining used in testing was chosen for its superior sound-absorbing qualities as well as its ease of handling. The lining, a polyurethane foam (tradename: Polyfoam J39), is commonly used in furniture production/restoration. Supplied originally as sheets (dimensions 1.37 m x 2.03 m x 0.05 m), a separate segment was fitted to each enclosure wall. Lining segments could be easily removed and installed by means of double-sided tape permanently fixed to about 3% of the enclosures' internal area.

Empirical tests done on two foam samples (each: diameter = 100 mm and thickness = 50 mm) disclosed a bulk density of 16 kg/m^3 and a porosity of (at least) 90%. Impedance tube tests of the same samples produced the absorption coefficient trace of Figure 3.3. The ranges of UNDAMPED resonances of both models being indicated, it is noteworthy that, despite overall good sound-absorbing qualities, the absorption coefficient is still quite low in

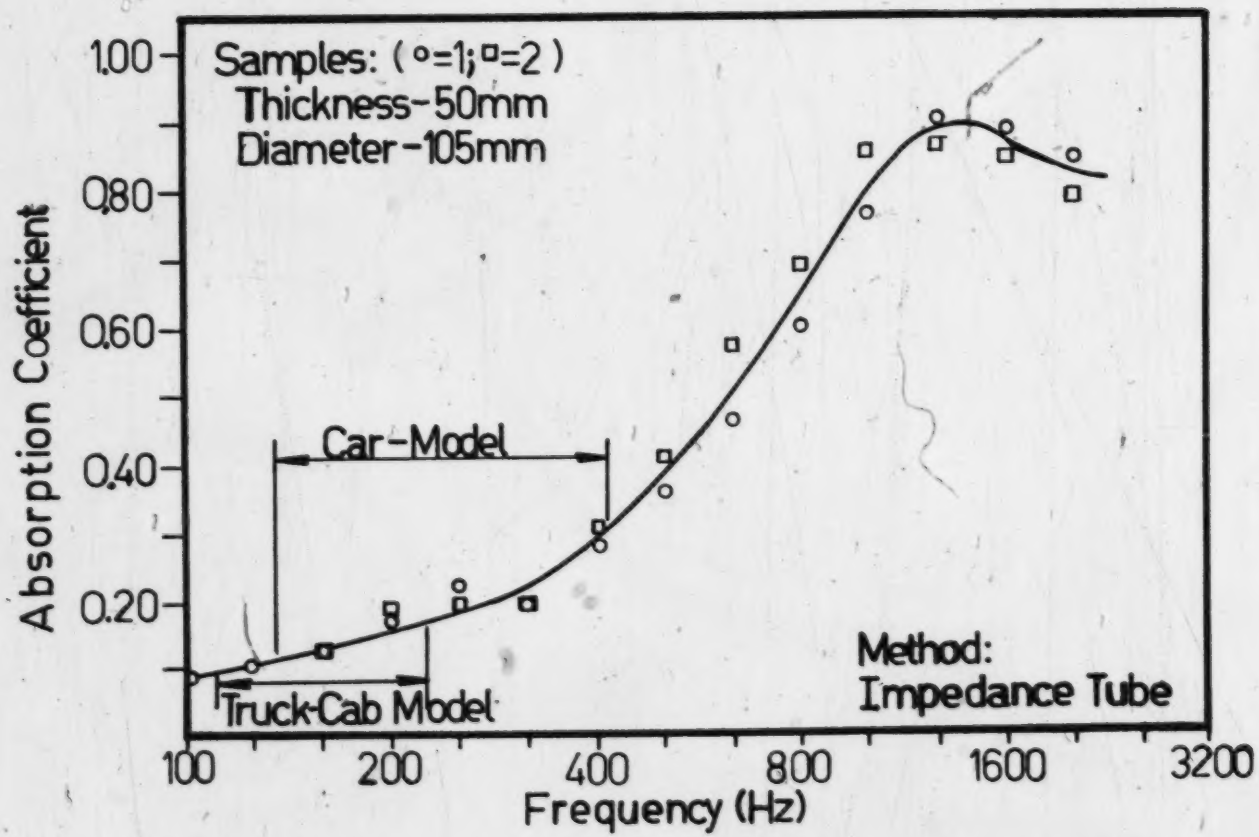

Figure 3.3 Acoustic Absorption Coefficient of Polyfoam J39.

the region of interest. (Note: as rule-of-thumb, the "hump" of the absorption coefficient trace occurs at a frequency whose wavelength is approximately four times the thickness of the lining. Thus, to have the hump centered at 200 Hz, a lining thickness of 0.43 m would be necessary -- obviously impractical in the context of highway vehicles. Nevertheless, in the fully-lined car-model resonances above 300 Hz could not be excited with appreciable amplitude.) The measured absorption coefficient data were used to estimate (see Appendix A2) the flow resistivity of the Polyfoam at 5500 rayls/meter.

Since each wall of an enclosure had been provided its own, fully-covering piece of lining, different combinations of lined walls could be tested. The influence of two variables could then be observed, namely:

- the ratio of lined area to total internal surface area (expressed as a percentage); and
- the particular location of the lining.

The various lining configurations tested in the two models are presented and described in Section 4.3. When fully lined, the internal volume of the truck-cab and car-models decreased by 20 and 26%, respectively.

3.3 Resonance Excitation

The objective of the experimental work was the excitation and measurement of individual cavity resonances in the low-frequency region. Recognizing the node-antinode

character of mode shapes (recall Eq. (2.4)), the placement of correctly-phased sources in the antinodal regions of a specific mode and excitation with either broadband noise or a pure tone should excite only the chosen mode. This technique had been partially successful in the work described in Section 1.6 and was therefore also applied in the present study.

The array of sources consisted of six, identical small-box loudspeakers. The driver chosen was a 4-inch diameter woofer (Philips AD5060) capable of a rated power output of 10 Watts. The enclosure constructed for each driver had external dimensions of 153 x 178 x 130 mm, was of 8-mm plywood and had all free internal volume filled with polyfoam (for suppression of box-resonances). Traces of source response to a white-noise input are given in Appendix A3. Although as large as practically possible (internal volume of the truck-cab and car models decreased by 1 and 2%, respectively, with all sources present), single-source excitation of resonant spectra was left unchanged if the five mute sources were removed.

Since neighboring antinodal regions of any mode are of opposite phase, the phase of any source must be adjustable separately, all sources being driven with the same electrical signal. This was achieved by using a small distribution box in which the power, taken from a single input, is distributed through separate switches (wired to permit reversal of polarity) to each source. The

distribution box was outside the model, individual source wires entering the model through a hole in one enclosure wall. In some instances, a common network layout with only a change of phase-setting could be used to excite different resonances. (The most frequently used network layouts with phase-setting are shown, for both models, in Appendix A3.)

The source network was driven by broadband noise (white noise) producing all frequencies between 20 and 20,000 Hz with equal amplitude. After amplification (by means of a locally-built 50-Watt power amplifier) the noise field inside the enclosure had a nominal sound pressure level of 100 dB (note: although excitation signal level was maintained at 5vRMS throughout all tests, in the fully-lined models nominal SPL dropped to 85 dB). Despite the high-level broadband input, resonant amplitude was usually such that locating the microphone pickup at a source-cone would disclose only the specific mode (not an increase of background level as would be intuitively expected).

3.4 Resonance Measurement

The acoustic response of the enclosures was measured and recorded by means of the following equipment.

A 1-inch condensor microphone (B&K 4145) mounted on a stand and usually aimed at the geometric center of the enclosure could be moved to wherever resonant response was greatest. (Note that in the truck-cab model most measurements were taken with the microphone in the upper corner of

one Endwall. Alternate microphone locations for this model are given in Appendix A3.) The measured signal was fed through a spectrometer (B&K 2113) to a Fast-Fourier-Transform (FFT) Analyzer (Nicolet 660A). The spectrometer served as both a power supply to the microphone and an amplifier of the measured signal. The FFT Analyzer transforms the input signal (time history of the acoustic pressure) into a plot of frequency versus amplitude and displays this information on an 800-line CRT screen. With the aid of a built-in Expander, measurement resolution for the truck-cab model was 0.2 Hz (0.4 Hz for the car-model). As the acoustic response displays constant small-scale variation, statistical averaging was used to collect and assimilate resonance data during a specific period of time. In most tests 150 readings of the response were averaged (representing 3 and 1.5 minutes of data collection for the truck-cab and car-models, respectively), though if the data trace displayed excessive roughness on the CRT an additional 150 samples were assimilated. (Some problems of resonance measurement that could be minimized through additional averaging are dealt with in Chapter 4.) A hard copy of each data trace was produced on an X-Y recorder (HP 7044A).

A sketch of all equipment used (input and measurement) is shown in Figure 3.4. The bulk of the tests were performed in an anechoic chamber (internal dimensions: 2.0 x 2.3 x 3.5 m) preventing interference of any unwanted sounds.

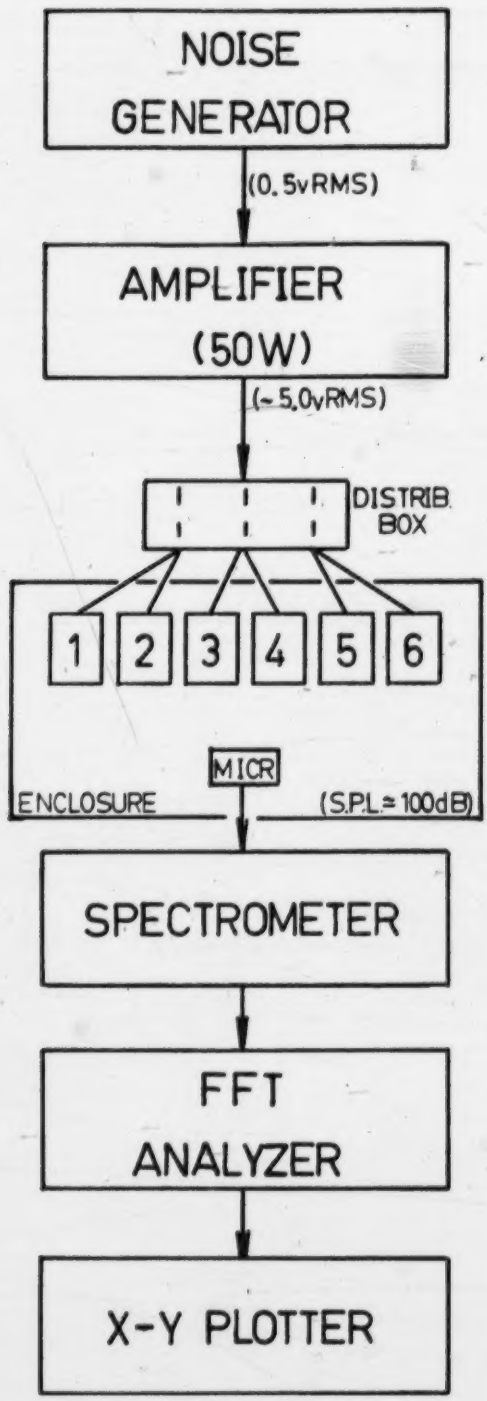

Figure 3.4 Schematic Diagram of Equipment Used.

4. METHOD

This chapter explains the method used to obtain the "formal" data sought by this study. Description of the problems encountered in resonance generation and how these were dealt with provides some insight into enclosure acoustics and allows unhindered presentation of formal data in the next chapter.

4.1 Truck-Cab Model

This section, describing excitation of fundamental acoustic resonances in the truck-cab model (both unlined and lined), outlines the basic method of obtaining acceptable resonance data.

As indicated earlier (Section 3.3), the basic procedure of resonance generation is uncomplicated. Choosing a specific resonance (for example, the fundamental longitudinal mode, 100) its expected mode shape would be noted -- in the case of the 100-mode, an antinode (of opposite phase) at either end of the longitudinal dimension and a node plane in center. Three sources would be assigned to each antinode (initially on the floor of the enclosure) and the polarity of one trio of sources set opposite to that of the other. White noise would then be supplied to the network and the microphone, fixed in a corner near the roof panel, used to measure the reverberant response. (The choice of microphone location is determined by the fact that any mode displays an antinode at a reflection-causing boundary. Thus, in a

perfectly-rectangular enclosure, any corner where three walls meet is a likely location for measurement of maximum amplitude of any resonance.) The most-frequently used network layouts (with phase-setting) for the truck-cab model can be found in Appendix A3.

Two problems appeared requiring modification of the basic procedure.

First, although network phase might have been set to excite one specific mode, other modes might also appear during measurement. The simplest case of this occurred when, with the network on the enclosure floor, phase would be set for mode 100 while both modes 100 and 110 would be measured. This was corrected by placing the sources at the midheight of the enclosure: each trio, then located on the horizontal node plane of the 110-mode, radiates with its own phase across the entire vertical section of the enclosure. By thus imposing the necessary signal-phase on both the upper and lower halves of the reverberant field, excitation of the tangential mode could be suppressed. (It was also possible to locate the outer sources of each trio at the midheight while placing opposite center sources at the floor and roof, respectively.) Another occurrence of this problem, more difficult to correct, was in excitation of the higher fundamental modes. Though sources would be located and phased for a specific tangential (or the one oblique) mode, lower fundamental resonances might also appear during measurement. If, during excitation of a tangential mode, a

component[3] axial mode appeared, it was first ensured that each antinode of the tangential mode contained at least one correctly-phased source. (Some tangential modes could be driven by placing two sources in each of three of the four antinodes.) If not sufficient to eliminate the unwanted resonance(s), the microphone would be moved from its "fixed" location and relocated or reoriented so that the unwanted mode(s) would either disappear from the CRT-display or appear at much-reduced amplitude. Microphone relocation, the only recourse if lower fundamental modes appeared during excitation of the oblique mode, was very effective in eliminating the higher fundamental modes during excitation of axial modes.

A second and much more serious problem was that of a "split peak" (see Figure 4.1). This occurred if, while exciting a single resonance, the measured response displayed a two-pronged peak. The amplitudes of the separate sub-peaks varied from less than 10% to over 50% of overall resonant amplitude and were not necessarily identical (symmetry about a central "dip"). Initial reaction is to consider one of the peaks as a neighboring resonance. However, differences of mode shape and frequency of the neighboring resonance (excited separately) are usually enough to rule out such possibilities. The conclusion then is that the splitting of a peak represents two (or more) plausible frequency-values for the particular resonance.

---

[3] "Component" axial modes of, for example, the 110-mode are modes 100 and 010.

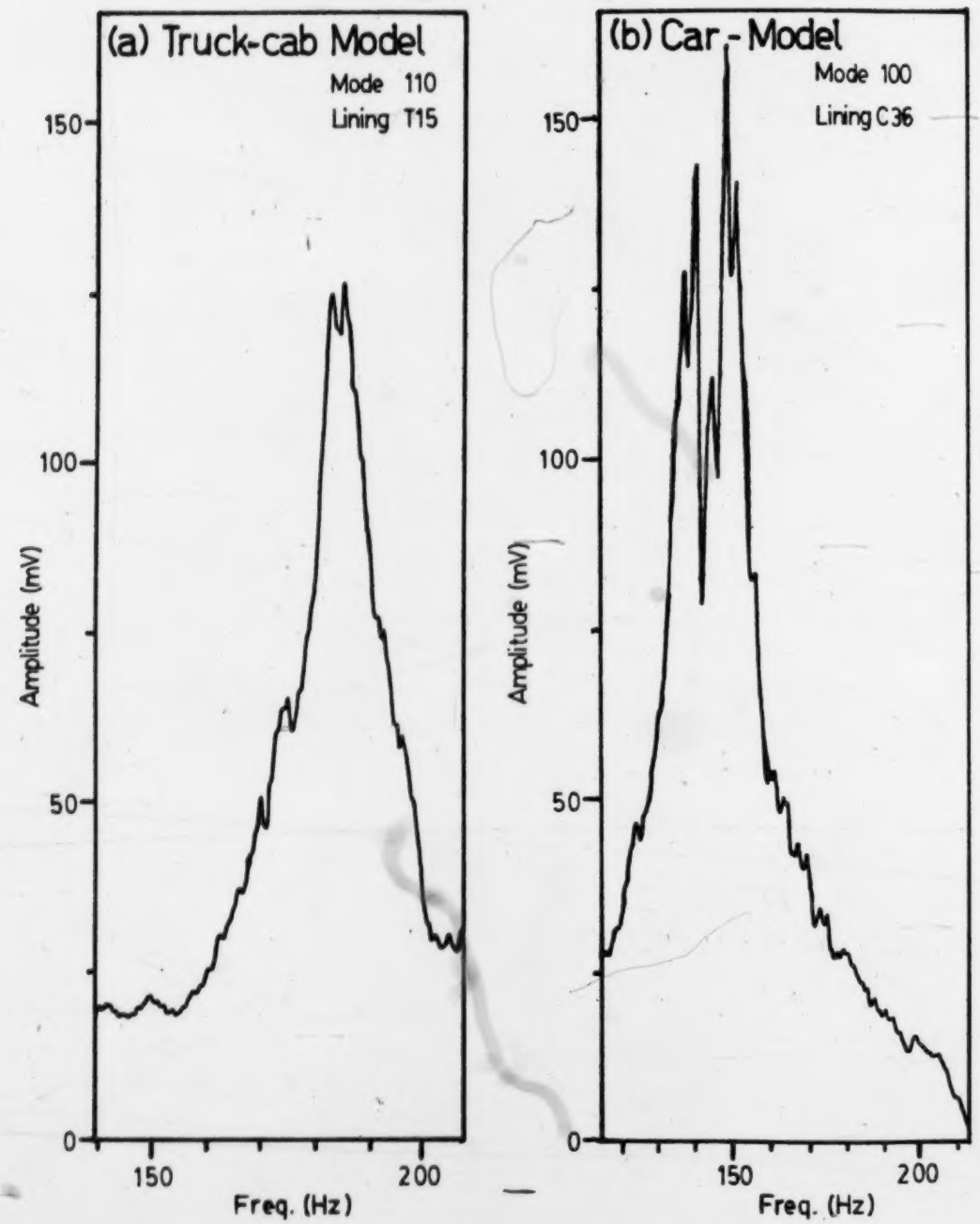

Figure 4.1 Sample Traces Containing a "Split Peak".

Several approaches were employed to eliminate splitting of peaks or, failing this, to obtain meaningful data despite the splitting. If sub-peaks differed in frequency by no more than 2 Hz (implying a small amplitude for each sub-peak), splitting could occasionally be eliminated by increasing the number of averages collected. (Note that, if analyzer bandwidth had been increased, splitting would not have been discernible.) If splitting persisted, alternate positions or orientations for the microphone would be tested. These modifications with, as a last resort, some repositioning of the source network, would normally eliminate the splitting. If, despite all attempts, the peak could not be reduced to a single frequency, either the sub-peak with the larger amplitude or the bottom of the central "dip" (if sub-peaks had identical amplitude) was used as the resonant frequency. If the sub-peaks differed by several cycles-per-second, implying distinct separate peaks, only relocation/reorientation of microphone or source network could be tried. In some cases a single peak could thus be generated at the frequency where the "dip" had been formerly. More often, such modification resulted in increased amplitude of one sub-peak and a reduction (disappearance) of the other. Typically, if the "dip" could be replaced or a sub-peak strengthened, overall resonant amplitude, visible on the CRT-display, would be increased.

Splitting of peaks tended to occur more readily and was much more difficult to eliminate in the unlined models (due

to the non-linear response resulting from interaction of the shell and the acoustic pressure wave; this is dealt with further in Section 5.3).

4.2 Car-Model

4.2.1 Unlined

Excitation of resonances in the car-model was to follow the same procedure as for the truck-cab model. Two additional problems were introduced, however, by the irregular shape of the enclosure. First, as the length of the car-model is almost twice the height dimension, frequencies of multiples of fundamental modes are interspersed among those of the higher fundamentals. Second, since no cross section of the car-model had rectangular shape, all mode shapes underwent distortion such that node planes became curved.

Initial attempts to identify the different frequencies met with very meager success. The enclosure was first excited with a single source to obtain a "complete" resonance spectrum (see Figure 4.2). Then, using either the single source or a specific (single mode) network layout, the microphone would be moved to various locations in the enclosure to measure the pressure (amplitude) distribution associated with one or more frequencies -- a process referred to as "mode tracking". Fundamental axial frequencies were readily obtained. Fundamental tangential

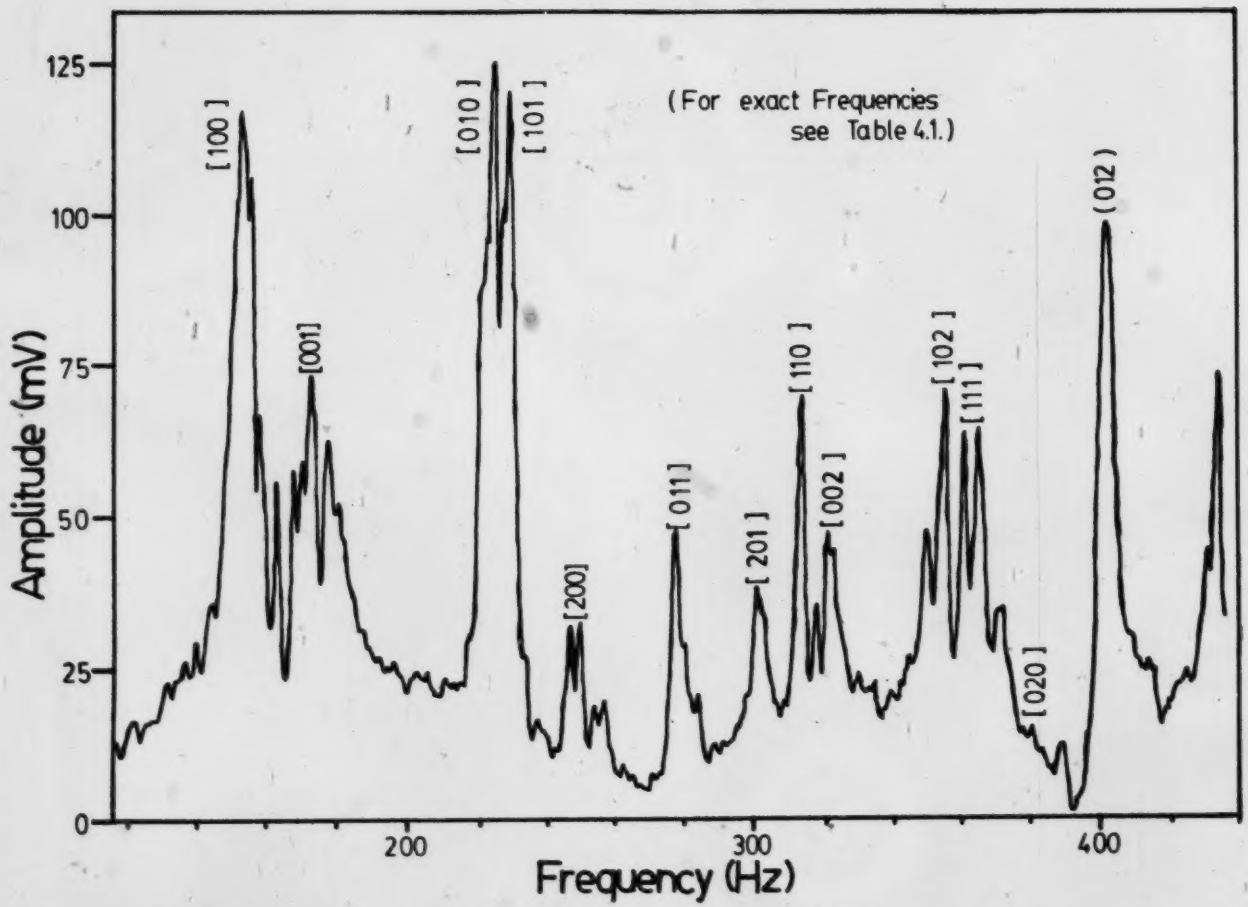

Figure 4.2 Single Source Excitation of Resonant Spectrum of Car-Model.

modes could not be identified clearly due to difficulty in locating precisely the pressure minima. Also, frequencies of what were assumed to be higher multiple resonances could not be suppressed, with the result that specific frequencies could not be associated with whatever nodal behaviour was discernible.

It was during these initial experimental measurements that the computer simulation of the car-model's resonant behaviour was performed‘ (as a "real-world" test of the finite element program under development; recall Section 2.2). The results obtained from this eigensolution (see Table 4.1) confirmed that higher multiples of the fundamental modes indeed do occur between the fundamental resonances. Also, curvature of the mode shapes was predicted (recall Figure 2.4). With these estimates of the various mode shapes, source network layouts were revised and testing for the higher fundamental modes resumed. All frequencies measured in the region of interest could then be identified and their mode shapes verified.

Excitation of individual resonances (most-used layouts in Appendix A3) disclosed that the problem of splitting of peaks was more severe in the car-model than in the unlined truck-cab model. By repeating a resonance test with identical source and microphone locations some time after making an initial measurement, changes of frequency or damping factor might occur, necessitating a choice as to

---

‘ The author is indebted to fellow graduate student Glen Stevenson for this simulation.

Table 4.1 Car-Model: Measured and Computed Frequencies.

Mode Label	Frequency (Hz)	
	Measured	Simulated
100	154.6	140.8
001	168.2	160.3
010	220.2	208.9
101	226.6	214.3
200	251.0	243.3
011	281.8	267.8
201	301.8	288.8
110	312.2	299.9
002	323.8	315.4
102	355.4	353.2
111	366.6	347.0
020	378.2	371.3

which data be accepted as "formal". Two examples of this selection process are cited, the first dealing with a split peak and the second with a variable peak width. The first, illustrated in Figure 4.3, concerns the fundamental longitudinal mode (mode 100). The peak of Figure 4.3a has a damping factor of 0.0192 which was deemed excessive when compared to a regression-estimated value of 0.0136 (determined by means of a linear regression based on all twelve car modes; see Chapter 5). The second attempt, generated at a much later date outside the anechoic testroom, produced a single-valued peak with a calculated damping factor of 0.0113. Although damping is below the regression value, the second attempt is the preferred choice. The second, somewhat more difficult, case involves mode 011 and is shown in Figure 4.4. Damping factors calculated for the three traces are 0.0052, 0.0101 and 0.0168, respectively, while the estimated (linear regression) value is 0.0083. Due to the shapes of the different peaks and their measured frequencies, Figure 4.4c was chosen as "correct". (Note that using either the second or third values of damping factor in the linear regression estimate makes almost no difference in its slope and intercept values.)

4.2.2 Lined

Besides some recurrence of unwanted resonances and the splitting of peaks, the major difficulty arising during

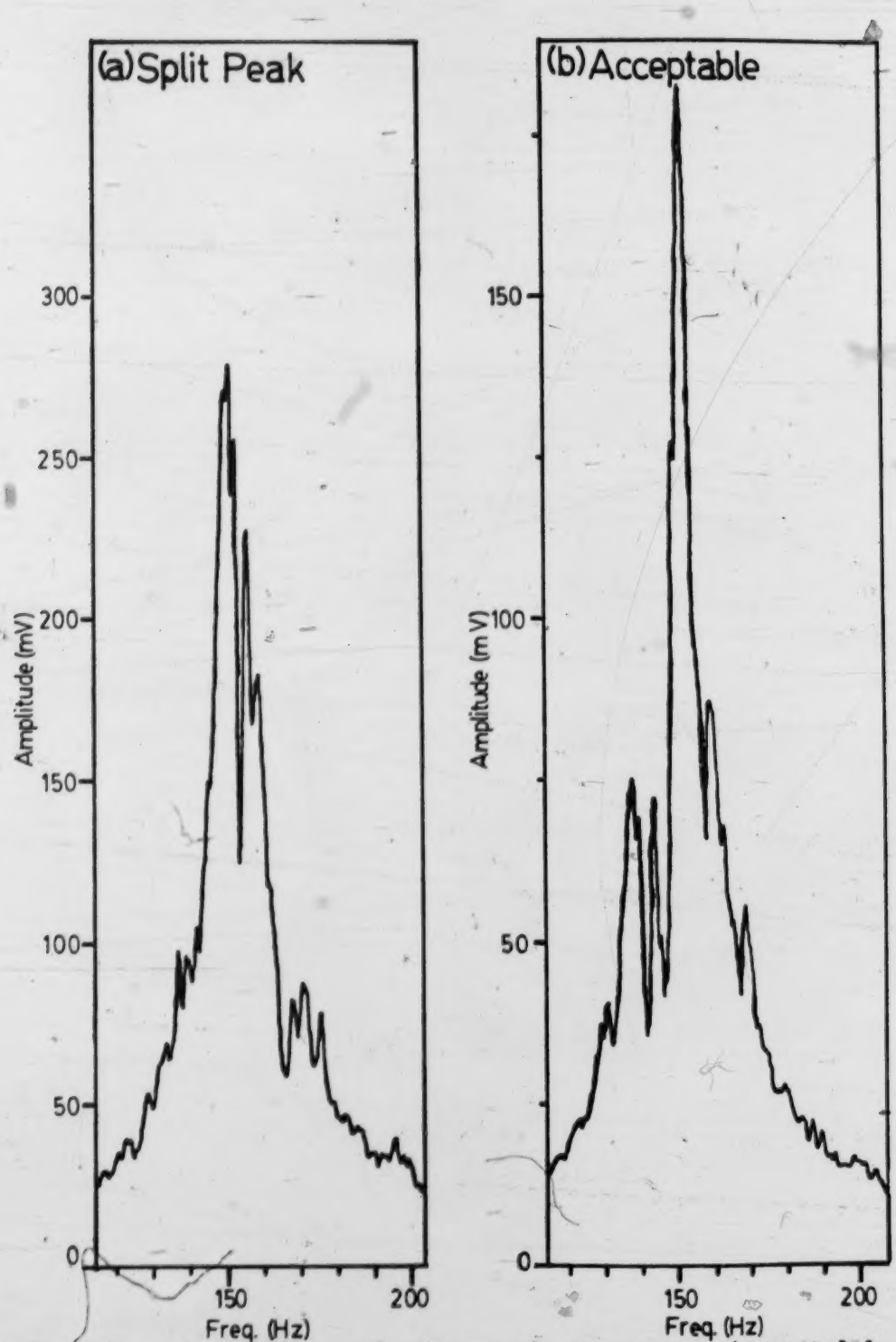

Figure 4.3 Variation of Measured Response (Car-Model: Mode 100).

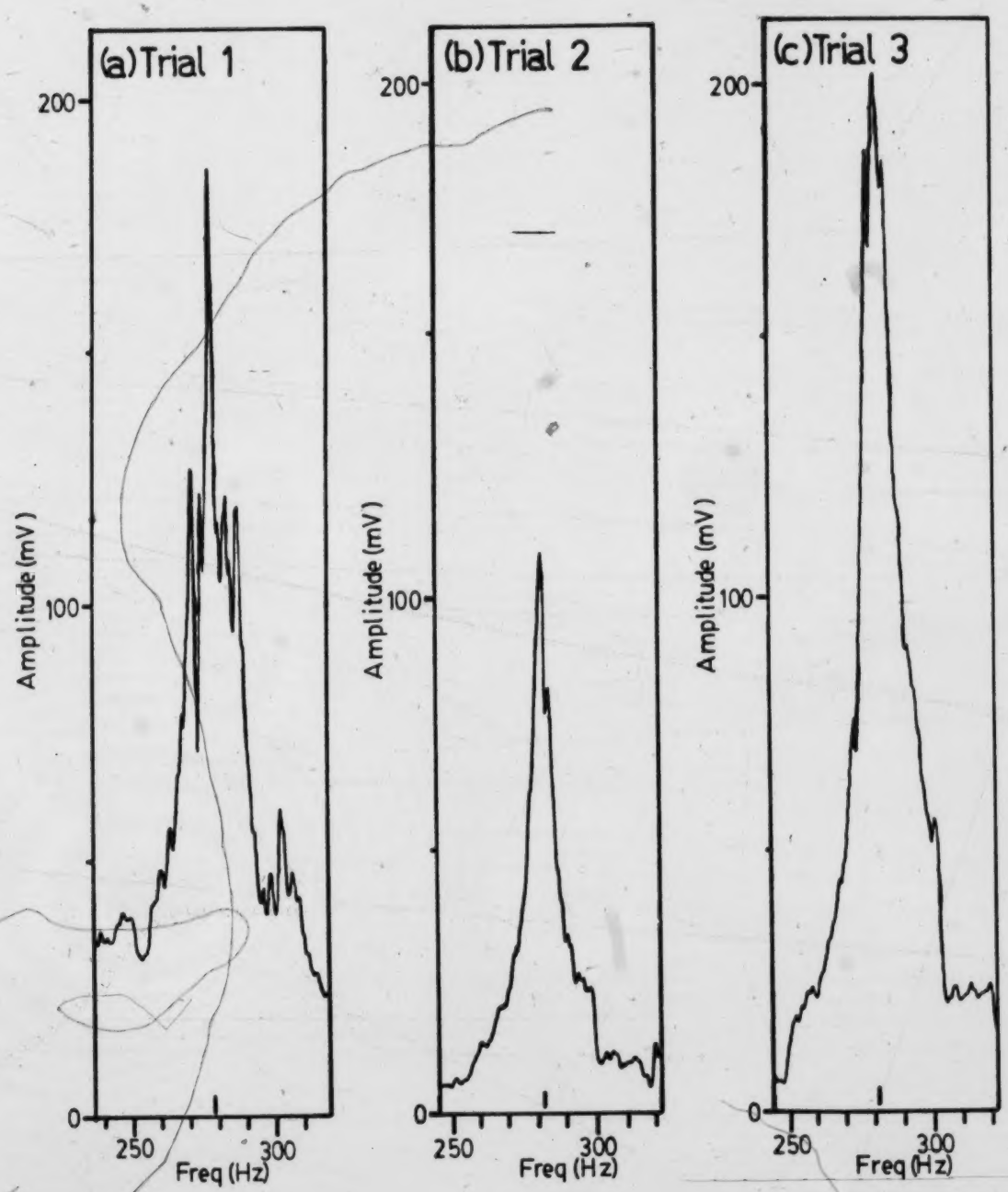

Figure 4.4 Variation of Measured Response (Car-Model: Mode 011).

testing of the lined car-model was the inability to adequately excite some of the resonances. This became especially noticeable for high percentages of area coverage where non-fundamental modes displayed such low amplitudes that analyzer gain had to be increased by a factor of ten to detect any resonant behaviour.

Excitation of unwanted modes and the appearance of split peaks were dealt with as before: relocation of sources and microphone. This was again used, though with very specific motivation, if resonances appeared to be undergoing excessive damping. In some cases it was found that a most unlikely layout-and-phasing of the network would excite a particular resonance: the layout in Figure 4.5 was thus used to excite modes 010 and 002. Another approach was to bring sources closer to one another to ensure effective interaction of their direct fields. Similarly, sources could be moved closer in to the reverberant field of the enclosure. In almost all such cases microphone position had to be carefully chosen (usually the end-result of much trial-and-error experimentation). A final method of recourse, if low-amplitude excitation of the mode occurred, was to increase analyzer gain to where the trace filled the entire CRT-display. Since both amplitude and frequency scales of the display were chosen to be linear (rather than logarithmic), damping factor could be determined by the usual method of measurement and calculation.

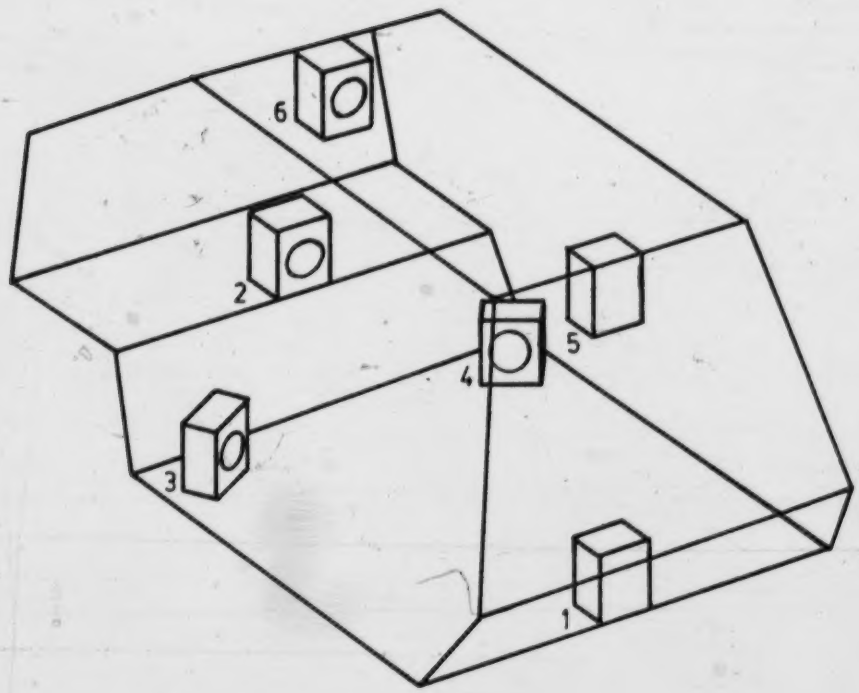

Figure 4.5 Supplementary Layout of Source Network.

Again, if for high-coverage linings traces appeared excessively rough on the CRT-display, additional averaging could be used to improve trace appearance.

4.3 Lining Configurations

The objective in testing was to study the damped resonant behaviour of the two models as a function of a discrete series of area coverages distributed evenly between the unlined and fully-lined states. By lining complete surfaces in various combinations (rather than increasing the areas of a randomly distributed series of patches) information could be obtained as to the specific influence of lining location. (Recall that modal damping factor and the changes of resonant frequency were the quantities of primary interest.)

4.3.1 Truck-cab model

The surfaces of the truck-cab model were named Endwalls, Horizontal walls and Sidewalls, being located normal to the length (1.52 m), height (1.42 m) and width (1.22 m), respectively (see also Figure 3.1).

After ascertaining the resonant behaviour of the seven fundamental modes in the unlined truck-cab model, resonance tests were initially repeated with three mutually orthogonal walls lined and all (six) walls lined (for coverages of 50% and 100% of internal surface area, respectively). Additional data were then collected by covering:

(i) three single walls (one E (15%), one H (16%) and one S (19%));

(ii) three pairs of opposite walls (both E (30%), both H (32%) and both S (38%));

(iii) three pairs of intersecting walls (one E plus one H (31%), one E plus one S (34%) and one H plus one S (38%));and

(iv) three "duct" linings (both E plus both H (62%), both E plus both S (68%) and both H plus both S (70%)).

An additional lining configuration tested could be practically realized in an actual operator cab: by lining the lower half of both Endwalls and the upper half of one Sidewall (effectively, the respective "doors" and "backwall" of the cab) a coverage of 25% was realized.

Lining configurations used in the truck-cab model are summarized in Table 4.2.

4.3.2 Car-model

The car-model consisted of ten surfaces labelled as shown in Figure 3.2; note that the Sidewalls are identically shaped. Again, the model's undamped acoustic response was determined, after which the model was lined completely and retested. To obtain a relatively even distribution of area coverages a limited number of lining configurations was chosen (with 9 unique panels the law of permutations indicates that over 500 combinations are possible) some consideration being given to what could be practically

Table 4.2 Lining Configurations Tested.

Truck-Cab		Car	
Lining	Surfaces Lined	Lining	Surfaces Lined
T00	none	C00	none
T15	E	C13	FW,SW
T16	H	C18	W_F,W_R
T19	S	C26	W_F,L,W_R
T25	2(E/2)+(S/2)	C33	FW,Fl,SW,P
T30	2E	C36	S_R,S_L
T31	E,H	C41	W_F,FW,W_R,RW,P,SW
T32	2H	C47	S_R,Fl,FW,W_F
T34	E,S	C53	W_F,L,W_R,Fl,SW,P
T35	H,S	C61	S_R,S_L,L,Fl
T38	2S	C64	all but S_R,S_L
T50	E,H,S	C70	all but W_F,W_R
T62	2E,2H	C76	all but L,Fl
T68	2E,2S	C100	all
T70	2H,2S		
T100	2E,2H,2S		

applied in an actual vehicle. The lining configurations are listed in Table 4.2. The total area covered by each lining is indicated in the lining name; for example, C13 indicates the lining covering 13% of the car-model's internal surface area (the letter T corresponds to the truck-cab model). The walls lined in each configuration are given by the abbreviations used in Figure 3.2.

PART III -- EVALUATION

5. DISCUSSION OF RESULTS

The present chapter deals concretely with that for which this study was undertaken -- the "formal" data (measured data listed in Tables A4.1 to A4.6). The acoustic quantities of primary interest are the damping factor (as defined in Section 2.4) and frequency shift (the change of resonant frequency) as these are altered by the presence of the lining. Resonant amplitude and mode shape, though both altered by the lining, are presently of lesser importance and are therefore considered only in regards to explaining behaviour of the primary variables.

Damping factor and frequency shift are thus "dependent" variables whose progressions are (to be) related to the "independent" variables of lining configuration and enclosure shape. Since each acoustic mode of an enclosure represents a very specific pressure distribution, the damping factor and frequency shift of each mode will be affected differently depending on lining location. The overall progression of a dependent variable is obtained when, for each lining configuration, data is averaged over all fundamental modes. Alternatively, averages can be derived for the different modal groups (axial, tangential and non-fundamental). In deriving the various averages of the dependent variables it is assumed that, in general, the extrema occurring in the progression of one mode are

cancelled by those occurring on the remaining modes. Thus scatter of (averaged) data will be lower for an overall progression (where data for all fundamental modes have been averaged) than for modal-group progressions.' Some information about the exact influence of lining location can be determined by comparing the modal progressions within a group. (Complete description of the influence of lining location was not an objective of this study, though the more obvious trends found are described.)

Results of the truck-cab and car models are discussed in separate sections after which a section is devoted to comparison of their acoustic responses. A summary of the major findings and their significance is found in the following chapter.

5.1 Truck-Cab Model

5.1.1 Damping factor

Resonant damping factor is observed to decrease with increase of resonant frequency in the unlined truck-cab model (Figure 5.1). Although scatter is large (reflected in a standard deviation of the data of 28% of measured range), none of the data are "wild" and the general decrease is clear.

' Scatter of data is given, in diagrams, as the variance of the data about the regression line; to permit comparison of scatter of damping and frequency shift data textual references to scatter are given as a percent of measured range.

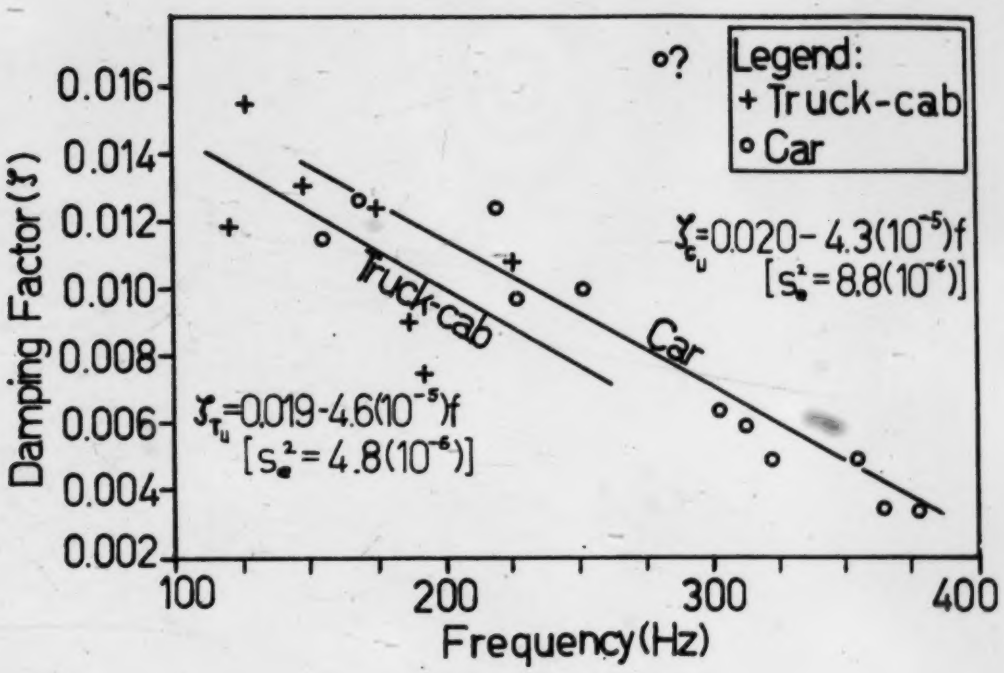

Figure 5.1 Resonant Damping in Unlined Enclosures.

Considering now the various lined states, the progression of damping factor averaged over all fundamental modes is shown in Figure 5.2. The discrete values of overall damping factor (ζ_T) are suitably approximated using the linear regression

$$\zeta_T = 0.011 + 3.9(10^{-4})S_L \qquad (5.1)$$

where S_L is the proportion of total internal surface area provided with the sound absorbent lining (expressed as a percentage). The regression provides an estimated mean damping factor of 0.011 in the unlined truck-cab model, which compares well with the measured (average) value of 0.0114. With the regression line passing through the range of measured data for all but one lining (T38), scatter of mean data about the regression is limited to 6% of the range of mean data. Maximum damping factor tends to occur on modes with the greatest number of nodes: for eleven of the fifteen lining configurations maximum damping factor occurred on a non-axial mode, six occurrences being the oblique mode.

If damping data are considered in terms of the three modal groups, the results are as shown in Figure 5.3. Three occurrences stand out, namely:

(i) accurate prediction of damping factor in the unlined model; values of 0.012, 0.010 and 0.010 predicted for the axial, tangential and oblique intercepts, respectively, display good agreement with the corresponding measured values of 0.013, 0.010 and 0.011 (recall that the oblique value represents a

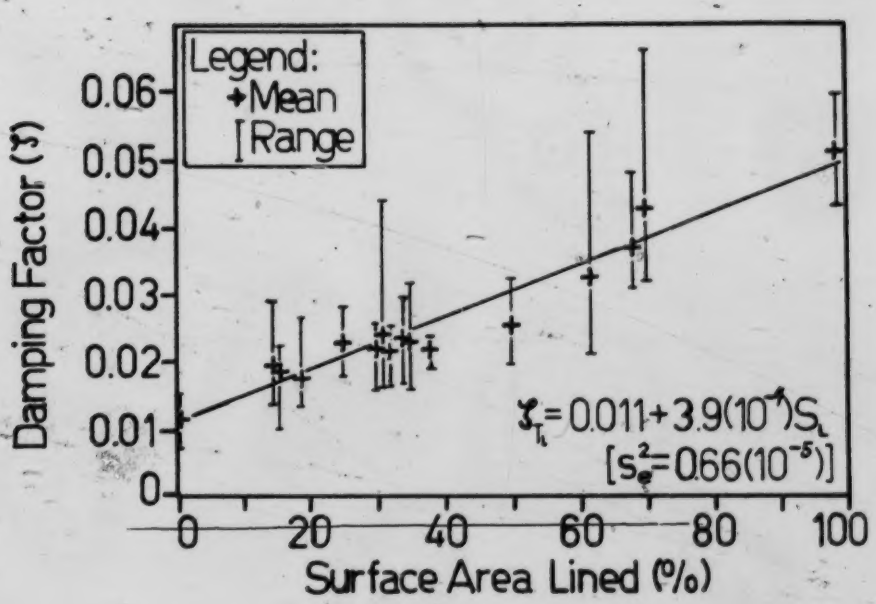

Figure 5.2 Overall Damping: Lined Truck-Cab Model.

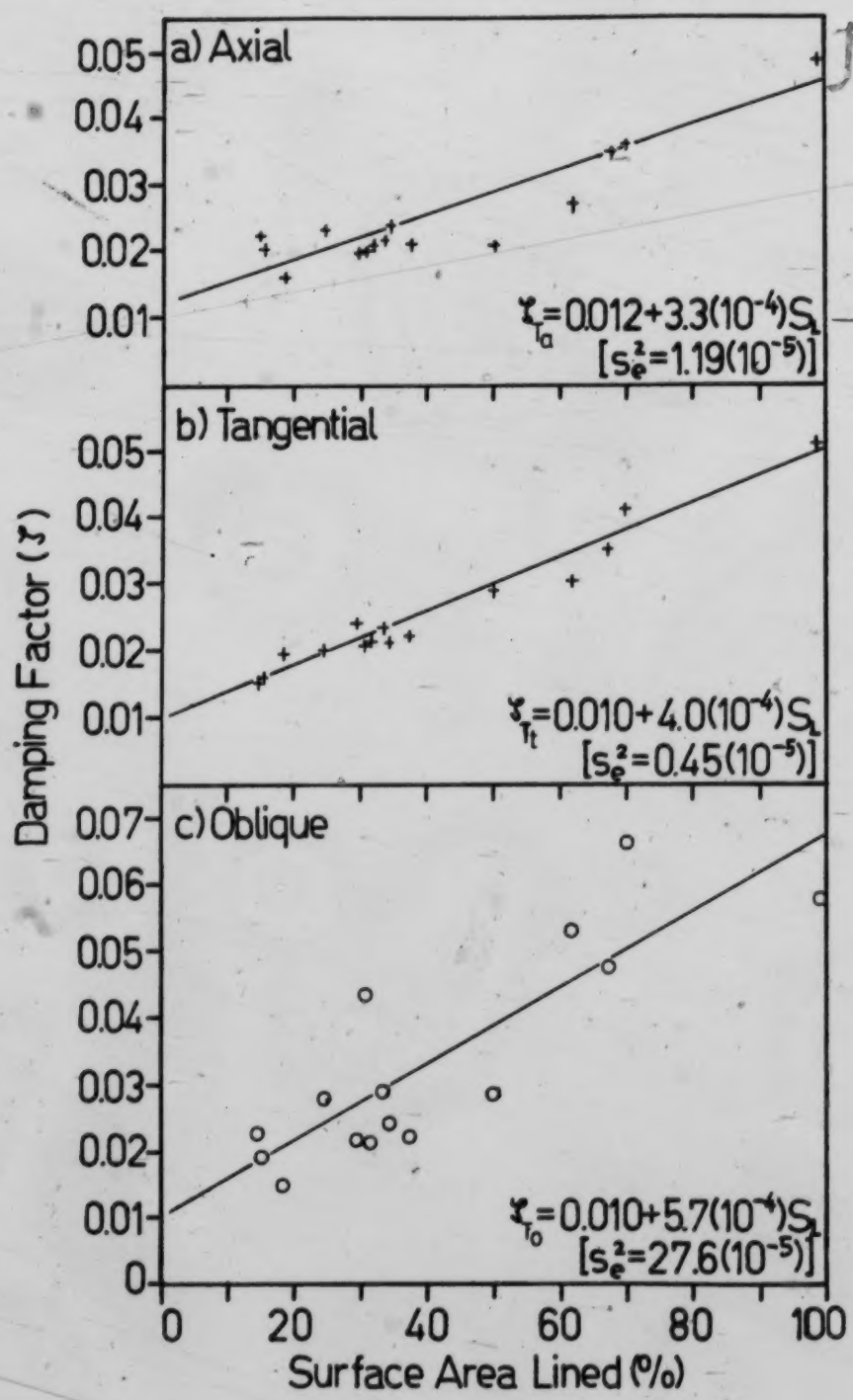

Figure 5.3 Modal-Group Damping: Lined Truck-Cab Model.

single mode).

(ii) the slope of a regression estimate increases as the number of nodal surfaces per modal group increases. (Note that this is consistent with the observation that maximum damping factor tends to occur on modes with a greater number of nodes.) Comparing the axial and tangential regression estimates, it will be seen that, due to the higher value of intercept and lower value of slope of the axial regression, at a particular value of area coverage the regression lines "cross over". Solving the axial and tangential regression equations simultaneously the coverage for which this occurs is 29% (damping factor 0.0214). Thus, since frequencies of the tangential modes exceed axial frequencies throughout all linings, the damping factor is observed to increase with increasing frequency if the amount of area-coverage exceeds 29%.

(iii) Data scatter is severe for the oblique mode (30% of measured range) and comparatively small for the axial and tangential data (9% and 5%, respectively, of the range of group-average data). The scatter of oblique data reflects a poorer repeatability of accurate generation of this mode and affirms the cancellation of local extrema which occurs in deriving averages of data. The slightly larger scatter of axial compared to tangential data is attributed to the lower sensitivity of the tangential modes to specific lining

location. Lining location can cause an excessive value of damping factor on either a single axial mode (as seen for lining T68 where damping on mode 001 exceeds damping on the remaining axial modes by almost 50%) or on all modes such that both modal and group-average data lie to one side of the regression line (as occurs at T25 and T50). (The significance of this latter occurrence is dealt with in the final section of this chapter.)

As a final comparison of averaged damping data, note that the tangential regression, given in Figure 5.3b, closely approximates the overall regression of damping factor as given by Eq. (5.1). This is due to the small difference between axial and tangential regression slopes and a high value of oblique regression slope.

If the damping factor progressions of individual members within a modal group are compared, insight can be gained into the exact influence of lining location. (To account for every location-dependent change of damping factor depends on considerations broader than those given here. The present purposes of accounting for lining location are (i) to discern whether extrema in group-averages are (not) a direct consequence of lining location and (ii) to contribute towards a better understanding of the "physics" of the phenomenon of acoustic energy dissipation.) Initially, using the damping factor of a single mode, it must be recognized which surfaces have been lined at each

data point and how damping factor at that point compares to damping on that mode for other lining configurations. Then, by comparing the progressions of different modes within a group, generalizations can be made concerning the significance of lining location for that mode type. In this way it was found that damping on an axial mode tends to display a local minimum if the lining is located normal to the standing wave of the mode (conversely, parallel to its node plane). Using Figure 5.4, this trend is seen for mode 010 (vertical) at T32 (floor and ceiling lined) and mode 001 (width) at T38 (both sidewalls lined). In such a case (lining normal to axial mode), two phenomena serve to keep damping factor low: first, recalling the frequency-dependence of the viscous boundary layer in the lining (Section 2.3), the lining is observed to have higher effective density relative to the lower-frequency axial modes; second, walls parallel to the axial standing wave are unlined, thereby sustaining high reflection of acoustic energy in the antinodal region. Thus, a local minimum of dissipation associated with sustained high reflection of acoustic energy results in the reduced damping factor. If walls parallel to the axial mode are lined, having normal walls unlined, modal damping remains relatively low due to high reflection of energy from the normal walls (compare damping at T30 and T38 on mode 001 in Figure 5.4). Note, using the same data (mode 001 at T30 and T38), the increase of damping factor (reflecting increased dissipation of energy) resulting from

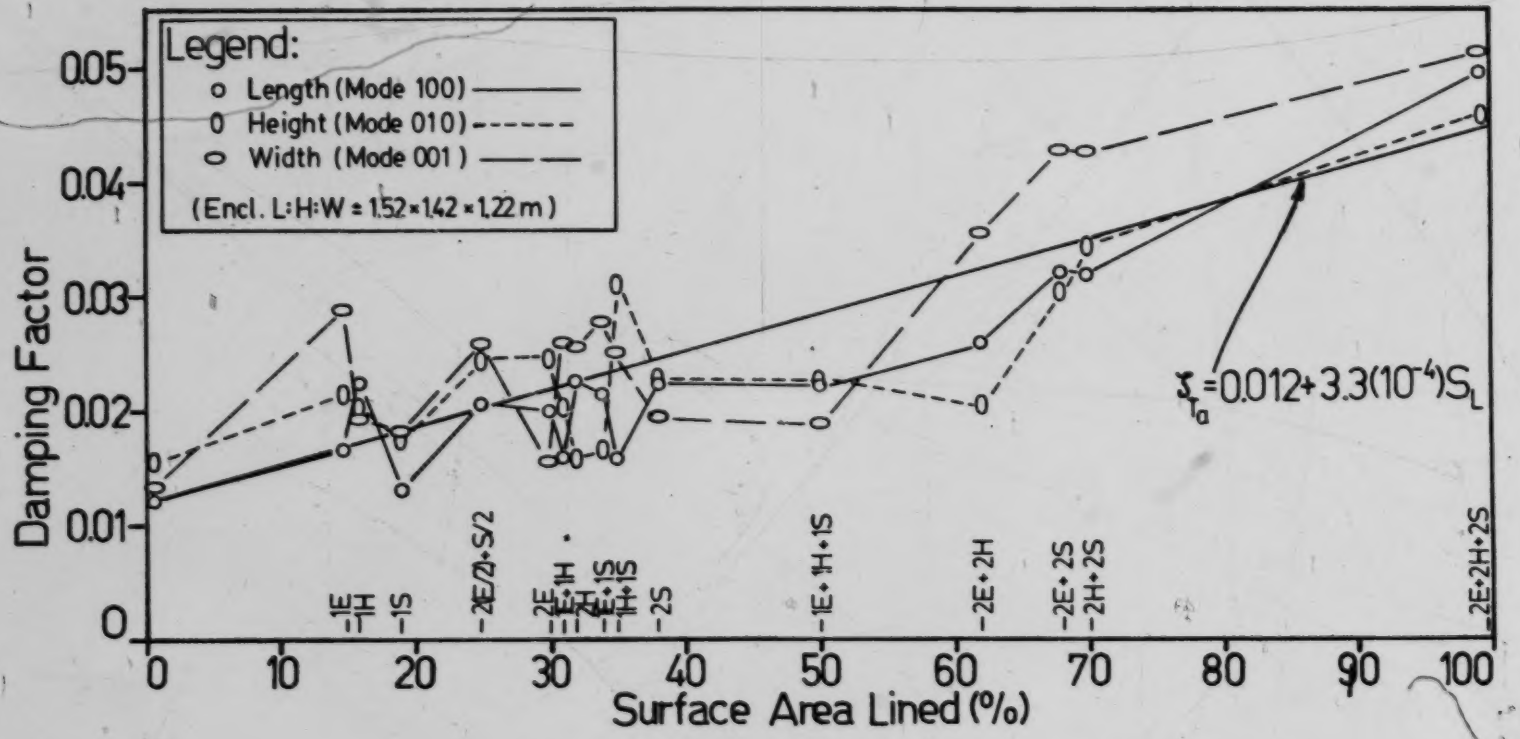

Figure 5.4 Axial Damping: Lined Truck-Cab Model.

the increase of covered area. Extending these considerations to the duct-like linings (T62, T68 and T70), the decrease of damping on mode 100 from T68 to T70 results from enhanced reflection of energy from the (normally-located) unlined endwalls and the lower value of damping on mode 010 at T68 is due to the unlined horizontal walls of this lining. Some of the inconsistencies of axial damping data with the stated trends (examples: (i) higher value of damping on mode 100 at T16 than at T15; (ii) higher value of damping on mode 001 at T32 than at T30 and T38) can be explained by accounting for the source-network layout used to excite the mode (Section 5.3). Tangential modes display local maxima of damping (see Figure 5.5) if lining is located on walls normal to the dimensions named in the mode label (that is, maxima of damping occur for mode 011 if some or all of the horizontal walls or sidewalls are lined).

Further consideration of the influence of lining location is given in later sections.

5.1.2 Frequency shift

Fundamental resonances in the unlined truck-cab model form three distinct groups: axial (120.9 Hz, 127.1 Hz and 148.5 Hz), tangential (175.1 Hz, 187.7 Hz and 193.3 Hz) and oblique (one mode at 226.6 Hz). Although modal frequencies shift by differing amounts for the various lining configurations (depending on lining location), overlapping of groups (where frequencies within one group shift into the

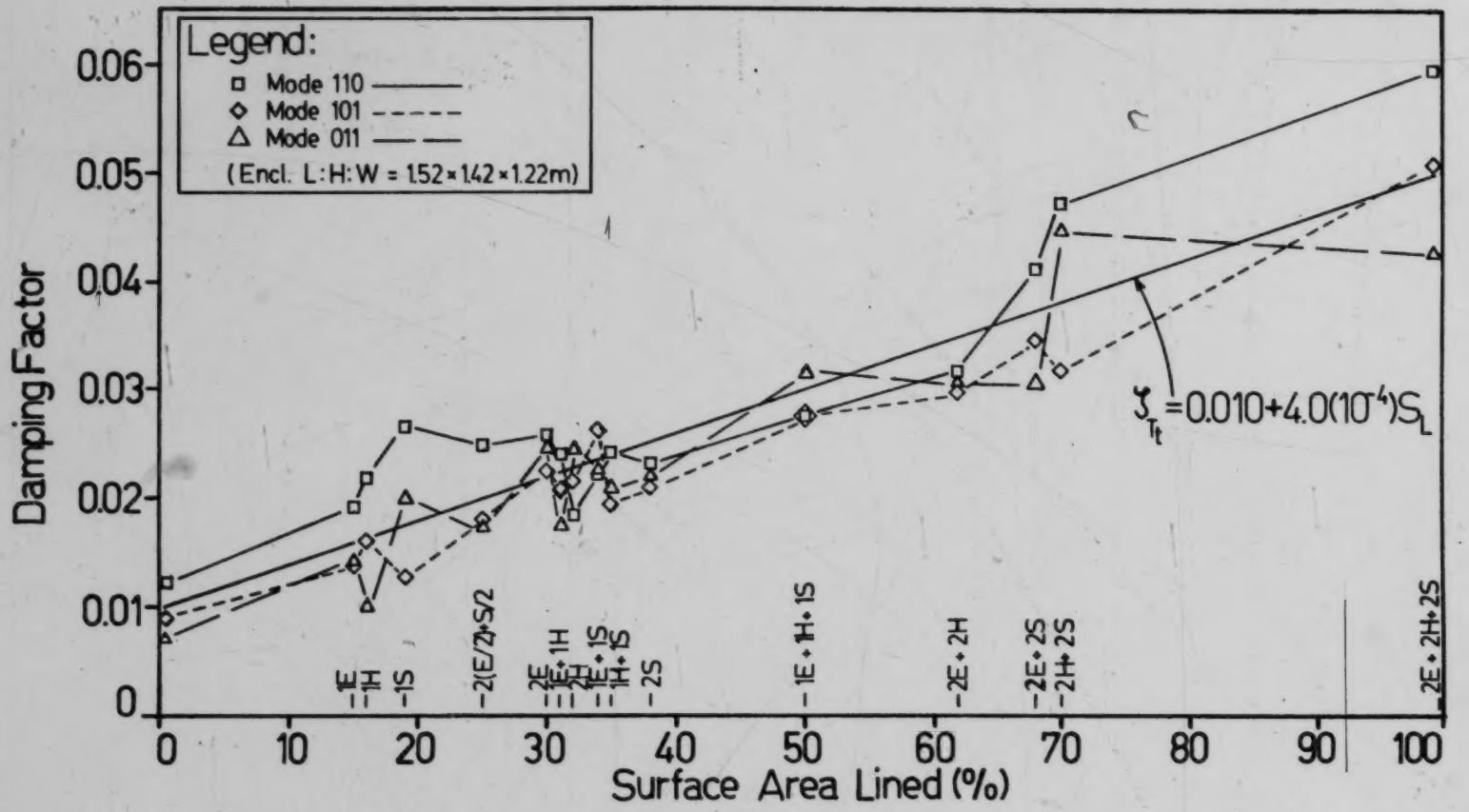

Figure 5.5 Tangential Damping: Lined Truck-Cab Model.

frequency region of a neighboring group) did not occur. As the proportion of lined area increased resonant frequency displayed a progressive decrease. Frequency shift, (defined as the difference of unlined and lined frequency-values of a mode, expressed as a percentage of unlined resonant frequency) is therefore negative and increases as the proportion of lined area increases. (Note that since all diagrams are plotted in terms of the increase of shift, a value higher along the ordinate-axis corresponds to a lower value of resonant frequency). Since increase of modal frequency (positive shift) was occasionally encountered, the absolute value of modal shift is used in the derivation of group-average data.

Derivation of overall-average data of frequency shift (all fundamental modes) leads to the plot of Figure 5.6 (shift data in Table A4.2). It is clear that, as for damping factor, shift data are suitably approximated by means of a linear regression. Scatter of overall-average data about the regression line is small (6% of the range of overall-average data); note that six of the data lie on the regression line. Range of measured shift increases with increase of lined area. The values of range which fall below the 0% level (reflecting positive frequency shift) occur only on axial modes and are a known consequence of lining location (described later).

As with the overall average, modal-group data are also suitably approximated by means of linear regressions (see

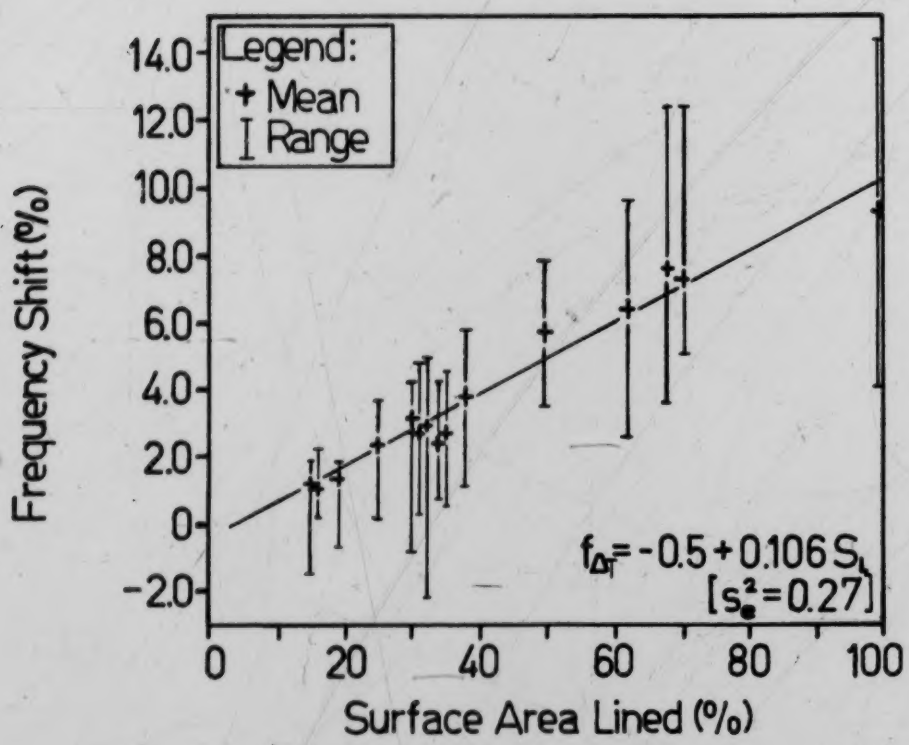

Figure 5.6 Overall Frequency Shift: Lined Truck-Cab Model.

Figure 5.7). Axial-group data (derived using absolute values of shift) are most susceptible to the influence of lining location and display a corresponding high degree of scatter (13% of range). Note that axial data before T30 tend to lie below the regression line while between T30 and T70 most data lie above it. In the latter region the high values occurring at T38, T50, T62 and T68 are in each case the result of an excessive value of shift on one of the modes (attributed to lining location). Scatter of data about the tangential regression is much lower at 5% of range, again reflecting the lower sensitivity of tangential modes to lining location. (For the large deviations occurring at both T50 and T68, shift of mode 011 coincides with the linear regression while those of modes 110 and 101 are high.) Scatter of oblique mode shift data is very low (7.3% of range). This indicates that resonant frequency is less susceptible to unaccounted-for influences (irregularities of excitation and measurement, panel flexibility, etc.) than damping factor (recall scatter of oblique damping data approached 30% of measured range). (It was found during testing that the center frequency of a resonance was almost always unmistakably clear while effort -- sometimes considerable -- might be needed to reduce the spread of a resonant peak; recall, for instance, the problem of a "split peak" described earlier.) As with damping factor, linear regressions of modal-group data display an increasing slope as the number of nodes per modal group increases.

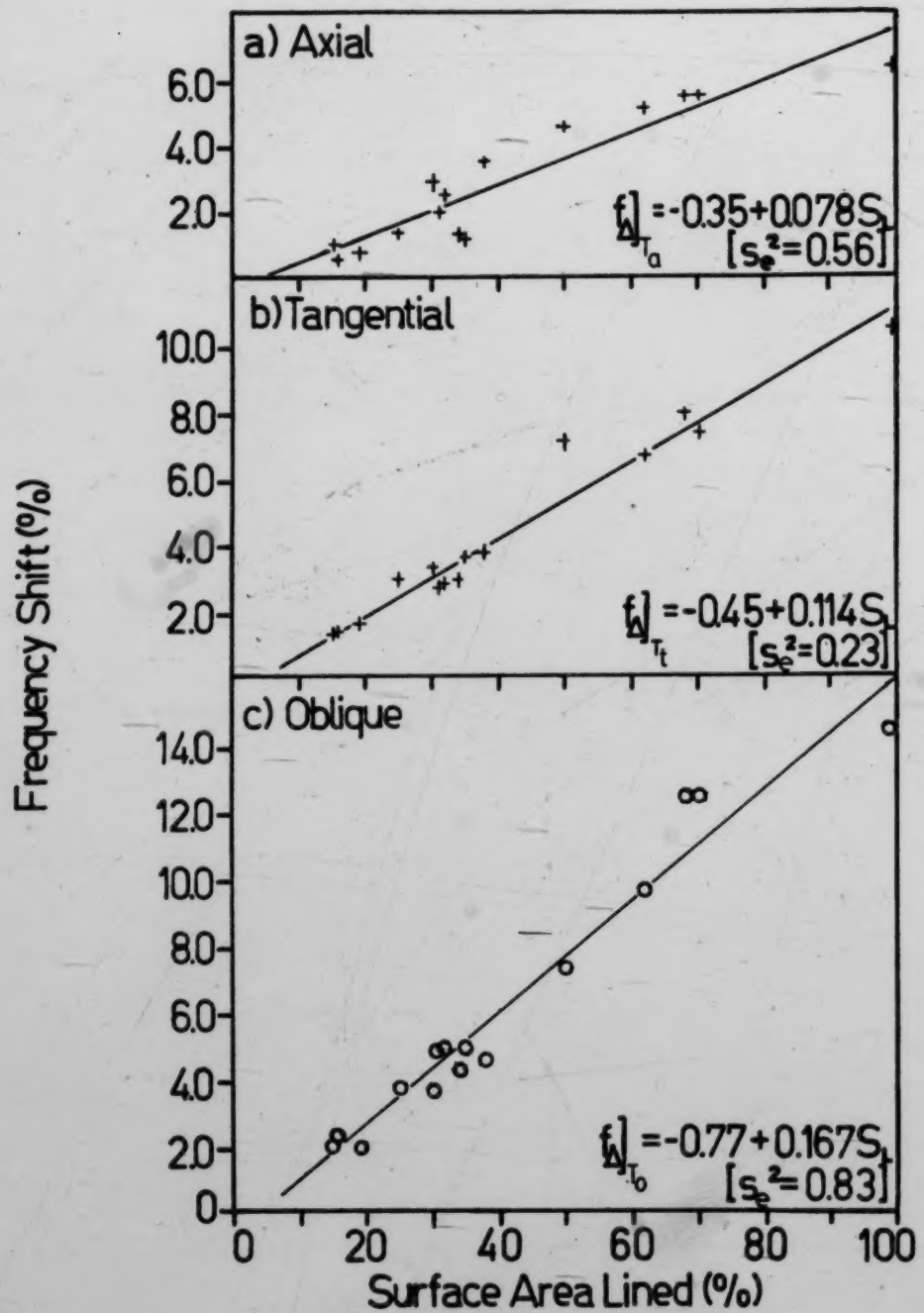

Figure 5.7 Modal-Group Frequency Shift: Lined Truck-Cab Model.

Maximum shift is thus likely to occur on the oblique mode and this was in fact observed in eleven of the fifteen configurations tested. Here again, the tangential regression closely approximates the overall average of shift (compare the Equations of Figures 5.6 and 5.7b). An interesting occurrence on all linear regression estimates of frequency shift is the prediction of a negative intercept -- that is, averaged data appear to suggest that modal frequency in the unlined model should exceed its actual value. It is suggested that for low area coverages the linear regression describing higher amounts of coverage is not applicable and that the shift line in fact curves in towards the origin of the graph (see also the last section of this chapter).

The influence of lining location on frequency shift is more consistent and therefore more readily discerned than its influence on damping factor. In terms of axial modes two trends were determined. First, the positive shift already mentioned tends to occur when lining is located normal to an axial mode and decreases as the amount of normally-located lining increases. As example of this the frequency of mode 100 increased by 1.5% if one Endwall was lined (T15) and increased by only 0.8% if both Endwalls were lined (T30). Recalling that for linings normal to axial modes damping factor is reduced, in part, because of the higher effective density of the lining to the axial standing wave, installation of the lining serves, in effect, to decrease the axial dimension causing the increase of frequency (by

lining one Endwall, the length dimension decreases by 3%). However, as the amount of lining (normal to the mode) increases, the dissipative effect of the lining is sufficient to cause frequency again to decrease. The above can be seen using Table A4.2. Observe, for example, the shift of mode 001: at T19 (one Sidewall lined), a positive shift of 0.4% was measured and at T38 (both Sidewalls lined) shift is negative at 1.1%. (Behaviour apparently inconsistent with the above occurs on mode 100 at T19 (one Sidewall lined) where shift was also positive and for mode 010 which, at T16, displayed negative shift (0.5%) and at T32 large positive shift (2.2%).) The second trend observed on axial modes is that these modes display local maxima of shift if lining is located on all walls parallel to the standing wave of the mode ("duct" linings; T62 for mode 001, T68 for mode 010 and T70 for mode 100, the latter two being overall maxima of shift at 5.8% and 7.9%, respectively). The remaining modes display shift consistent with having been lined partially normal/partially parallel to their respective standing waves. As example, mode 001 displays a large shift (7.4%) for T62 (Sidewalls unlined) and lesser shifts of 3.6% and 5.5%, respectively, for T68 and T70 (Horizontal walls unlined, Endwalls unlined, respectively). The increase of shift from T68 to T70 is simply a reflection of increased area coverage. Concerning the tangential modes, maximum shift occurs for two of the modes (101 and 011) when the lining is ductlike and parallel to the intersection of

the node planes (T68 for mode 101 and T70 for mode 011).

5.2 Car Model

As indicated in the previous section, damping factor and frequency shift in the truck-cab model are suitably described by means of linear regressions. This was seen to hold true for the car-model also. Discussion of the influence of lining location, begun with study of the truck-cab model results, is extended by considering the car-model's damping and shift data.

Resonance testing of the car-model also included measurement of five non-fundamental resonances as these were interspersed among the higher fundamental resonances. Treated as a separate modal group, non-fundamental data are NOT included in the derivation of overall averages of damping factor and frequency shift (though, for comparison, modal-group data are derived).

5.2.1 Damping factor

Damping factor in the unlined car-model displays a very pronounced decrease with increasing frequency (see Figure 5.1). The linear regression describing this trend is based on all twelve resonant modes. The high value of scatter (22% of range) is largely the result of the "wild" datum at 282 Hz (this point was chosen as the "best" of three possible values; recall Section 4.2.2). Visual inspection of Figure 5.1 indicates that nine of the car-model's twelve resonant

damping data lie within 0.001 (vertically) of the regression line. This is equivalent to 8% of measured range and affirms the high degree of linearity of the data. (The 28%-of-range scatter of truck-cab data is also visually discernible.)

The variation of damping factor (averaged over all fundamental modes) with area lined is shown in Figure 5.8. While range measured at each data point tends to increase with area lined, averaged data display low scatter (6% of range) and are more regularly distributed about the regression line than was observed for the truck-cab model. Thus, the linear approximation is seen to be good. Maximum damping factor occurred for eleven of thirteen linings on a fundamental mode; six of these were on tangential modes (also true for the unlined car-model) and five on axial modes.

Linear regressions of modal-group damping data are shown in Figure 5.9. Comparing the axial, tangential and non-fundamental averages it is again seen that regression slope increases with the number of nodes per modal group. The lower value of oblique regression slope (compared to tangential slope) is ascribed to the two low values of oblique damping for linings C53 and C100. (Recall firstly that the oblique regression is based on a single mode making large scatter more likely. Further, the datum at C100 reflects the high degree of measurement uncertainty inherent to higher modes when area coverage becomes large.) Regression intercepts are seen to decrease with increasing modal

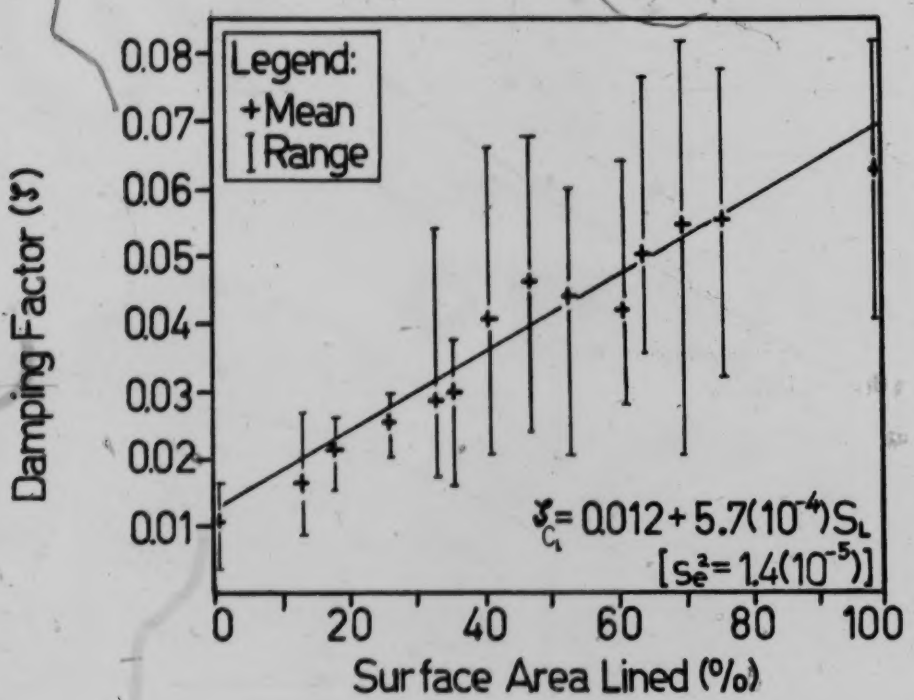

Figure 5.8 **Overall Damping: Lined Car-Model.**

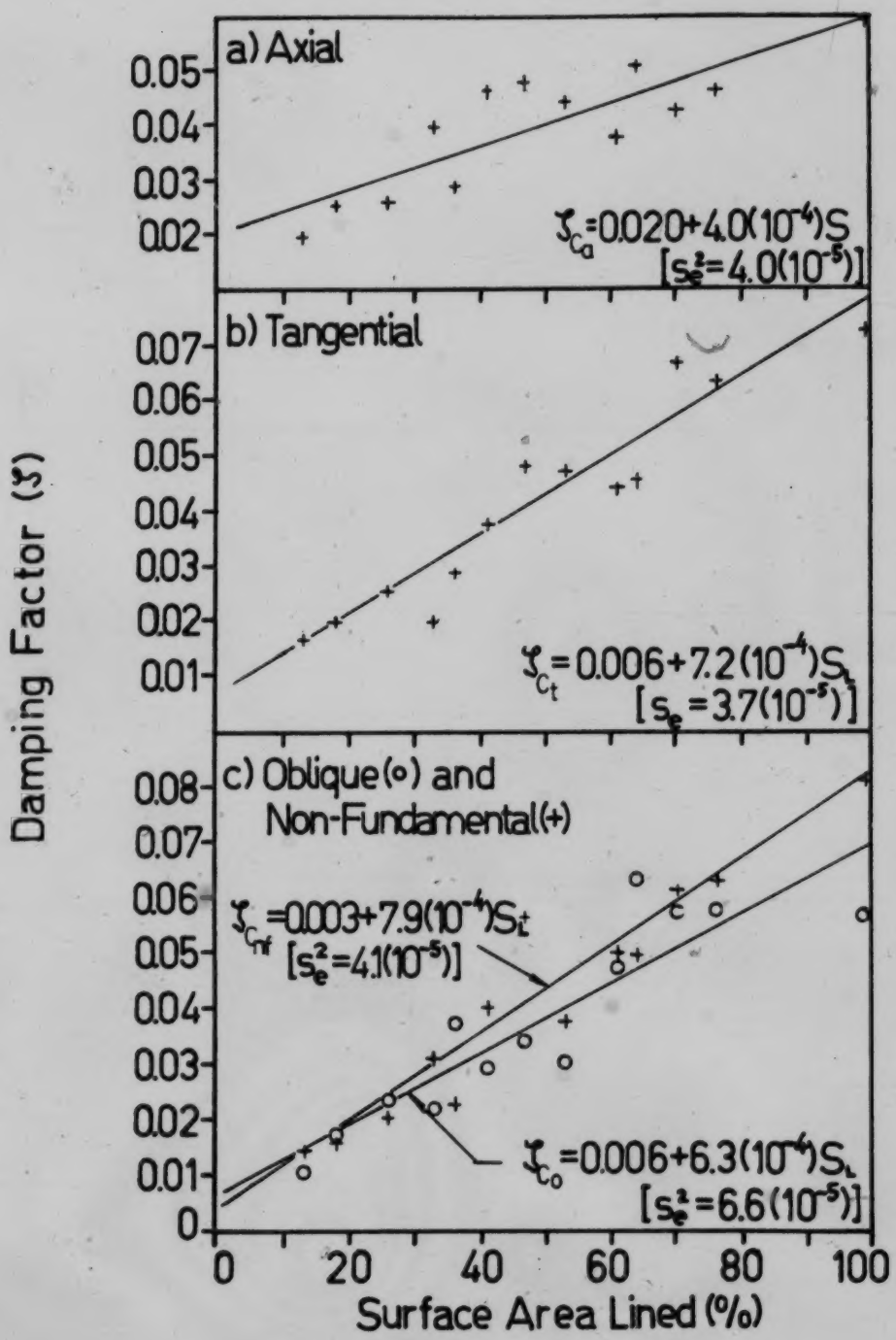

Figure 5.9 Modal-Group Damping: Lined Car-Model.

complexity which is consistent with the behaviour observed in Figure 5.1. Scatter of modal-group data about their respective linear regressions is approximately double that of the overall regression (averaging 12.5% for the four modal groups and 6% for the overall regression). For both the axial and tangential regressions, if a data point is (vertically) remote from the regression line (linings C33, C41, C47, C53 and C64 for the axial regression and C33, C47 and C70 for the tangential regression), the tendency found is that damping on one mode is excessive while that on the remaining modes is very near that predicted by the regression line. (For linings C47, C53 and C64 only mode 100 displays an excessive value of damping factor.) This reaffirms that the axial regression is more sensitive to the influence of lining location than the tangential regression. Note that for the latter, the data other than those considered remote, are extremely well-behaved. The tangential and axial regressions display a "crossover" (beyond which damping factor increases with frequency) at 42% of area lined. (Since this is high due to the large values of axial damping on single modes at the midrange of coverages, the "true" value of crossover will occur for a coverage of approximately one-third of total surface area.) The slope of the tangential regression of the car-model is one-fifth greater than that of its overall damping regression (recall that for the truck-cab model the tangential and overal damping regressions were effectively

identical). This is due primarily to the larger difference of axial and tangential regression slopes in the car-model.

As regards the influence of lining location on the car-model's resonances, inspection of Figures 5.10 and 5.11 reveals the following:

(i) damping on axial modes tends to be high (above an individual mode's mean progression) if lining is located near the mode's regions of maximum pressure amplitude. For mode 100 (longitudinal) this is seen in lining the front and rear "windows" (W_F and W_R) and the "firewall"; for mode 001 (width) local maxima of damping factor occur if the lower boundary is lined (firewall, floor, slantwall and panel); for mode 010 (vertical) local maxima of damping are seen where the floor and lid form part of the lining. Observe that by locating lining near the regions of maximum amplitude, the panels which intersect at the antinode no longer radiate the acoustic energy as effectively as when unlined. Pressure antinodes occur for the longitudinal fundamental mode at the intersection of the front window and firewall as well as at the bottom of the rear wall, and, for the transverse (width) mode at the intersections of floor and sidewalls. Figure 5.10 further shows the consistently low damping factor of mode 010 (pressure antinodes at the intersections of front window and lid and of floor and slantwall). This is attributed to the short vertical dimension resulting

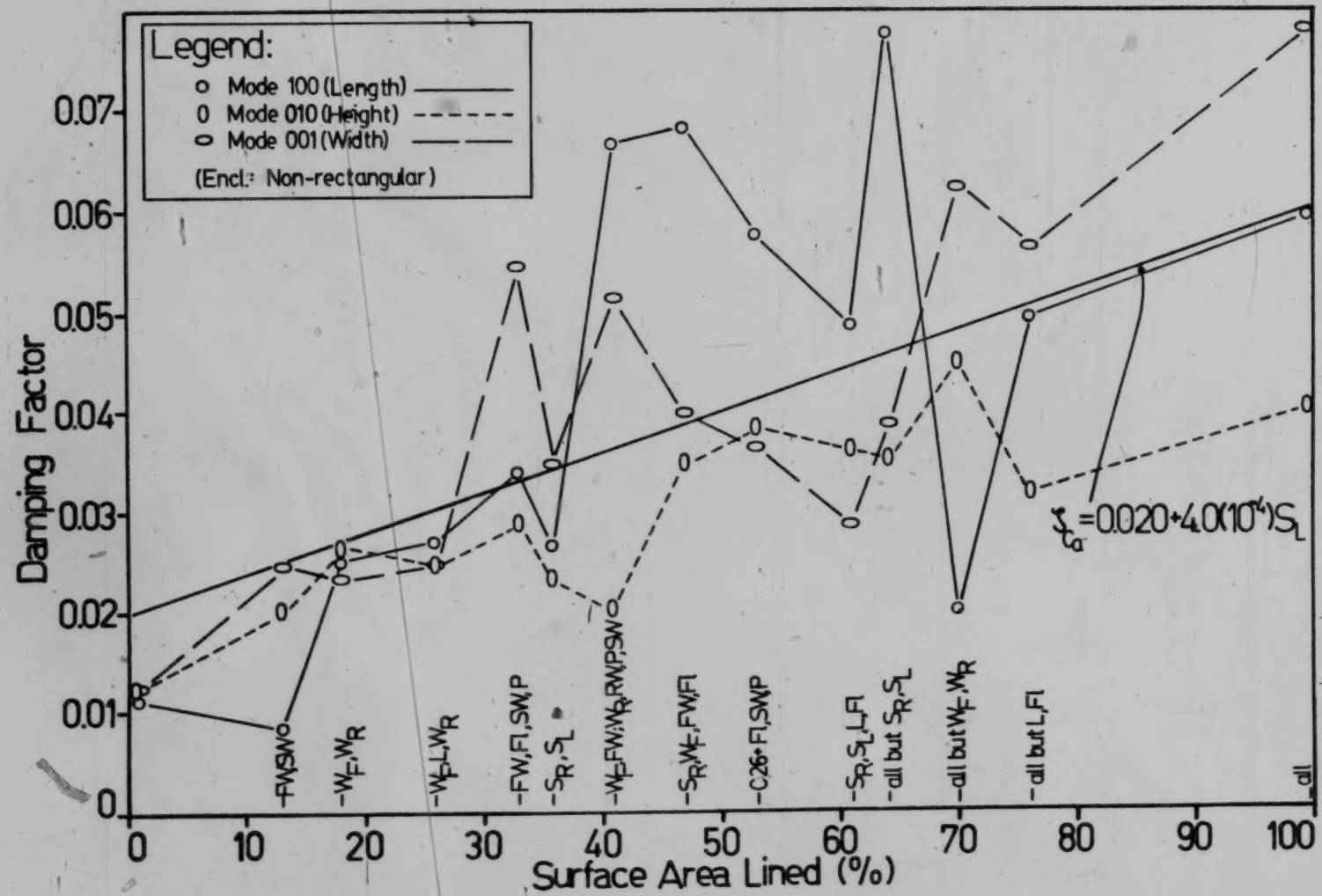

Figure 5.10 Axial Damping: Lined Car-Model.

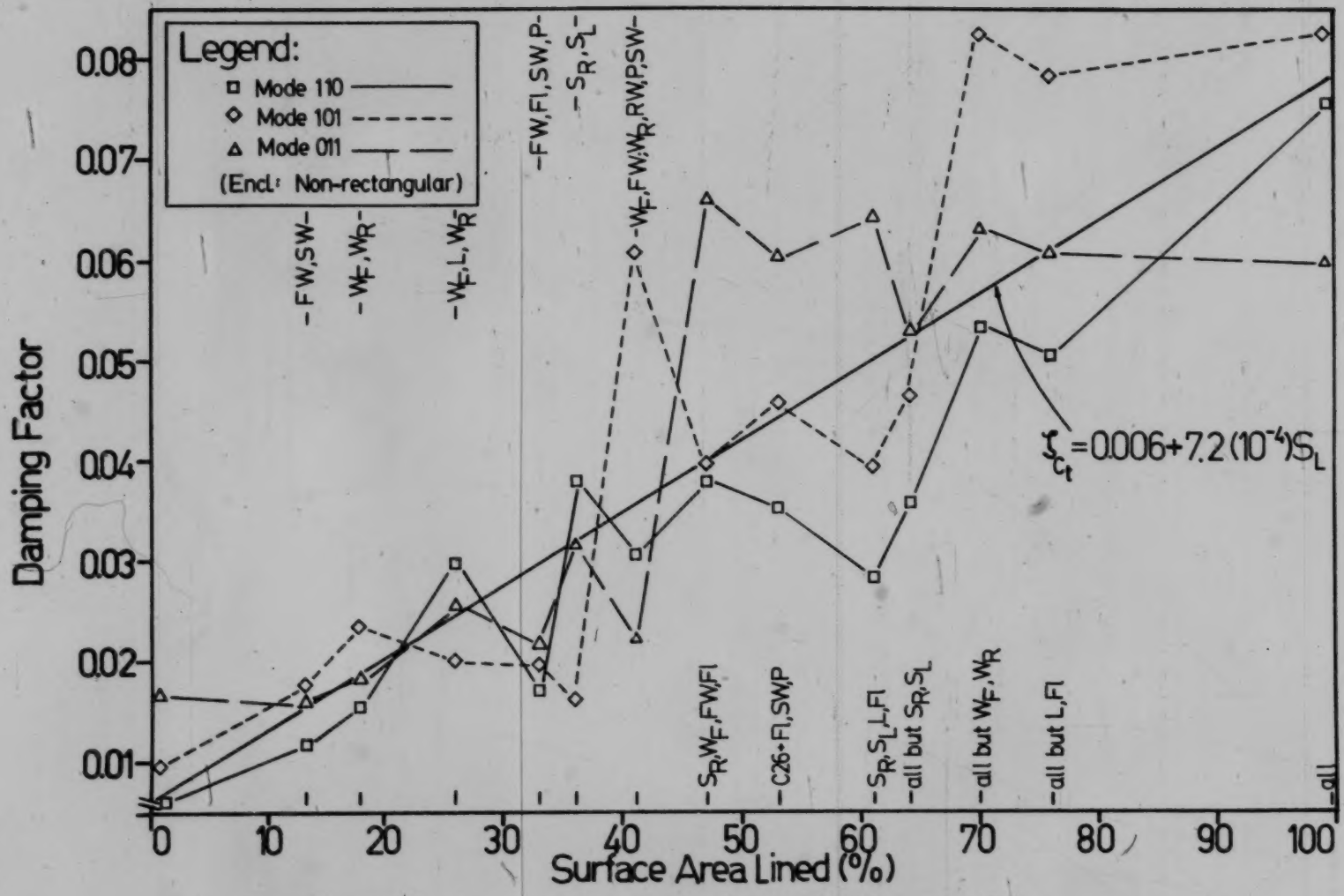

Figure 5.11 Tangential Damping: Lined Car-Model.

in low mass-high stiffness acoustic properties. The large scatter in the data of mode 100 is mainly the result of splitting of peaks: for all of linings C41, C47, C53 and C64 mode 100 could not be generated as a distinct-frequency resonant peak. (For higher coverage linings well-formed resonances were again obtained. Response amplitude, which had remained high for the aforementioned linings, decreased to approximately one-third for the remaining linings.)

(ii) Damping on tangential modes also attains local maxima if lining is located on panels adjacent to the modal antinodes. As example of this, observe the value of damping factor on mode 011 for lining C47 where, by placing the lining on (among others) one sidewall and the floor, the lining is directly adjacent to three of the mode 011 antinodes (running lengthwise at the top and bottom of both sidewalls; note that pressure amplitude is always greatest for the lower antinodes). Similar behaviour is seen on mode 110 for linings C26, C47 and C61 (the latter being an example of low damping factor if antinodes are unlined) and for mode 101 at lining C41. The low scatter of tangential-group data (Figure 5.9b) is a reflection of the consistent distribution of modal damping data about the regression estimate plotted in Figure 5.11.

5.2.2 Frequency shift

Modal frequency shift in the lined car-model, while again negative and increasing with lined area, displays some trends not observed in the truck-cab model. First, whereas in the truck-cab model some positive shift was encountered, none occurred in the car-model tests. Second, since modal groups in the car-model overlapped, changes of modal sequence (compared to the unlined case) occurred as the members of the more-complex groups again displayed greater amounts of shift (see also Table A4.5). Finally, the increase of resonant wavelength, implicit in the decrease of resonant frequency, was given some special attention.

As seen in Figures 5.12 and 5.13 frequency shift in the car-model shows behaviour very similar to that in the truck-cab model. Frequency shift data averaged over all fundamental modes (Figure 5.12) display good linearity. The larger deviation of points C33, C64 and C70 from the overall regression can be explained in terms of divergent points at these linings in the modal-group plots of Figure 5.13 (for example, at C33 the tangential (averaged) datum is low due to low values of shift on both modes 011 and 110). The axial and tangential data display low scatter about the regression estimates (11% and 8% of measured range, respectively) and tangential regression slope exceeds axial slope by approximately one-sixth. Oblique data contain an obviously wild point at C64 (NOT used in obtaining the regression line). Scatter of data is large about the oblique regression while

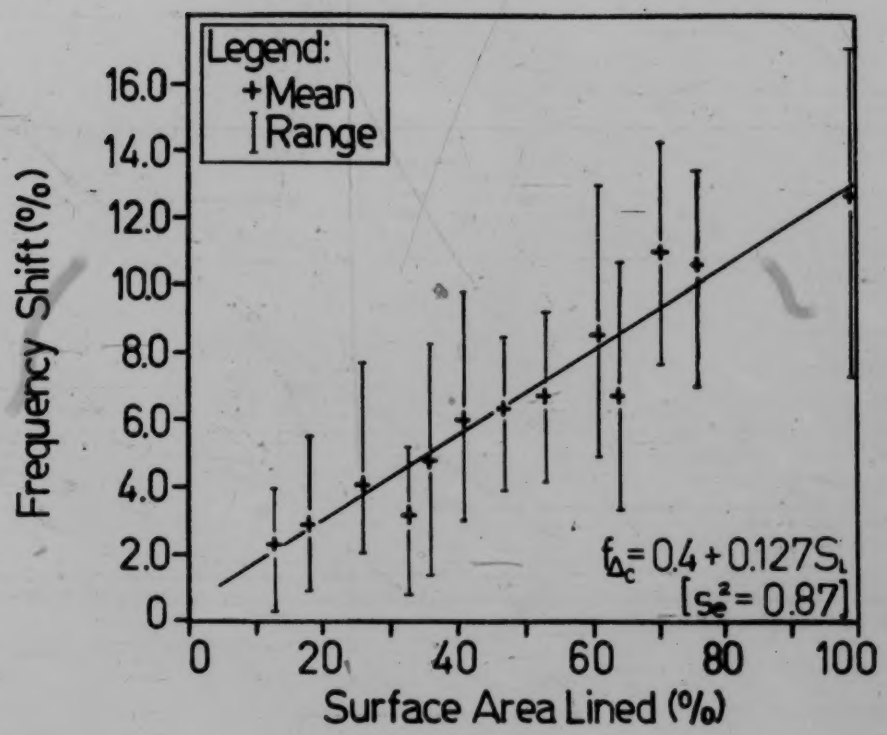

Figure 5.12 **Overall Frequency Shift: Lined Car-Model.**

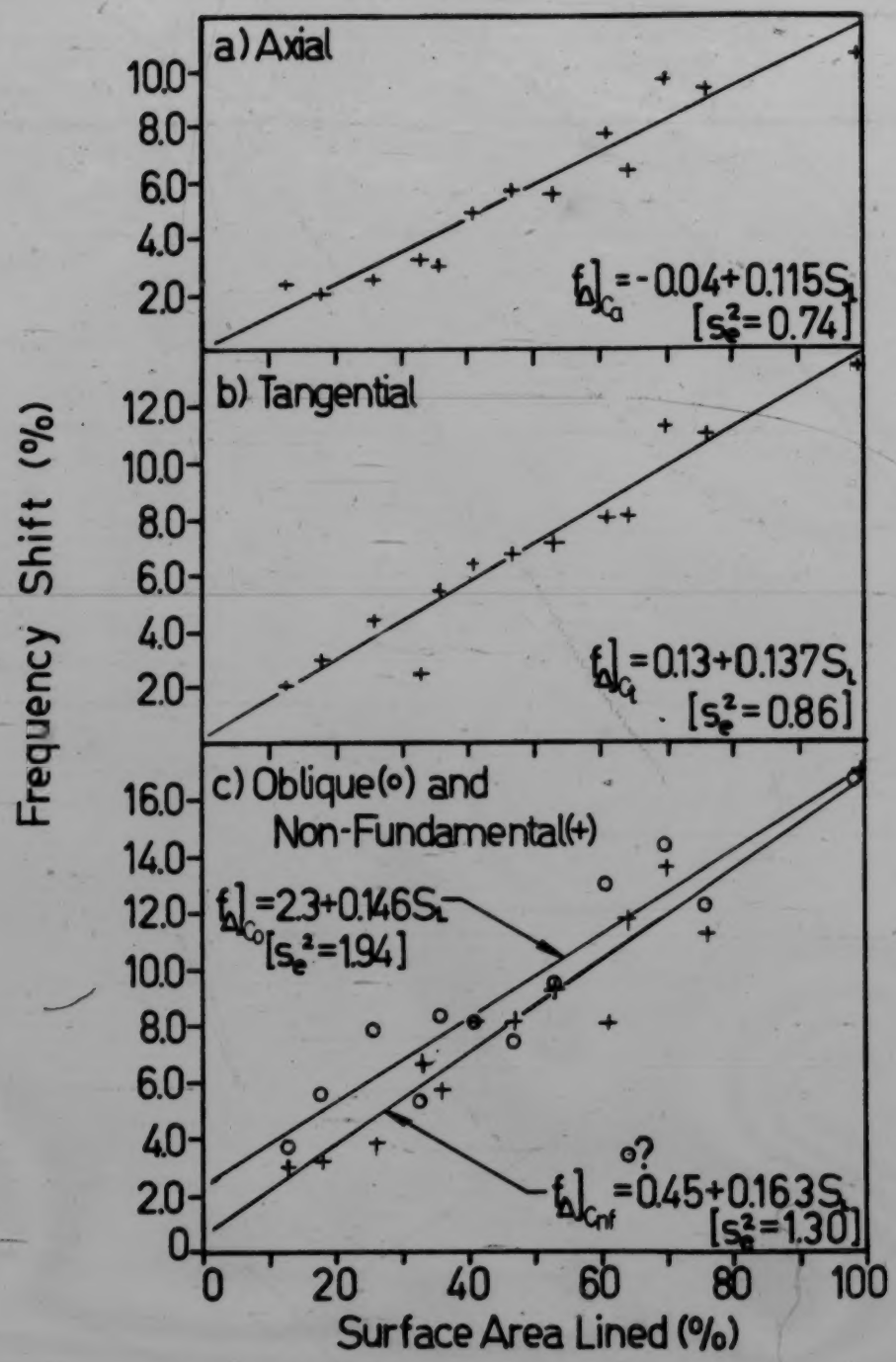

Figure 5.13 Modal-Group Frequency Shift: Lined Car-Model.

that about the non-fundamental regression is limited by the averaging process. Changes of modal sequence are reflected in that regression slope of the tangential group exceeds that of the axial group: for linings C64 to C100, the resonant frequency of mode 101 was less than that of mode 010 (in the unlined model the reverse is true). Such reversals of sequence did not occur between different members within a modal group. In comparing the regression estimates of Figures 5.12 and 5.13, it is observed that a negative intercept is predicted for the axial regression alone (note, however, that no positive shift actually occurred). Maximum frequency shift occurred in the fully-lined model on ten of the twelve modes considered (both modes 010 and 011 reached their overall maxima with lining C70).

The influence of specific lining location on car-model resonances is summarized as follows. As with the truck-cab model, fundamental axial modes display larger amounts of shift when lined parallel to the direction of the standing wave (for example, linings C13 and C61 for mode 100) and lesser shift when lining is normal to the standing wave (example: linings C33, C53 and C64 for mode 010). (The only non-fundamental axial mode which conforms consistently with this fundamental-axial shift pattern is mode 002). Of the fundamental tangential modes, two (modes 011 and 110) display large shift if the sidewalls are lined. The local minimum shift of mode 110 for lining C64 (sidewalls alone

UNlined) suggests (an unexpected) dependence of radiation/reflection of the antinodal signal upon the sidewalls for this mode. Shift of mode 101 displays a local maximum for lining C41 (where the front and rear of the model have been lined) and appears insensitive to lining of the sidewalls (this latter occurrence being unexpected). Of the two non-fundamental tangential modes, only mode 201 demonstrates some consistency of frequency shift with the trend cited for the truck-cab model: local maxima of shift if lining is located parallel to the intersection of the node planes (a local maximum shift was observed for mode 201 for lining C47).

The change of resonant frequency resulting from the lining of the enclosures also implies a change of resonant wavelength (recall that the product of frequency and wavelength is a constant, namely, sonic speed). Thus as frequency decreases resonant wavelength must increase. The result of this can be observed in the relocation of nodal planes, an example of which is given for the vertical axial mode in Table 5.1. (Note that the designations "Front" and "Rear" in Table 5.1 refer to the regions beneath the Front-window and Rear-window, respectively; the letter W indicates a measurement taken at the midwidth of the car-model.) From the data in the table, it is clear that the node plane tends to shift towards the lined surface. Note that at a highly reflective boundary the phase shift between reflected and incident components of the pressure wave is fixed

Table 5.1 Relocation of Nodal Surface (Mode 010).

Location	Lining	Vertical distance from plane of floor (cm) C00	C26
Front	Rt.	30	45
	W	--	41
	Lf.	30	50
Midlength	Rt.	36	46
	W	--	45
	Lf.	--	48
Rear	Rt.	42	60
	W	--	55
	Lf.	46	75
Freq. (Hz)		221.6	213.8

(approximately 90°) while at a porous lining phase shift changes depending on lining impedance. Thus the node plane must shift away from the reflective boundary.

5.3 Comparison of Models

In Table 5.2 a summary is given of the acoustic response (in terms of damping factor and frequency shift) of the two models tested. Comparison can thus be made of the influence on acoustic response of (i) enclosure volume, (ii) enclosure shape and (iii) shell material.

The regressions of damping factor versus resonant frequency in the unlined models are very similar. Since the regressions predict approximately the same zero-frequency damping factor of 0.02 (for this reason taken to be a characteristic of the medium, air), the difference of slope is significant and not a chance occurrence (the latter being conceivable due to the larger scatter of truck-cab model data). The more rapid decrease of damping factor in the truck-cab model is a result of its larger volume: as the reverberant field is larger, the effect of natural absorption of acoustic energy provided by the enclosing material is reduced. Lower scatter of the car-model data (which includes the five non-fundamental modes) results from its more uniform sound field (due to irregular shape) and the greater uniformity and density of its steel shell: the higher porosity of wood and more uneven layer of varnish (hand-painted) in the truck-cab model contribute to more

Table 5.2 Comparison of Acoustic Response of Truck-Cab and Car Models[1].

Ordinate (y)	Abscissa (x)	Group	TRUCK-CAB Intercept (A)	TRUCK-CAB Slope (B)	TRUCK-CAB Scatter (% of range)	CAR Intercept (A)	CAR Slope (B)	CAR Scatter (% of range)
Damping Ratio (UNLINED MODELS)	Frequency (Hz)	---	0.019	$-4.6(10^{-4})$	28	0.020	$-4.3(10^{-4})$	22
Damping Ratio	Lined Area (percent)	Axial	0.012	$3.3(10^{-4})$	9	0.020	$4.0(10^{-4})$	15
		Tangential	0.010	$4.0(10^{-4})$	5	0.006	$7.2(10^{-4})$	11
		Oblique	0.011	$5.7(10^{-4})$	30	0.006	$6.3(10^{-4})$	15
		Overall	0.011	$3.9(10^{-4})$	6	0.012	$5.7(10^{-4})$	6
		Non-Fund.	---	---	---	0.003	$7.9(10^{-4})$	10
Frequency Shift (percent)	Lined Area (percent)	Axial	-0.35	0.078	13	-0.04	0.115	11
		Tangential	-0.45	0.114	5	0.13	0.137	8
		Oblique	-0.77	0.167	7	2.30	0.146	11
		Overall	-0.50	0.106	6	0.40	0.127	7
		Non-Fund.	---	---	---	0.45	0.163	8

[1] A linear relationship of the form $y = A + Bx$ is assumed.

random behaviour and therefore greater scatter of its unlined damping data. Finally, since the frequency ranges of the models overlap (see Figure 5.1), the difference of damping factor caused by the use of different enclosing materials, though measurable, is not great.

Turning to the variations of damping factor and frequency shift with area coverage, the two models again display very similar behaviour with, in all but one (modal-group) variation, regression slope of the car-model exceeding that of the truck-cab model. Note that, in general, overall averages display lesser scatter of data than the component modal-group averages.

In comparing the linear regressions of overall damping factor, the higher intercept of the car-model is unexpected since damping factor is known to decrease with frequency and the range of car-model resonances lies above that of the truck-cab model (recall Figure 5.1). The high value of overall intercept is a direct reflection of the (extremely) high axial intercept which, in turn, resulted from the high damping factor on individual axial modes in the range C33 to C64 (recall Figure 5.10). If the identified high values of axial damping factor are momentarily disregarded and a regression estimate assumed between the mean measured intercept (0.012) and the derived linear regression value of the fully-lined case (note that remaining axial data are then also more suitably approximated) intercept/slope values

of 0.012 and $4.8(10^{-4})$ would be obtained for the AXIAL regression. (Note that this conforms well with the value of 0.014 predicted at 150 Hz by the damping-frequency regression of the unlined model.) The overall regression of damping factor would then have intercept/slope values of 0.009 and $6.1(10^{-4})$. Thus, an overall regression in which only the "well-behaved" axial damping data are used, provides an intercept (as estimate of mean damping factor in the unlined model) which is more consistent with both Figure 5.1 and the remaining modal-group damping intercepts of Table 5.2 as well as a regression slope nearer that of the tangential and oblique regressions. Comparing, then, the damping factor regressions of the two models in terms of the various group-averages, regression slope is seen, in all cases, to be greater for the car-model. This is the result of the car-model's reverberant field being both smaller (due to model dimensions) and more uniform (due to irregular shape) than that of the perfectly-rectangular truck-cab model. (Irregular enclosure shape causes more random reflection and thereby greater dissipation of reverberant acoustic energy.) The greater scatter of axial and tangential data about their respective linear regressions for the car-model is a reflection of the greater susceptibility of these modes to the "peak-splitting" phenomenon which was encountered consistently throughout the car-model tests. (Vibrations of the highly flexible steel panels were visually indiscernible but clearly perceived by placing the

hand on various panels; recall that excitation of the reverberant field occurred at nominally 100 dB. Panel vibration amplitude, though less than a millimeter, causes slight variations of internal dimension and, along with the elastic response of the panels, may be sufficient to cause the multiple frequency values of specific resonances referred to as peak splitting. Nonconstancy of axial dimensions may inherently also contribute to this.)

Concerning frequency shift, the main difference between the overall averages of the two models is the negative intercept (positive shift) of the truck-cab model (note that all modal-group regressions of truck-cab model frequency shift also display a negative intercept). As positive shift was not encountered in the car-model tests, irregular model shape appears to ensure that the dissipative effect of the lining overrides any tendency of the pressure wave to undergo enhanced reflection from the lining. Note that for all but the oblique regression, regression slope in the car-model exceeds that of truck-cab model which affirms the higher, more effective dissipation of acoustic energy occurring in the car-model. (The low scatter of oblique shift data in the truck-cab model (in itself remarkable as scatter of the non-averaged oblique data is usually high) affirms the validity of its regression slope.) The lower scatter of tangential shift data than that of axial shift data seen in both models (and observed also in terms of damping factor in both models) reaffirms the lower

susceptibility of the tangential modes to the influence of lining location.

The final paragraph of this section is a qualitative comparison of the dissipation of acoustic energy in the two models. In the car-model it was found that dissipation of acoustic energy was greatest if lining was provided on the walls projecting outward from a given mode's pressure antinodes. Note that if unlined, these panels reflect essentially all incident energy back to the reverberant field. Turning now to the truck-cab model and using excitation of its fundamental longitudinal mode as example, the sources, though discrete, can be conceived of as line sources parallel to and midway between the two horizontal walls and located in front of the two endwalls (see Figure A3.3). For lining configurations where the endwalls are left unlined (serving as a highly reflective baffle) the two horizontal walls serve as a more effective continuation of the baffle than the sidewalls as the former are parallel to the line-source. Thus if the horizontal walls only are lined, damping factor is high while if the sidewalls only are lined the enhanced radiation provided by the unlined horizontal walls serves to keep damping of mode 100 relatively low. This explains the observed high damping of mode 100 at T15 and low damping at T19; note that if the line sources were rotated by 90° (that is, parallel to and midway between the sidewalls) it is expected that damping of mode 100 will be low for T15 and higher for T19. Two

conclusions apparent from the above are (i)that dissipation of acoustic energy in the antinodal regions is the most effective means of reducing resonant noise levels and (ii)that in considering the extrema of axial damping factor, layout of the source network relative to lining location must also be taken into account. Additional evidence of the former is that damping of the truck-cab model's tangential modes was highest if lining was located along the modal pressure antinodes. Regarding the second conclusion, observe on Figure 5.10 that for each of the extreme values of damping on mode 100 the lining was located on the most reflective panels, relative to this mode, while the "line-sources" were, in each case, adjacent to these panels along the front-floor and rear-panel of the model (see Figure A3.4).

5.4 A Proposition

Recall from Sections 5.1 and 5.2 that all progressions of damping factor and frequency shift for both the perfectly-rectangular and complex-shaped enclosures are suitably described by means of linear regressions. Nevertheless, distribution of data points about the various regression lines provides sufficient evidence to propose the following:

> Though nominally linear increases, the true variations of damping factor and frequency shift with increase of area coverage appear to be sinusoidal. Amplitude of the sinusoidal variation decreases as the number of nodes per modal group increases while its period decreases as enclosure shape becomes more complex.

Evidence of this trend can be found for both models in most plots of averaged data. For the car-model this is best seen in Figure 5.13a where frequency shift (averaged) is plotted for the axial modes. Using Table A4.5, it is apparent that the low values of axial shift at C36 and C64 are due to a local minimum occurring on a single group-member (mode 001 in both cases) and if revised average data are derived excluding the low values (resulting in shifts of 3.9% and 7.5%, respectively) these values are both closer to the regression line and more consistent with the proposed variation. Similar treatment of the high values of axial shift (occurring at C13, C61 and C70) results in revised data (1.6%, 6.0% and 7.8%, respectively) which also are closer to the regression line and consistent with the sinusoidal variation. The revised data and the associated sinusoidal variation are shown in Figure 5.14. By thus recognizing where extrema occur on individual modes, data of most group-averages (including non-fundamental and overall averages) of damping factor and frequency shift will be seen to conform with the proposed variation. (The sinusoidal variation is not directly applicable to car-model oblique data due to excessive scatter.) Considering now the truck-cab model, data of Figure 5.2 (overall damping), Figure 5.3a and 5.3b (axial and tangential damping factor) and Figure 5.7a (axial frequency shift) display the sinusoidal behaviour about their regression lines. Note that all averaged data of damping factor (overall, axial and

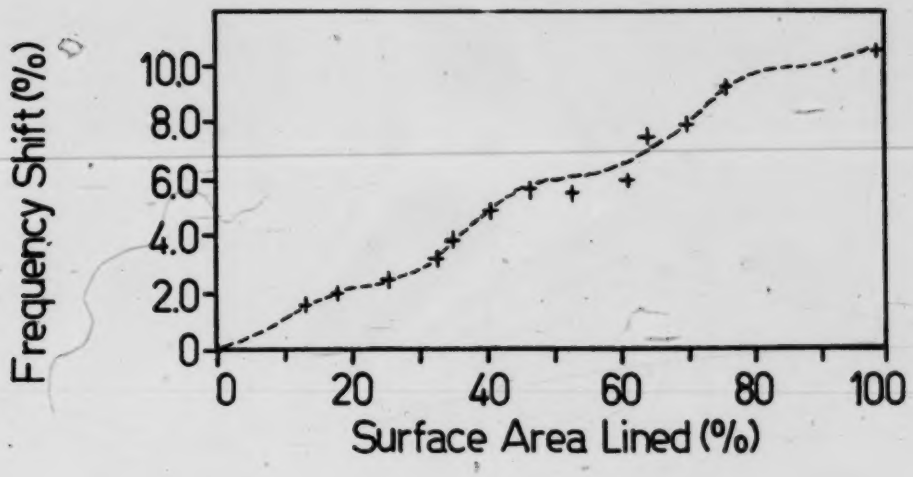

Figure 5.14 Revised Axial Frequency Shift (Car-Model).

tangential) display crossings of their regression lines at approximately T32 and T68. Frequency shift data of the truck-cab model display crossings of the regression in the same locations though phase of the frequency shift data is opposite that of damping data (where the damping variation is convex upwards, the variation of frequency shift is concave). Since the axial shift variation is concave to approximately T30, it is likely that prior to T15 concavity of the true variation is maintained such that the true intercept of the curve is in fact zero (not negative as suggested by the linear regression). In comparing the two models in terms of the respective variations of axial shift (Figure 5.7a and Figure 5.14) it is apparent that while the truck-cab model displays at least two crossings of the linear regression the car-model data display at least four. Hence the suggested decrease of period as enclosure shape becomes more complex. Finally, recalling from Table 5.2 that scatter of axial (group) data in all cases exceeds that of tangential data, it appears that amplitude of the sinusoidal variation decreases as the number of nodes per modal group increases. (Decreased amplitude is thus, in effect, a direct consequence of the reduced sensitivity of the more complex modes to the influences of lining location.)

Eventual use of numerical modelling to simulate the progressions of damping factor and frequency shift should allow the proposed variation to be affirmed or refuted. Although lining location and source-network layout must

necessarily remain of influence (causing local extrema on individual modal progressions) the "eccentricities" of excitation and measurement (in the form of investigator error, unaccounted-for influences such as panel flexibility and surface finish, etc.) will be bypassed. Thus the average progressions generated will be the theoretical mean progressions.

6. CONCLUSION

The purpose of the present study has been to consider dissipation of the resonant acoustic energy of small-room enclosures as dependent on variation of an absorbent lining. By varying the configuration (and thereby extent) of a constant-thickness lining and observing the effect on individual resonances, as well as groups of modes, progressions of damping factor and frequency shift were derived. An array of discrete, identical sources permitted excitation of individual fundamental modes. Problems encountered in exciting resonances acceptably were overcome through trial-and-error experimentation. In what follows, the major findings of the analytical study are summarized and matters warranting further investigation are cited.

Damping factor decreases linearly with increasing frequency in both unlined models (damping at 400 Hz is approximately one-quarter that at 100 Hz (nominal value: 0.012)). Damping factor decreases more rapidly in the truck-cab model (reflected in a 7% higher value of regression slope) due to its smaller ratio of surface area-to-volume. Also, scatter of damping data is greater in the truck-cab model due to uneven surface finish and non-uniform wall material. Regression lines of unlined damping data predict a common zero-frequency damping factor (value: 0.02) for both models. The trend of decreasing damping factor with increasing frequency is reversed if the lining

is applied to more than one-third of the internal surface area. (The calculated "crossover" coverage of 42% in the car-model is recognized to be high due to high values of damping on a single axial mode; the figure of one-third, as rule-of-thumb, is thus applicable to both models.)

Damping factor, as dependent on increasing area coverage, displays linear increase in all of the various modal averages considered. Damping data averaged over all fundamental modes display low scatter (6%) about their regression estimate. The overall regression line, for each lining configuration tested, passes through the measured range of damping data (one exception being noted). Axial-group data are most susceptible to the influences of lining location and therefore display greater scatter of data. Regression slope of the tangential-group data exceeds that of axial data by approximately 25%. Oblique mode data, representing only one mode, display large scatter (15% to 30% of measured range) and for one model (truck-cab) a value of regression slope exceeding that of the tangential regression by 30%. Modal-group data of the lowest five non-fundamental modes (car-model only), where no distinction has been made as to mode type, display the largest value of regression slope and a moderate amount of data scatter (10%). Regression intercepts, as estimates of mean unlined damping factor, correspond well with those measured. As the difference between tangential and axial regression slope

decreases (oblique slope assumed to exceed tangential slope) the tangential slope provides a reasonable estimate of the slope of the overall regression estimate of damping factor.

The method of data-reduction used involves derivation of both overall and modal-group (axial, tangential and non-fundamental) average values of damping factor and frequency shift. This approach, by minimizing the influences of both lining location and measurement irregularities, provides very low values of data scatter of overall averages (6%). Although progressions of the individual modes within a group differ only slightly from one another, averaged progressions between different modal groups differ significantly (as seen in comparing regression slope-values in Table 5.2).

Resonant frequency is seen to decrease as the amount of lined area increases. Expressed as a percentage of the unlined resonant frequency, frequency shift increases linearly with lined area. Averaged data of frequency shift display trends very similar to those of damping factor: reduction of scatter about a regression line as the number of modal data per averaged datum increases and increase of regression slope as modal complexity increases. For both models, regression slope of the overall average of shift is closely approximated by the tangential regression slope (the latter exceeding the former by 7% for both models). Group-average regression estimates (including overall) of

frequency shift in the truck-cab model predict negative intercepts (positive shift). Positive shift (increase of resonant frequency) was encountered on only the axial modes of the truck-cab model. (Although the car-model axial regression also displays a negative intercept, no increase of frequency was obse.ved.) Axial modes are, also in terms of frequency shift, the mode type most susceptible to lining location. Oblique shift data of the truck-cab model display low scatter (7%) and a regression-estimated slope which exceeds that of the car-model by 13%.

As to the influence of lining location, it is apparent that maximum dissipation of acoustic energy (as seen in local maxima of damping factor and frequency shift) is realized by placing lining on panels adjacent to modal pressure antinodes. Such placement of the lining dissipates energy in the regions where energy density is highest; the energy content of the reverberant field is reduced and the resonant amplitude (alt. overall noise level) decreases. Axial modes in the perfectly-rectangular enclosure display maxima of damping and shift when lined parallel to the modal standing wave and in the irregularly-shaped enclosure when lined along the mode's antinodal regions. Tangential modes tend to display maxima of damping and shift if the enclosure, regardless of shape, is lined as a duct parallel to the intersection of the modal node planes. (Axial modes in a perfectly-rectangular enclosure tend to

undergo positive shift when lined normal to the modal standing wave.)

The extent of influence of lining location can be aggravated (or inhibited) depending on the layout of the source network. Although source location must sometimes be compromised to achieve acceptable excitation of a resonant mode, careful study of data generated will disclose local extrema of the dependent quantities. The method of multiple-source excitation provides great flexibility in generating acceptable data and is thus a most effective means of isolating resonances.

Enclosure characteristics (volume, shape and wall material) can also be identified as to their influence on resonant acoustic response. The larger enclosure volume of the truck-cab model results in a more rapid decrease of damping factor (with resonant frequency) in the unlined model. Also, regression slope of all but oblique frequency shift (Table 5.2) being greater for the car-model, is in part attributed to its smaller reverberant volume (as enclosure volume decreases the ratio of surface area-to-volume increases and reverberant acoustic energy is more readily dissipated). An additional cause of greater slope of car-model regressions is the model's irregular shape: reflection of acoustic energy is more diffuse in the car-model, making its reverberant field more uniform and the

dissipation of acoustically-transmitted energy more efficient. Differences of enclosure wall material and surface finish lead to the reduced scatter of data about the regression of damping factor versus frequency in the unlined car-model. The high flexibility of the car-model enclosure is likely to have been a major contributor to the consistency of "peak-splitting" encountered in this model.

Although considerable information has been generated about damped resonant response in small-room enclosures, several matters warrant further investigation. First (and most basic) concerns measurement repeatibility. Comparing, for the truck-cab model's oblique mode, the excessive scatter of damping data (30% of range) to the low value of shift scatter (7%), more insight is necessary as to the factors which determine damping factor as well as the extent of their influence. (Note that greater scatter of damping data was also observed for all car-model modal groups; Table 5.2). Second, in attempting to account more rigorously for extrema of modal damping and shift, consideration must be given to, among others:

- microphone location -- whether resonant damping is different when measured near or away from the lining;
- panel flexibility -- the relative influence of walls with and without seams on modes (standing waves) of differing orientation; and
- the relative positioning of the source network and

the lining.

Finally, in addition to the numerical modelling to affirm or refute the posited sinusoidal variation, testing of a different thickness of lining could be undertaken. The influence of lining thickness on amplitude and period could then be determined.

In conclusion, it is evident that the information generated by this study is directly applicable to the problem of acoustic resonance in vehicle passenger compartments. Having recognized that placement of the lining in the antinodal regions of the resonant modes leads to maximum dissipation of acoustic energy (thereby preventing its reflection/radiation about the enclosure), designs of new vehicles can allow adequate space in appropriate locations for absorbent material. Similarly, in existing vehicles with noise problems, lining can be more strategically located.

BIBLIOGRAPHY

Aspinall, D.T. (1972) "The Reduction of Airborne Engine-Noise by Palliative Treatments (Second Report)", Motor Industry Research Association, Report No. 1972/1.

Bristow, J.R. (1952) "Noise in Private Cars", Proceedings of the Institution of Mechanical Engineers: Automotive Division, London, pp. 9-22.

Craggs, A. (1971) "The Transient Response of a Coupled Plate-Acoustic System Using Plate and Acoustic Finite Elements", Journal of Sound and Vibration, 15, pp. 509-528.

Craggs, A. (1972) "The Use of Simple Three-Dimensional Acoustic Finite Elements for Determining the Natural Modes and Frequencies of Complex-Shaped Enclosures", Journal of Sound and Vibration, 23(3), pp. 331-339.

Craggs, A. (1973) "An Acoustic Finite Element Approach for Studying Boundary Flexibility and Sound Transmission Between Irregular Enclosures", Journal of Sound and Vibration, 30(3), pp. 343-357.

Craggs, A. (1982) "A Note on the Theory and Application of a Simple Pipe Acoustic Element", Journal of Sound and Vibration, 85(2), pp. 292-295.

Craggs, A. (1984) "Absorption Finite Elements in Acoustics", Paper No. 8 in "Application, Reliability and Training in Finite Element Method Technology", Proceedings of the Fourth World Congress on Finite Element Methods (J. Robinson, ed.), Publ.: Robinson and Associates, Dorset,

England.

Delany, M.E. and Bazley, E.N. (1970) "Acoustical Properties of Fibrous Absorbent Materials", Applied Acoustics (3), pp. 105-116.

Gladwell, G.M.L. (1964) "A Review of Noise and Vibration in Motor Cars", Journal of Sound and Vibration, 1(2), pp. 202-210.

Howell, L.J. (1980) "An Overview of Structures and Acoustics Technology in Automotive Applications", SAE Transactions, Paper 800611, pp. 2143-2159.

Jennequin, G. (1971) "Is the Computation of Noise Level Inside a Car Feasible?", I. Mech. E. publication, Vibration and Noise in Motor Vehicles, Paper C108/71, pp. 132-137.

Jha, S.K. and Priede, T. (1972) "Origin of Low Frequency Noise in Motor Cars", Proceedings of the 14th FISITA Conference, London, England, pp.1/48-1/55.

Kuttruff, H. (1973) Room Acoustics, Applied Science Publishers Ltd., London, England.

Le Salver, R. and Jennequin, G. (1972) "Méthode de Calcul Pour les Bruits Basse Fréquence dans un Habitacle de Voiture", Proceedings of the 14th FISITA Conference, London, England, pp. 89-100.

Morse, P.M. (1981) Vibration and Sound, Published by the American Institute of Physics for the Acoustical Society of America.

Nakamura, H., Sato, S. and Sakagami, J. (1961) "On Cavity Resonance of a Car Room and its Abatement", SAE preprint 1961 (Abstract in SAE Journal, May 1961, page 104).

Nefske, D.J. and Howell, L.J. (1978) "Automobile Interior Noise Reduction Using Finite Element Methods", SAE Transactions, Paper 780365, pp. 1727-1737.

Nefske, D.J. and Sung, S.H. (1985) "Structural-Acoustic System Analysis Using the Modal Synthesis Technique", Proceedings of the International Modal Analysis Conference, Orlando, Florida, pp. 864-868.

Petyt, M., Lea, J. and Koopman, G.H. (1975) "A Finite Element Method for Determining the Acoustic Modes of Irregularly Shaped Cavities", Journal of Sound and Vibration, 45(4), pp. 495-502.

Raff, J.A. and Perry, R.D.H. (1973) "A Review of Vehicle Noise Studies Carried out at the Institute of Sound and Vibration Research with a reference to some recent research on petrol engine noise", Journal of Sound and Vibration, 28(3), pp. 433-470.

Shuku, T., Yoshida, A., Nagai, M. and Watari, A. (1972) "Reduction of Interior Car Noise by Control of Cavity Resonance", Proceedings of the 14th FISITA Conference, London, England, Paper 1/9, pp. 1/56-1/62.

Smith, D.L. (1976) "Experimental Techniques for Acoustic Modal Analysis of Cavities", Proceedings of the Internoise '76 Conference, Washington, D.C., pp. 129-132.

Stead,G. (1973) A Finite Element Approach to Sound Transmission Between Rooms, M.Sc. Thesis, University of Alberta, Dept. of Mech. Engineering.

West, J. (1966) "The Reduction of Airborne Engine-noise by Palliative Treatments (First Report)", Motor Industry Research Association, Report 1966/7.

Zwikker,C. and Kosten,C.W. (1949) Sound Absorbing Materials, Elsevier Publishing Company,Inc., New York.

APPENDIX A1 -- ESTIMATION OF CAVITY RESONANCES OF TRUCK-CAB MODEL

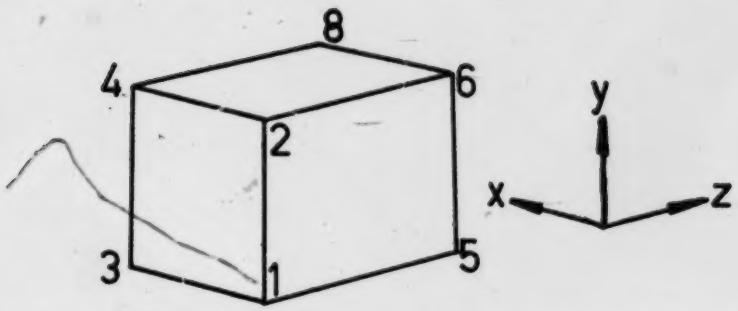

Using the above 8-node element, the program of the following pages chain-assembles 60 such elements to form a global matrix of the entire model. Nodal coordinates are read in for only one element (line 109, data lines 154 to 161) since all elements are identical for the perfectly-rectangular enclosure. The node numbers of each element are read in (line 110, data lines 162 to 175) after which the element [S] and [P] matrices (recall Eq. 2.6) are generated (line 123) and assembled (lines 124 and 125) to form the global matrices. Subroutine NROOT then provides the eigensolution of resonant frequencies (and mode shapes).

The following table compares the modal measured frequencies to those estimated (a) with the numerical simulation and (b) with the rectangular-enclosure formula (Eq. 2.5).

Mode	Measured (Hz)	Simulated	"Exact"
100	120.9	114.3	113.4
010	127.1	123.9	121.4
001	148.5	146.9	141.9
110	175.1	168.6	166.1
101	187.7	186.1	181.6
011	193.3	192.2	186.8
111	226.6	223.6	218.5

```
C          (NPROG=ABSENC)
C  THIS PROG CALCULATES THE RESPONSE FOR A PARTICULAR
C  ENCLOSURE BY ASSEMBLING 80 - 8 NODE ELEMENTS
C  TO USE MORE THAN 80 ELEMENTS, SET NELMND  OF ELEMENTS
C  RESET IDX AND M ACCORDINGLY.
      REAL SD(120,120),PD(120,120),IGVC(120,120)
      DIMENSION X1(8),Y1(8),Z1(8),XEE(80,8)
      REAL EP(8,8),ES(8,8)
      DIMENSION FREQ(8),EVC(8),W2(8)
      REAL W(120)
      READ(5,4)NELP,NELL,IDX,LEIG
      READ(5,3) (X1(K),Y1(K),Z1(K),K=1,8)
      READ(5,4) ((NGE(J,JJ),JJ=1,8),J=1,NELP)
      PI=3.141592654
      CS=343.0
        DO 22 J=1,IDX
        DO 22 I=1,IDX
      SD(I,J)=0.0
   22 PD(I,J)=0.0
        IE=8
        N=3
        NCORN=8
        NUN=1
        IEX=8
      DO 26 K=1,NELP
      CALL HXSG(X1,Y1,Z1,ES,EP,N)
   30 CALL ACAS(SD,ES,NCORN,NUN,IEX,IDX,NGE,K,NELP)
      CALL ACAS(PD,EP,NCORN,NUN,IEX,IDX,NGE,K,NELP)
   26 CONTINUE
      CALL NROOT(IDX,SD,PD,W,IGVC)
      DO 28 I=1,LEIG,8
        IA = I+8
        DO 27 II=1,IA
          I2=II-I+1
          IW=IDX-II
          W2(I2)=W(IW)
   27 FREQ(I2) = CS*SQRT(ABS(W2(I2)))/(2.0*PI)
      WRITE(6,6)((W2(L),L=1,8),(FREQ(K),K=1,8))
      DO 28 J=1,IDX
        DO 28 IB=I,IA
          IND=IDX-IB
          ID=IB-I+1
   28     EVC(ID)=IGVC(J,IND)
   28 WRITE(6,8)J,(EVC(K),K=1,8)
    1 FORMAT(4E10.5)
    2 FORMAT('RS=',E15.5,'THICK=',E15.5,'POR=',E15.5,'DAMP',E15.5)
    3 FORMAT(3F5.3)
    4 FORMAT(8I4)
    6 FORMAT('0'/T3,'EIGENVALUES-FREQUENCY(HZ)'/'0',T5,8(E13.4)/
     1   T11,6(F8.1,7X)/'0',T3,'EIGENVECTORS'/'0')
    8 FORMAT(I4,8(E13.4))
        STOP
        END
C  DATA FOR 80 ELEMENT MODEL
     2.3E+1     2.0E0      1.0E0      5.0-3
  80  12  120  18
 0.000 0.000 0.000
 0.000 0.355 0.000
 0.305 0.000 0.000
 0.305 0.355 0.000
 0.000 0.000 0.407
 0.000 0.355 0.407
 0.305 0.000 0.407
 0.305 0.355 0.407
   1   2  21  22   6   7  26  27
   2   3  22  23   7   8  27  28
   3   4  23  24   8   9  28  29
   4   5  24  25   9  10  29  30
   6   7  26  27  11  12  31  32
   7   8  27  28  12  13  32  33
C.........
C.......... ETC ..........
C.........
  88  80 109 110  84  85 114 115
  91  82 111 112  86  87 116 117
  92  83 112 113  87  88 117 118
  93  84 113 114  88  89 118 119
  94  85 114 115  89 100 119 120
C ***************************************************************
C *
C *         SUBROUTINE HXSG(X,Y,Z,ES,EP,N)
C *
C *   FORMS S AND P MATRICES FOR 8 NODE 3D ISOPARAMETRIC
C *   ACOUSTIC ELEMENT
C *
C ***************************************************************
C *
C *   INPUT
C *
C *   X,Y,Z.....ARRAYS CONTAINING THE ASSOCIATED CARTESIAN
C *             CO-ORDINATES OF THE NODES OF THE ELEMENT IN
C *             CORRECT SPIRAL ORDER.
C *
C *   N.........INTEGRATION CODE INTEGER
C *             -IF USED WITH SUBROUTINE TRINT N IS THE NUMBER
C *              OF POINTS USED IN NUMERICALLY INTEGRATING OVER
C *              THE ELEMENT
C *             -IF USED WITH SUBROUTINE GAUSSO, N=+D IS THE
C *              NUMBER OF POINTS USED IN NUMERICALLY
C *              INTEGRATING OVER THE ELEMENT, WHERE D IS 2
C *              OR 3 DEPENDING ON WHETHER THE ELEMENT IS A
C *              TWO OR THREE DIMENSIONAL ELEMENT
C *
C ***************************************************************
C *
C *   OUTPUT
C *
C *   EP........ELEMENT P MATRIX
C *
C *   ES........ELEMENT S MATRIX
C *
C *   *NOTE*:THE ABOVE ARE RELATED TO ACOUSTICS VIA THE
C *          MATRIX EQUATION
C *
C *                  [S](A)-B[P](A)=(0)
C *
C *          WHERE  (A)...IS A COLUMN VECTOR OF NODAL
C *                       ACOUSTIC PRESSURES
C *                 (0)...IS A NULL COLUMN VECTOR
C *                  B....IS EQUAL TO THE NATURAL FREQUENCY
```

```
C *                          IN RADIANS/SEC DIVIDED BY THE SPEED
C *                          OF SOUND, ALL SQUARED  (W/C)**2
C *
C*************************************************************
C *
C *    VARIABLES
C *
C *    D.........DIMENSION IDENTIFIER TO DISTINGUISH BETWEEN
C *              2 AND 3 DIMENSIONAL ELEMENTS IN THE ELEMENT
C *              SUBROUTINES
C *
C *    ENN.......ONE-DIMENSIONAL ARRAY CONTAINING THE
C *              INTERPOLATION FUNCTIONS FOR A SINGLE POINT
C *              OF INTEGRATION
C *
C *    ENXEZ.....TWO-DIMENSIONAL ARRAY CONTAINING THE NATURAL
C *              CO-ORDINATE DERIVATIVES OF THE INTERPOLATION
C *              FUNCTIONS (FIRST ROW IS W.R.T. XI, SECOND ROW
C *              IS W.R.T. ETA, THIRD ROW IS W.R.T. ZETA) FOR
C *              A SINGLE INTEGRATION POINT
C *
C *    EXYZ......TWO-DIMENSIONAL ARRAY CONTAINING PRODUCT OF
C *              [JIN] POST-MULTIPLIED BY [ENXEZ]
C *
C *    F.........ARRAY OF CO-ORDINATES FOR NUMERICAL INTEGRATION
C *
C *    FF........TWO-DIMENSIONAL ARRAY CONTAINING THE RESULTS OF
C *              [ENN]T*[ENN], WHERE THE "T" SIGNIFIES THE
C *              TRANSPOSE OF THE MATRIX
C *
C *    FS........TWO-DIMENSIONAL ARRAY CONTAINING THE RESULTS OF
C *              [ENXEZ]T*[JIN]T*[JIN]*[ENXEZ], WHERE THE "T"
C *              SIGNIFIES THE TRANSPOSE OF THE MATRIX
C *
C *    JAC.......TWO-DIMENSIONAL ARRAY CONTAINING ELEMENTS OF
C *              THE JACOBIAN MATRIX FOR TRANSFORMING BETWEEN
C *              CARTESIAN AND NATURAL CO-ORDINATES (WHERE THE
C *              NUMERICAL INTEGRATION IS PERFORMED IN THE
C *              NATURAL CO-ORDINATE SYSTEM)
C *
C *    JIN.......INVERSE OF THE JACOBIAN MATRIX
C *
C *    W.........ARRAY OF WEIGHTING VALUES FOR NUMERICAL
C *              INTEGRATION
C *
C *    XI,ETA,...ASSIGNED NATURAL CO-ORDINATES OF THE ELEMENT
C *    ZETA      NODES
C *
C*************************************************************
C *
C *    SUBROUTINES
C *
C *    DIDET.....FORMS INVERSE OF 2 OR 3 DIMENSIONAL JACOBIAN
C *              MATRIX [JIN] AND CALCULATES THE DETERMINANT
C *              OF THE JACOBIAN MATRIX "DETJ"
C *
C *    FJACT.....FORMS 2 OR 3 DIMENSIONAL JACOBIAN MATRIX [JAC]
C *
C *    FSFFT.....PERFORMS FOLLOWING MATRIX OPERATIONS:
C *                   [FS]=[EXYZ]T*[EXYZ]
C *                   [FF]=[ENN]T*[ENN]
C *              WHERE "T" SIGNIFIES THE TRANSPOSE OF THE MATRIX
C *
C *    GAUSSO....LOADS CO-ORDINATES AND WEIGHTING VALUES FOR
C *              GAUSS QUADRATURE INTEGRATION SCHEME
C *
C *    TRINT.....LOADS CO-ORDINATES AND WEIGHTING VALUES FOR
C *              AREA CO-ORDINATE INTEGRATION SCHEME FOR
C *              TRIANGULAR ELEMENTS
C *
C *    VEXYZT....PERFORMS FOLLOWING MATRIX OPERATION:
C *                   [EXYZ]=[JIN]*[ENXEZ]
C *
C*************************************************************
C
      SUBROUTINE HXSS(X,V,Z,ES,EP,N)
C
      REAL X(8),V(8),Z(8),ES(8,8),EP(8,8),DETJ,FF(8,8)
      REAL FS(8,8),EXYZ(3,8),ENXEZ(3,8),ENN(1,8),F(4),W(4)
      REAL XI(8),ETA(8),ZETA(8),JAC(3,3),JIN(3,3)
      INTEGER D
C
C
      DATA XI/2*-1.,2*1.,2*-1.,2*1./,ETA/-1.,1.,-1.,1.,-1.,1.,
     1    -1.,1./,ZETA/4*-1.,4*1./
C
      DO 10 I=1,8
      DO 10 J=1,8
      ES(I,J)=0.0
   10 EP(I,J)=0.0
C
C LOAD GAUSS QUADRATURE VALUES
C
      CALL GAUSSO(F,W,N)
C
C FORM S AND F MATRICES USING AN N**3 POINT
C INTEGRATION SCHEME
C
      D=3
      NU=8
      DO 20 II=1,N
      DO 20 JI=1,N
      DO 20 KI=1,N
      XE=F(II)
      YE=F(JI)
      ZE=F(KI)
C
C FORM SERENDIPITY INTERPOLATION FUNCTIONS
C
      DO 12 I=1,8
      A=XE*X(I)+1.0
      B=YE*ETA(I)+1.0
      C=ZE*ZETA(I)+1.0
      ENN(1,I)=A*B*C/8.0
      ENXEZ(1,I)=X(I)*B*C/8.0
      ENXEZ(2,I)=ETA(I)*A*C/8.0
   12 ENXEZ(3,I)=ZETA(I)*A*B/8.0
C
      CALL FJACT(ENXEZ,X,Y,Z,JAC,D,NU)
      CALL DIDET(JAC,JIN,DETJ,D)
```

```
      CALL VEXY2Y(ENXE2,JIN,EXY2,D,NU)
      CALL FSFPT(EXY2,ENN,FS,FP,D,NU)
C
      DO 15 I=1,6
      DO 15 J=1,6
      ES(I,J)=ES(I,J)+FS(I,J)*W(II)*W(JJ)*W(KK)*DETJ
   15 EP(I,J)=EP(I,J)+FP(I,J)*W(II)*W(JJ)*W(KK)*DETJ
   20 CONTINUE
      RETURN
      END
C*********************************************************************
C
      SUBROUTINE GAUSSO(F,W,N)
C
C LOADS GAUSS QUADRATURE ABSCISSAE AND WEIGHTING FUNCTION VALUES
C
C*********************************************************************
C
      REAL F(6),W(6)
      INTEGER N
C
C N IS THE DEGREE OF QUADRATURE TO BE USED
C
      GO TO(10,20,30,40),N
   10 CONTINUE
      WRITE(6,15)
   15 FORMAT(' ***************************************************'/
     &       ' N MUST BE 2, 3, OR 4 IN SUBROUTINE GAUSSO'/
     &       ' ***************************************************')
      RETURN
C
   20 F(2)=.5773503
      F(1)=-F(2)
      W(1)=1.0
      W(2)=1.0
      RETURN
C
   30 R=1.0/9.0
      V=.7745967
      F(1)=-V
      F(2)=0.0
      F(3)=V
      W(1)=5.0*R
      W(2)=8.0*R
      W(3)=5.0*R
      RETURN
C
   40 V1=.8611363
      V2=.3399810
      W1=.3478548
      W2=.6521452
      F(1)=-V1
      F(2)=-V2
      F(3)=V2
      F(4)=V1
      W(1)=W1
      W(2)=W2
      W(3)=W2
      W(4)=W1
      RETURN
      END
C*********************************************************************
C
      SUBROUTINE FJACT(ENXE2,X,Y,Z,JAC,D,NU)
C
C FORMS JACOBIAN MATRIX FOR D-DIMENSIONAL ELEMENT WITH
C NU NODES
C
C*********************************************************************
C
      INTEGER D
      REAL ENXE2(D,NU),X(NU),Y(NU),Z(NU),JAC(D,D)
C
      DO 5 I=1,D
      DO 5 J=1,D
    5 JAC(I,J)=0.0
C
      DO 10 I=1,NU
      DO 10 J=1,D
      JAC(J,1)=JAC(J,1)+ENXE2(J,I)*X(I)
      JAC(J,2)=JAC(J,2)+ENXE2(J,I)*Y(I)
      IF(D.EQ.2)GO TO 10
      JAC(J,D)=JAC(J,D)+ENXE2(J,I)*Z(I)
   10 CONTINUE
      RETURN
      END
C*********************************************************************
C
      SUBROUTINE DIDET(A,AI,DET,D)
C
C FORMS THE INVERSE AND EVALUATES THE DETERMINANT OF
C A DXD MATRIX (D MUST BE EITHER 2 OR 3)
C
C*********************************************************************
C
      INTEGER D
      REAL A(D,D),AI(D,D),DET
C
      IF(D.EQ.3)GO TO 100
      IF(D.EQ.2)GO TO 200
      WRITE(6,10)
   10 FORMAT(' ***********************************************'/
     &       '  D MUST BE 2 OR 3 IN SUBROUTINE DIDET'/
     &       ' ***********************************************')
      RETURN
C
  100 CONTINUE
      DET=A(1,1)*(A(2,2)*A(3,3)-A(3,2)*A(2,3))-
     &    A(1,2)*(A(2,1)*A(3,3)-A(3,1)*A(2,3))+
     &    A(1,3)*(A(2,1)*A(3,2)-A(3,1)*A(2,2))
C
      AI(1,1)=(A(2,2)*A(3,3)-A(3,2)*A(2,3))/DET
      AI(1,2)=-(A(1,2)*A(3,3)-A(3,2)*A(1,3))/DET
      AI(1,3)=(A(1,2)*A(2,3)-A(2,3)*A(1,3))/DET
      AI(2,1)=-(A(2,1)*A(3,3)-A(3,1)*A(2,3))/DET
      AI(2,2)=(A(1,1)*A(3,3)-A(3,1)*A(1,3))/DET
      AI(2,3)=-(A(1,1)*A(2,3)-A(2,1)*A(1,3))/DET
      AI(3,1)=(A(2,1)*A(3,2)-A(3,1)*A(2,2))/DET
      AI(3,2)=-(A(1,1)*A(3,2)-A(3,1)*A(1,2))/DET
      AI(3,3)=(A(1,1)*A(2,2)-A(2,1)*A(1,2))/DET
```

```
      RETURN
C
  200 CONTINUE
      DET=A(1,1)*A(2,2)-A(1,2)*A(2,1)
      AI(1,1)=A(2,2)/DET
      AI(1,2)=-A(1,2)/DET
      AI(2,1)=-A(2,1)/DET
      AI(2,2)=A(1,1)/DET
      RETURN
      END
C*************************************************************
C
      SUBROUTINE VEXYZT(ENXEZ,JIN,EXYZ,D,NU)
C
C FORMS INTERMEDIATE MATRIX FOR DEVELOPMENT OF
C D-DIMENSIONAL EE MATRIX
C
C*************************************************************
C
      INTEGER D
      REAL ENXEZ(D,NU),EXYZ(D,NU),JIN(D,D)
C
      DO 10 I=1,D
      DO 10 J=1,NU
      EXYZ(I,J)=0.0
      DO 10 K=1,D
   10 EXYZ(I,J)=EXYZ(I,J)+JIN(I,K)*ENXEZ(K,J)
      RETURN
      END
C*************************************************************
C
      SUBROUTINE FSFPT(EXYZ,ENN,FS,FP,D,NU)
C
C FORMS THE KERNEL MATRICES FS AND FP FOR D-DIMENSIONAL
C ACOUSTIC ELEMENT WITH NU NODES
C
C*************************************************************
C
      INTEGER D
      REAL EXYZ(D,NU),ENN(1,NU),FS(NU,NU),FP(NU,NU)
C
      DO 10 I=1,NU
      DO 10 J=1,NU
      FS(I,J)=0.0
   10 FP(I,J)=ENN(1,J)*ENN(1,I)
C
      DO 20 I=1,NU
      DO 20 J=1,NU
      DO 20 K=1,D
   20 FS(I,J)=FS(I,J)+EXYZ(K,I)*EXYZ(K,J)
      RETURN
      END
      SUBROUTINE ACAS(A,AE,NCORN,NUN,IEX,IOX,NSE,K,NEL)
      REAL A(IOX,IOX),AE(IEX,IEX)
      INTEGER NSE(NEL,NCORN)
C        ASSEMBLES ELEMENT INTO GLOBAL MATRIX
C        NCORN = # CORNERS,  NUN = # UNKNOWNS PER CORNER
      DO 10 NR = 1,NCORN
      DO 10 NC = 1,NCORN
      DO 10  J = 1,NUN
      DO 10  I = 1,NUN
      A(I+NUN*(NSE(K,NR)-1),J+NUN*(NSE(K,NC)-1)) =
     1 A(I+NUN*(NSE(K,NR)-1),J+NUN*(NSE(K,NC)-1)) +
     2 AE(I+NUN*(NR-1),J+NUN*(NC-1))
   10 CONTINUE
      RETURN
      END
      SUBROUTINE EIGEN(A,R,N,MV)
      DIMENSION A(1),R(1)
C
C        ..................................................................
C
C        IF A DOUBLE PRECISION VERSION OF THIS ROUTINE IS DESIRED, THE
C        C IN COLUMN 1 SHOULD BE REMOVED FROM THE DOUBLE PRECISION
C        STATEMENT WHICH FOLLOWS.
C
C     DOUBLE PRECISION A,R,ANORM,ANRMX,THR,X,Y,SINX,SINX2,COSX,
C    1                 COSX2,SINCS,RANGE
C
C        THE C MUST ALSO BE REMOVED FROM DOUBLE PRECISION STATEMENTS
C        APPEARING IN OTHER ROUTINES USED IN CONJUNCTION WITH THIS
C        ROUTINE.
C
C        THE DOUBLE PRECISION VERSION OF THIS SUBROUTINE MUST ALSO
C        CONTAIN DOUBLE PRECISION FORTRAN FUNCTIONS.  SORT IN STATEMENTS
C        40, 68, 75, AND 78 MUST BE CHANGED TO DSORT.  ABS IN STATEMENT
C        62 MUST BE CHANGED TO DABS.  THE CONSTANT IN STATEMENT 5 SHOULD
C        BE CHANGED TO 1.0D-12.
C
C        ..................................................................
C
C        GENERATE IDENTITY MATRIX
C
    5 RANGE=1.0E-6
      IF(MV-1) 10,25,10
   10 IQ=-N
      DO 20 J=1,N
      IQ=IQ+N
      DO 20 I=1,N
      IJ=IQ+I
      R(IJ)=0.0
      IF(I-J) 20,15,20
   15 R(IJ)=1.0
   20 CONTINUE
C
C        COMPUTE INITIAL AND FINAL NORMS (ANORM AND ANRMX)
C
   25 ANORM=0.0
      DO 35 I=1,N
      DO 35 J=1,N
      IF(I-J) 30,35,30
   30 IA=I+(J*J-J)/2
      ANORM=ANORM+A(IA)*A(IA)
   35 CONTINUE
      IF(ANORM) 165,165,40
   40 ANORM=1.414*SQRT(ANORM)
      ANRMX=ANORM*RANGE/FLOAT(N)
C
C        INITIALIZE INDICATORS AND COMPUTE THRESHOLD, THR
C
```

```
      IND=0
      THR=ANORM
   45 THR=THR/FLOAT(N)
   50 L=1
   55 M=L+1
C
C        COMPUTE SIN AND COS
C
   60 MQ=(M*M-M)/2
      LQ=(L*L-L)/2
      LM=L+MQ
   62 IF( ABS(A(LM))-THR) 130,65,65
   65 IND=1
      LL=L+LQ
      MM=M+MQ
      X=0.5*(A(LL)-A(MM))
   68 Y=-A(LM)/ SQRT(A(LM)*A(LM)+X*X)
      IF(X) 70,75,75
   70 Y=-Y
   75 SINX=Y/ SQRT(2.0*(1.0+( SQRT(1.0-Y*Y))))
      SINX2=SINX*SINX
   78 COSX= SQRT(1.0-SINX2)
      COSX2=COSX*COSX
      SINCS =SINX*COSX
C
C        ROTATE L AND M COLUMNS
C
      ILQ=N*(L-1)
      IMQ=N*(M-1)
      DO 125 I=1,N
      IQ=(I*I-I)/2
      IF(I-L) 80,115,80
   80 IF(I-M) 85,115,90
   85 IM=I+MQ
      GO TO 95
   90 IM=M+IQ
   95 IF(I-L) 100,105,105
  100 IL=I+LQ
      GO TO 110
  105 IL=L+IQ
  110 X=A(IL)*COSX-A(IM)*SINX
      A(IM)=A(IL)*SINX+A(IM)*COSX
      A(IL)=X
  115 IF(MV-1) 120,125,120
  120 ILR=ILQ+I
      IMR=IMQ+I
      X=R(ILR)*COSX-R(IMR)*SINX
      R(IMR)=R(ILR)*SINX+R(IMR)*COSX
      R(ILR)=X
  125 CONTINUE
      X=2.0*A(LM)*SINCS
      Y=A(LL)*COSX2+A(MM)*SINX2-X
      X=A(LL)*SINX2+A(MM)*COSX2+X
      A(LM)=(A(LL)-A(MM))*SINCS+A(LM)*(COSX2-SINX2)
      A(LL)=Y
      A(MM)=X
C
C        TESTS FOR COMPLETION
C
C        TEST FOR M = LAST COLUMN
C
  130 IF(M-N) 135,140,135
  135 M=M+1
      GO TO 60
C
C        TEST FOR L = SECOND FROM LAST COLUMN
C
  140 IF(L-(N-1)) 145,150,145
  145 L=L+1
      GO TO 55
  150 IF(IND-1) 160,155,160
  155 IND=0
      GO TO 50
C
C        COMPARE THRESHOLD WITH FINAL NORM
C
  160 IF(THR-ANRMX) 165,165,45
C
C        SORT EIGENVALUES AND EIGENVECTORS
C
  165 IQ=-N
      DO 185 I=1,N
      IQ=IQ+N
      LL=I+(I*I-I)/2
      JQ=N*(I-2)
      DO 185 J=I,N
      JQ=JQ+N
      MM=J+(J*J-J)/2
      IF(A(LL)-A(MM)) 170,185,185
  170 X=A(LL)
      A(LL)=A(MM)
      A(MM)=X
      IF(MV-1) 175,185,175
  175 DO 180 K=1,N
      ILR=IQ+K
      IMR=JQ+K
      X=R(ILR)
      R(ILR)=R(IMR)
  180 R(IMR)=X
  185 CONTINUE
      RETURN
      END
C
C     ..................................................................
C
C        SUBROUTINE NRDOT
C
C        PURPOSE
C           COMPUTE EIGENVALUES AND EIGENVECTORS OF A REAL NONSYMMETRIC
C           MATRIX OF THE FORM B-INVERSE TIMES A.  THIS SUBROUTINE IS
C           NORMALLY CALLED BY SUBROUTINE CANOR IN PERFORMING A
C           CANONICAL CORRELATION ANALYSIS.
C
C        USAGE
C           CALL NRDOT (N,A,B,XL,X)
C
C        DESCRIPTION OF PARAMETERS
C           N  - ORDER OF SQUARE MATRICES A, B, AND X.
C           A  - INPUT MATRIX (N X N).
C           B  - INPUT MATRIX (N X N).
```

```
C            XL - OUTPUT VECTOR OF LENGTH M CONTAINING EIGENVALUES OF
C                 B-INVERSE TIMES A.
C            X  - OUTPUT MATRIX (M X M) CONTAINING EIGENVECTORS COLUMN-
C                 WISE.
C        SUBROUTINES AND FUNCTION SUBPROGRAMS REQUIRED
C           EIGEN
C
C        METHOD
C           REFER TO W. W. COOLEY AND P. R. LOHNES, 'MULTIVARIATE PRO-
C           CEDURES FOR THE BEHAVIORAL SCIENCES', JOHN WILEY AND SONS,
C           1962, CHAPTER 3.
C
C     ..................................................................
      SUBROUTINE NROOT(M,A,B,XL,X)
      DIMENSION A(1),B(1),XL(1),X(1)
C     ..................................................................
C
C        IF A DOUBLE PRECISION VERSION OF THIS ROUTINE IS DESIRED, THE
C        C IN COLUMN 1 SHOULD BE REMOVED FROM THE DOUBLE PRECISION
C        STATEMENT WHICH FOLLOWS.
C
C     DOUBLE PRECISION A,B,XL,X,SUMV
C
C        THE C MUST ALSO BE REMOVED FROM DOUBLE PRECISION STATEMENTS
C        APPEARING IN OTHER ROUTINES USED IN CONJUNCTION WITH THIS
C        ROUTINE.
C
C        THE DOUBLE PRECISION VERSION OF THIS SUBROUTINE MUST ALSO
C        CONTAIN DOUBLE PRECISION FORTRAN FUNCTIONS.  SORT IN STATEMENTS
C        110 AND 175 MUST BE CHANGED TO DSORT.  ABS IN STATEMENT 110
C        MUST BE CHANGED TO DABS.
C
C     COMPUTE EIGENVALUES AND EIGENVECTORS OF B
C
      K=1
      DO 100 J=2,M
      L=M*(J-1)
      DO 100 I=1,J
      L=L+1
      K=K+1
  100 B(K)=B(L)
C
C        THE MATRIX B IS A REAL SYMMETRIC MATRIX.
C
      MV=0
      CALL EIGEN (B,X,M,MV)
C
C     FORM RECIPROCALS OF SQUARE ROOT OF EIGENVALUES.  THE RESULTS
C     ARE PREMULTIPLIED BY THE ASSOCIATED EIGENVECTORS.
C
      L=0
      DO 110 J=1,M
      L=L+J
  110 XL(J)=1.0/ SQRT( ABS(B(L)))
      K=0
      DO 115 J=1,M
      DO 115 I=1,M
      K=K+1
  115 B(K)=X(K)*XL(J)
C
C     FORM (B**(-1/2))PRIME * A * (B**(-1/2))
C
      DO 120 I=1,M
      N2=0
      DO 120 J=1,M
      N1=M*(I-1)
      L=M*(J-1)+I
      X(L)=0.0
      DO 120 K=1,M
      N1=N1+1
      N2=N2+1
  120 X(L)=X(L)+B(N1)*A(N2)
      L=0
      DO 130 J=1,M
      DO 130 I=1,J
      N1=I-M
      N2=M*(J-1)
      L=L+1
      A(L)=0.0
      DO 130 K=1,M
      N1=N1+M
      N2=N2+1
  130 A(L)=A(L)+X(N1)*B(N2)
C
C     COMPUTE EIGENVALUES AND EIGENVECTORS OF A
C
      CALL EIGEN (A,X,M,MV)
      L=0
      DO 140 I=1,M
      L=L+I
  140 XL(I)=A(L)
C
C     COMPUTE THE NORMALIZED EIGENVECTORS
C
      DO 150 I=1,M
      N2=0
      DO 150 J=1,M
      N1=I-M
      L=M*(J-1)+I
      A(L)=0.0
      DO 150 K=1,M
      N1=N1+M
      N2=N2+1
  150 A(L)=A(L)+B(N1)*X(N2)
      L=0
      K=0
      DO 180 J=1,M
      SUMV=0.0
      DO 170 I=1,M
      L=L+1
  170 SUMV=SUMV+A(L)*A(L)
  175 SUMV= SQRT(SUMV)
      DO 180 I=1,M
      K=K+1
  180 X(K)=A(K)/SUMV
      RETURN
      END
End of file
```

APPENDIX A2 -- ESTIMATION OF FLOW RESISTIVITY OF POROUS MATERIALS

The flow resistivity of a sample acoustic absorbent lining is estimated by comparing analytically-simulated curves of acoustic absorption coefficient to the measured trace obtained with the aid of a standard impedance tube. The program uses the isothermal speed of sound (290 m/sec) and assumes a density of air of 1.21 kg/m^3. Sample thickness is read in as data and a value of resistivity assumed. The absorption coefficient trace is then calculated for stepwise increase of frequency and compared by overlaying on the measured trace (see Figure A2.1).

Specific acoustic impedance (Z_o) of the lining is first determined (lines 50 and 51; derivation of the real (Z_1) and imaginary (Z_2) parts of this quantity makes use of the theory of Delany and Bazley (1970)). The impedance of the lining relative to the diffuse sound field is next determined (real and imaginary components, respectively, in lines 60 and 61) using (Zwikker (1949), Eq. 1.05):

$$Z = Z_o \coth \gamma l \qquad \text{(A2.1)}$$

(the real and imaginary components of $\coth \gamma l$ are approximated (Zwikker (1949), Eq. 1.15) by means of P1 and P2, respectively). Estimation of the complex components of the propagation coefficient γ (G1 and G2) also employs the theory of Delany-Bazley. Finally, absorption coefficient is determined (line 62; reference: Kuttruff (1973), Eq. II.8).

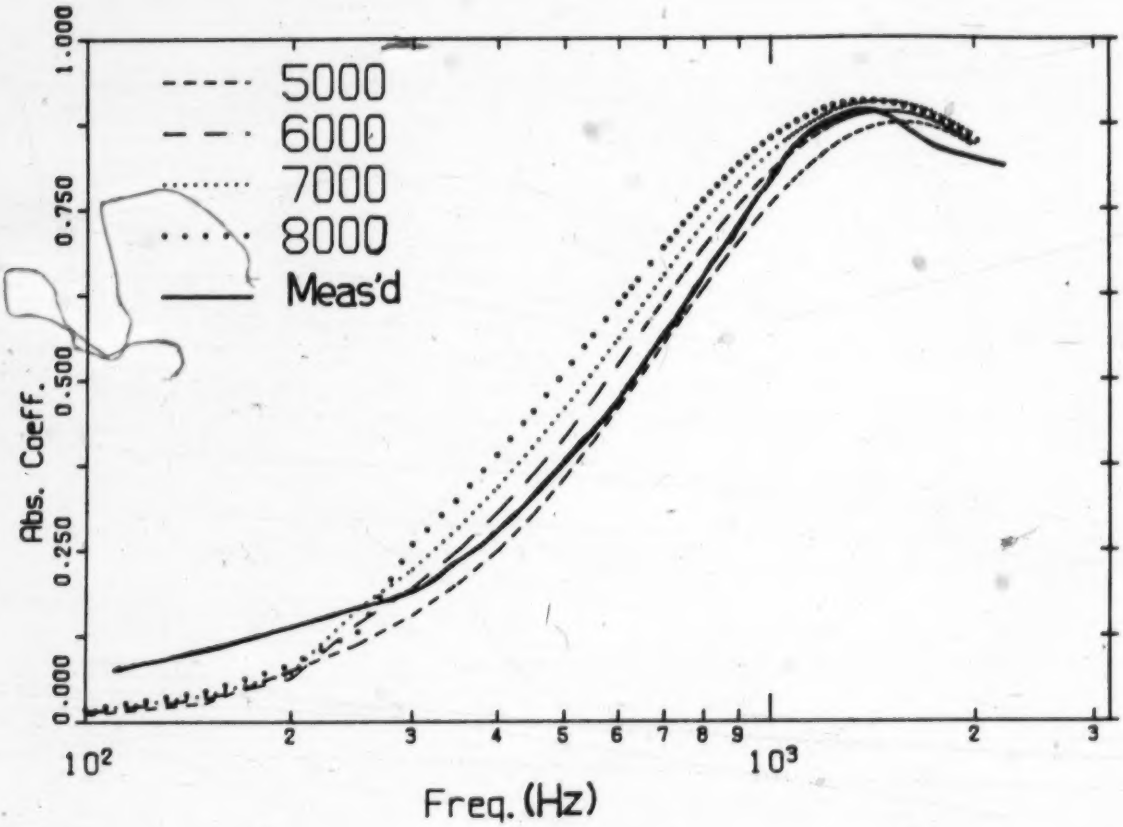

Figure A2.1 **Estimation of Flow Resistivity**

```
      C          (MPROG=ABSO)   DETERMINATION OF ACOUSTIC
      C          ABSORPTION COEFFICIENTS.
            INTEGER F,RS,F1,MS
            REAL LS,X(40),Y(40),ALPH(20),Z(40)
            REAL*8 TITL(4)/'5000','6000','7000','8000'/
            READ(5,1)MC,K1,RS,MA,RMA
            READ(5,2)(ALPH(I),I=1,12)
            READ(5,3)(ALPH(I),I=13,20)
            MF = 0
            KC = 4
            PI = 3.1415926
            MA = MA*0.001
            DO 27 RS = 5000,8000,1000
         19 WRITE(6,11)MC,RS,MA
            RS = RS
            DS = 1.0-0.01*(RS/2000)**0.8887
            WRITE(6,12)DS
            D7 = 1-((1-DS)**0.8887
            LS = 1*(1-DS)**0.3333
            WRITE(6,13)LS
      C        CORRECT FOR POROSITY
            M = MA*LS
      C        CORRECT FOR AREA POROSITY
            PS = DS/D7
            C = MC/PS
            WRITE(6,14)C
            WRITE(6,15)
            RS = RMA
            DO 20 I=1,40
         20 Y(I) = 0.0
            DO 25 F=50,2000,50
              F1 = F/50
              X(F1) = F
              D2 = F*2*PI
              R3 = 0.5+0.55*SQRT(D2/RS)
              IF(R3 .GT. 1.0)GOTO 21
                RSN=RS
                GOTO 22
         21     RSN = R3*RS
         22   R4 = 0.45*SQRT(RS/D2)
              IF(R4 .GT. 1.0)GOTO 23
                RH = RS*1.3
                GOTO 24
         23     RH = RS*(1+R4)
         24     A = 1.0/SQRT(PS)
                B = SQRT(K1*K1+(RSN/(RH*D2))**2)
                B = SQRT(B)
                D = -RSN/(K1*RH*D2)
               T1 = ATAN(D)
               Z1 = A*B*COS(T1/2)
               Z2 = A*B*SIN(T1/2)
               G1 = D2*PS*Z1/C
               G2 = D2*PS*Z2/C
               V1 = 2*G1*M
               V2 = 2*G2*M
               V2 = -V2
                Q = COSH(V2)-COS(V1)
               P1 = (SINH(V2))/Q
               P2 = (SIN(V1))/Q
               Z3 = Z1*P1+Z2*P2
               Z4 = Z2*P1-Z1*P2
               A1 = 4.0*Z3/((Z3+1)**2+Z4**2)
      C           MULTIPLY BY AREA POROSITY
               A1 = A1*D7
               Y(F1) = A1
              WRITE(6,16)F,A1
         25 CONTINUE
            MF = MF + 1
            KC = KC+10
      C     IF(MF .LT. 4)GOTO 26
      C  26 CALL CSPL2(X,Y,40,MF,KC,50.0,200.0,0.75,0.0,0.2,5.0,ALPH)
         26 CALL CSPL(X,Y,Z,40,MF,2,1,KC,0,2.0,1.5,5.0,0.0,0.25,4.0,ALPH,-5)
            MF = IABS(MF)
            CALL CSPEPS(-5.75,0.75,TITL(MF),5,0.3,0.5)
         27 CONTINUE
      C     CALL CSPL(X,Y,Z,40,MF,2,1,0,0,2.0,1.3,5.0,0.0,0.25,4.0,ALPH,-5)
            1 FORMAT(3I5,2E12.5)
            2 FORMAT(12A4)
            3 FORMAT(8A4)
           11 FORMAT(' ',80('_')/' ','INPUT PARAMETERS:'/' ','REF. SOUND',
           1   ' SPEED =',I5,' METERS/SEC.'/' ','FLOW RESISTIVITY =',I5,
           2   ' RAYLS/METER'/' ','THICKNESS =',F5.5,' METER'/' ',80('_'))
           12 FORMAT(' ','POROSITY =',E11.4,' UNITS')
           13 FORMAT(' ','EXT. LENGTH =',F7.4,' METERS')
           14 FORMAT(' ','SPEED OF SOUND =',F10.5,' METERS/SEC ')
           15 FORMAT(' ',80('_')/' ','FREQUENCY',4X,'% ABS.')
           16 FORMAT(3X,I5,7X,F8.3)
              STOP
              END
      C   TRIAL DATA:ABSO FOR VARIABLE RESISTIVITY (13/8/85)
          200    1 1000     .500E+03     .1315+01
      AB.CO. - VAR. RS.(THK=50mm)
      Freq.              Abs. Coeff.
      C
      C
      C
      C
End of file
```

APPENDIX A3 -- BROADBAND RESPONSES AND MOST-USED LAYOUTS OF EQUIPMENT

Presented first is a trace of typical response of the individual sources to broadband noise in the range 0-20,000 Hz (Figure A3.1). Thereafter follows the responses of all six sources in the range of 0-1,000 Hz (Figure A3.2); note the similarity of response of the different sources. All such response traces were generated with each source one-half meter from the floor of the (otherwise empty) anechoic chamber, with the microphone aimed directly at the source-cone at 1 meter distance and the source being excited by a 3-volt(RMS) signal.

In the remaining pages of this Appendix are found the source-network layouts which allowed acceptable excitation of each resonance for most lining configurations. Layouts are given for both models. As indicated, some layouts can be used to excite several modes by simply changing network phase.

Also given for both models are the most frequently used microphone locations. For the truck-cab model most readings were made with the microphone in its "fixed" location though, if response in this corner was poor, the microphone was usually moved to the named location. In the car-model, where no "fixed" location common to measurement of all modes was used, the listed location was the most likely region to suitably measure the resonance.

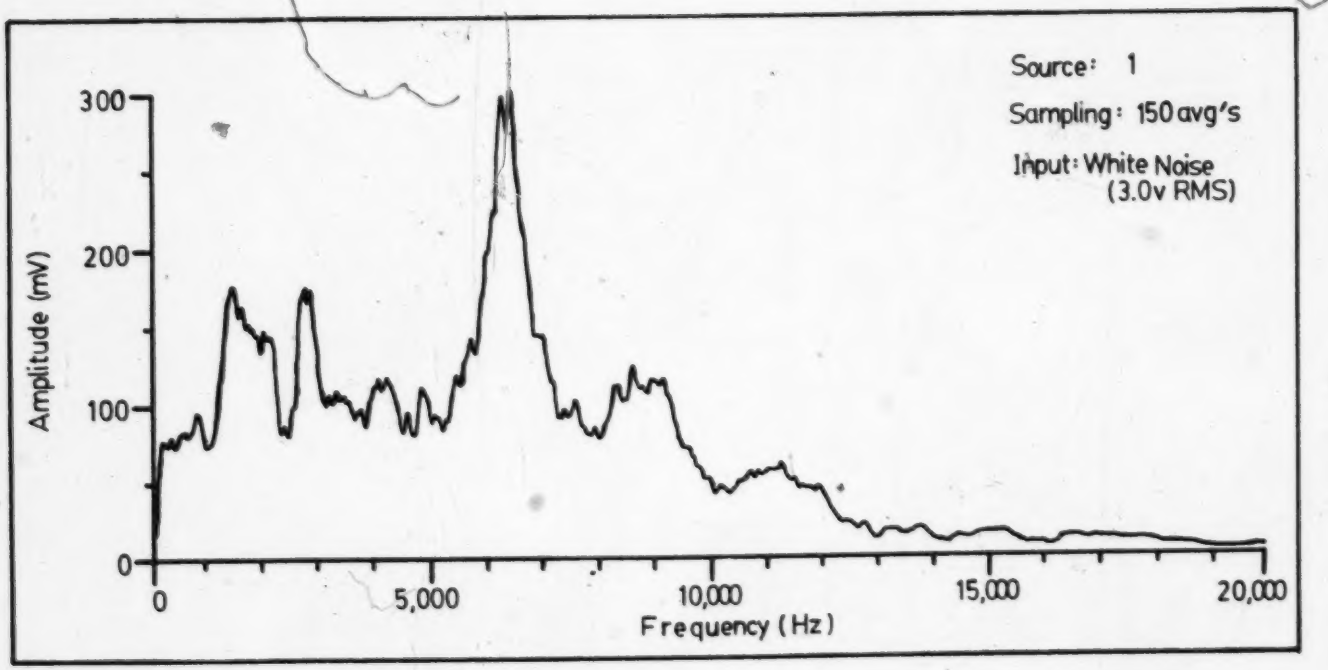

Figure A3.1 **Typical Response of Sources to Broadband Noise.**

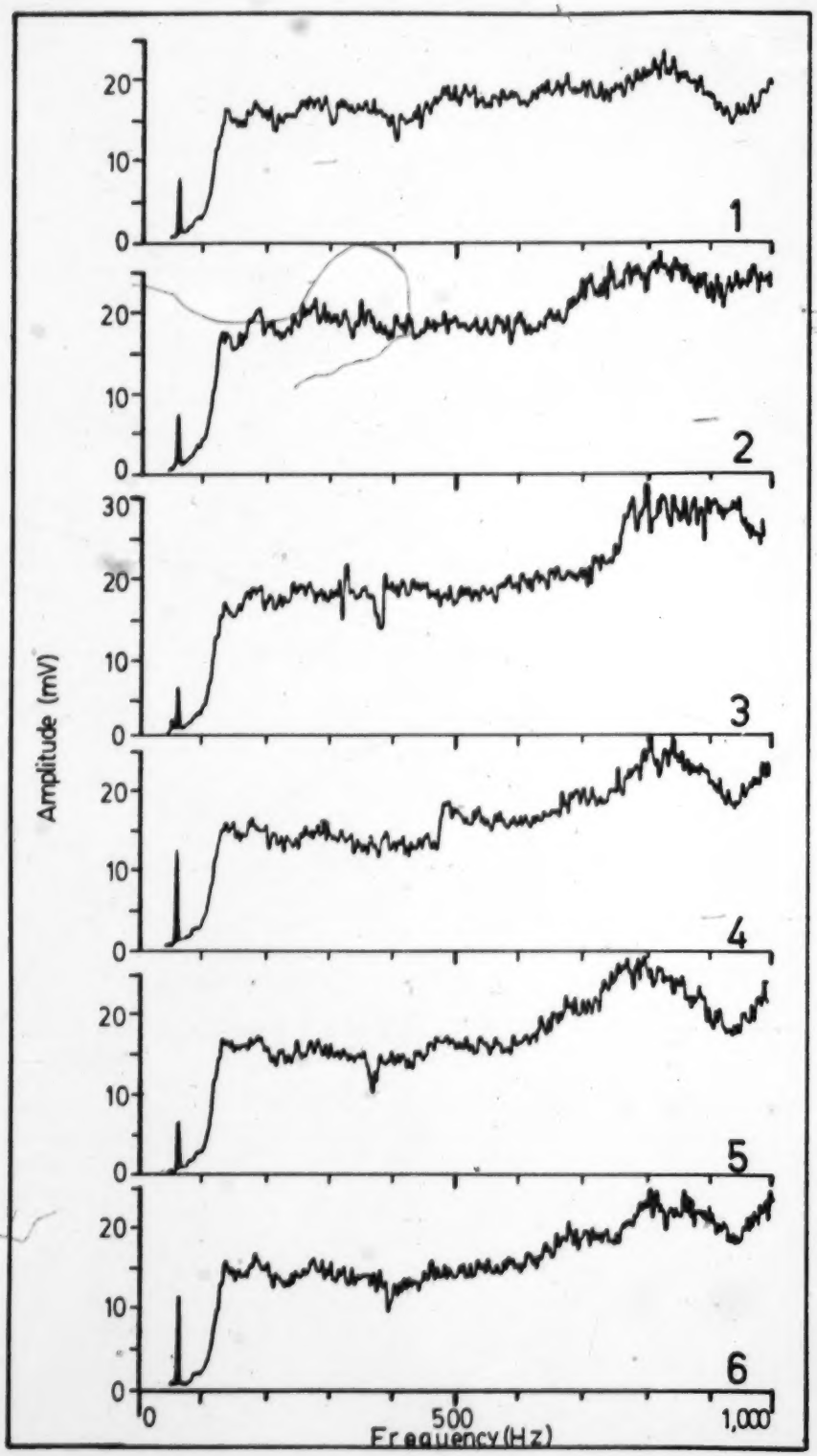

Figure A3.2 Response of Individual Sources (0-1,000 Hz).

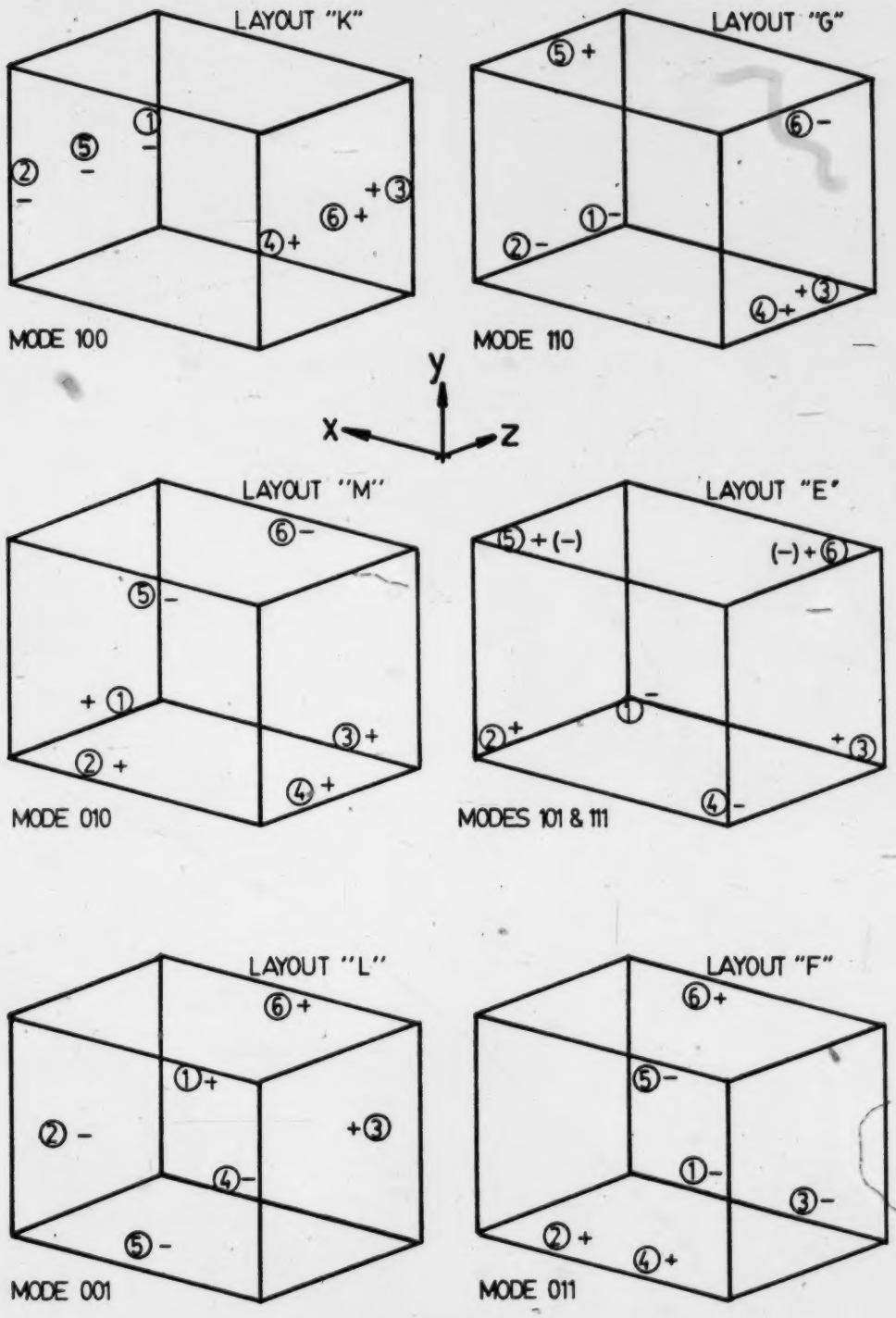

Figure A3.3 **Most-Used Network Layouts: Truck-cab Model**

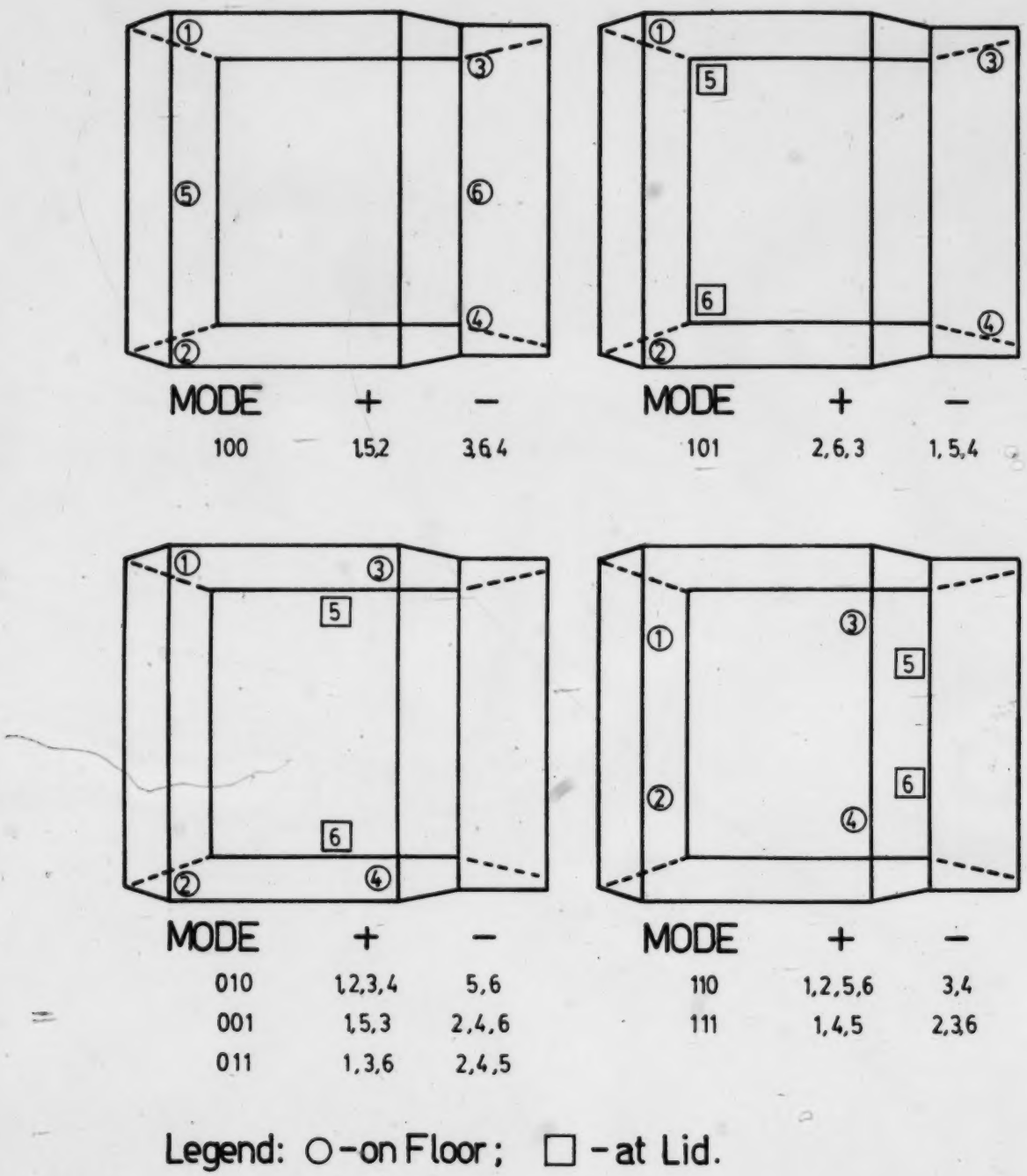

Figure A3.4 Most-Used Network Layouts: Car-Model (Fund. Modes)

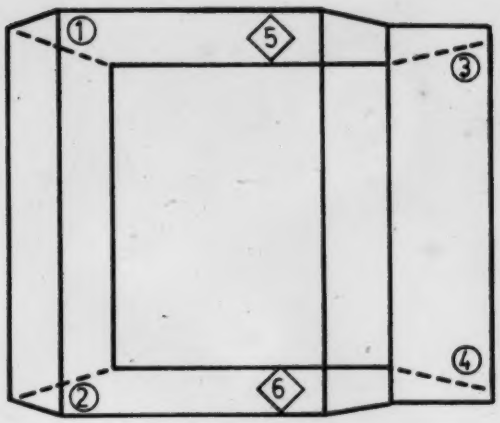

MODE	+	−
200	1, 2, 3, 4	5, 6
201	1, 6, 3	2, 5, 4

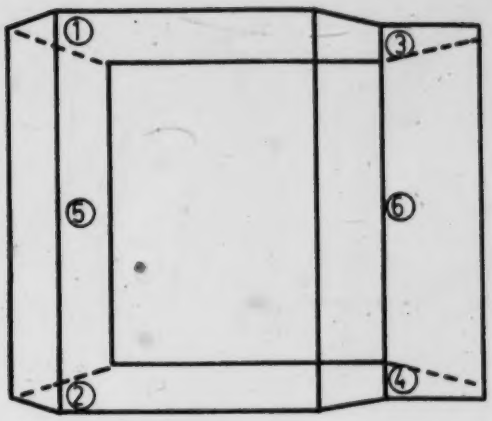

MODE	+	−
002	1, 2, 3, 4	5, 6
102	1, 2, 6	5, 3, 4

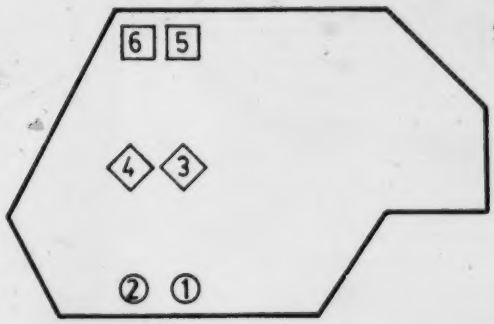

SIDEWALL:
Right - 1, 3, 5
Left - 2, 4, 6

MODE	+	−
020	1, 2, 5, 6	3, 4

Legend: ○-Floor; ◇-Midheight; □-Lid.

Figure A3.5 **Most-Used Network Layouts: Car-Model (Non-Fund. Modes)**

MICROPHONE (RE-)LOCATION

TRUCK-CAB MODEL (ALTERNATIVE LOCATION TO "FIXED")

MODE 100 -- Midpoint of endwall

010 -- At midlength of the floor, usually along a sidewall

001 -- At midheight of sidewall

110 -- Midpoint of seam endwall-floor

101 -- Midheight of seam endwall-sidewall

011 -- Midpoint of seam floor-sidewall

111 -- To any other corner of same endwall

CAR-MODEL

Microphone location identified with a 3-letter symbol, explained below.

MODE 100 RpL	MODE 200 RpW	MODE 002 FfL
001 LhL	011 L1L	102 RpW
010 LfL	201 RpL	111 R1L
101 RhL	110 R1W	020 FhL

Symbol explanation:

First position (length)	Second position (height)	Third position (width)
F -- front	f -- floor	L -- left
L -- midlength	p -- panel	W -- midwidth
R -- rear	h -- midheight	R -- right
	1 -- lid	

APPENDIX A4 -- TABLES OF MEASURED DATA

Table A4.1 Truck-Cab Model -- Damping Factor (x10³).

Lining >	T00	T15	T16	T19	T25	T30	T31	T32	T34	T35	T38	T50	T62	T68	T70	T100
Mode																
100	11.8	16.7	22.4	13.2	20.7	19.9	15.8	22.6	21.4	15.8	22.4	22.4	26.2	32.3	32.1	49.6
010	15.4	21.4	20.2	17.5	24.4	24.4	20.2	15.8	16.5	31.3	22.9	22.5	20.6	30.6	34.0	46.0
001	13.0	28.9	19.4	18.1	25.9	15.5	25.8	25.6	27.8	25.2	19.4	18.9	35.7	43.0	42.8	51.4
110	12.3	19.2	21.9	26.6	25.0	25.8	24.0	18.5	22.3	24.3	23.4	27.8	31.7	41.4	47.4	59.8
101	8.9	13.8	16.2	12.7	18.1	22.5	20.8	21.6	26.4	19.5	21.1	27.8	29.7	34.8	31.8	50.8
011	7.4	14.1	10.0	20.0	17.7	24.6	17.6	24.7	22.5	21.1	22.0	31.8	30.9	30.7	44.6	42.9
111	10.7	22.8	19.2	14.9	28.2	21.8	43.8	21.4	29.1	24.2	22.7	28.6	53.3	47.9	66.2	57.9
Averages																
Axial	13.4	22.3	20.7	16.3	23.7	19.9	20.6	21.3	21.9	24.1	21.6	21.3	27.5	35.3	36.3	49.0
Tang.	9.5	15.7	16.0	19.8	20.3	24.3	20.8	21.6	23.7	21.6	22.2	29.1	30.8	35.6	41.3	51.2
Overall	11.4	19.6	18.5	17.6	22.9	22.1	24.0	21.5	23.7	23.1	22.0	25.7	32.6	37.2	42.7	51.2

Table A4.2 Truck-Cab Model -- Frequency Shift (%).

Lining >	T00	T15	T16	T19	T25	T30	T31	T32	T34	T35	T38	T50	T62	T68	T70	T100
Mode																
100	120.9	+1.49	0.17	+0.66	0.17	+0.83	0.33	1.16	1.32	0.50	5.79	3.47	5.29	4.80	5.79	4.14
010	127.1	0.47	0.47	1.10	2.83	3.46	0.63	+2.20	1.89	0.63	3.46	3.46	2.52	7.87	5.04	6.92
001	148.5	0.94	0.81	+0.40	0.94	4.18	4.85	3.91	0.67	2.29	1.08	6.46	7.41	3.64	5.52	7.81
110	175.1	1.48	0.69	1.26	2.74	3.71	2.34	2.40	2.40	3.48	3.31	7.77	6.28	8.57	6.62	9.59
101	187.7	1.28	1.39	1.60	2.56	4.16	2.77	2.24	4.05	4.05	4.05	6.50	6.50	8.31	6.82	10.8
011	193.3	0.83	1.86	1.86	3.31	1.76	2.69	3.52	2.38	3.10	3.52	5.07	6.93	6.82	8.38	10.8
111	226.4	1.99	2.25	1.90	3.67	3.58	4.81	4.90	4.20	4.90	4.55	7.24	9.58	12.4	12.4	14.4
Averages																
Axial		0.97	0.48	0.72	1.31	2.82	1.94	2.42	1.29	1.14	3.44	4.46	5.07	5.44	5.45	6.29
Tang.		1.20	1.31	1.57	2.87	3.21	2.60	2.72	2.94	3.54	3.63	6.45	6.57	7.90	7.27	10.4
Overall		1.21	1.09	1.25	2.32	3.10	2.63	2.90	2.41	2.71	3.68	5.71	6.36	7.49	7.22	9.21

Table A4.3 Truck-Cab Model -- Resonant Amplitude (mV).

Lining >	T00	T15	T16	T19	T25	T30	T31	T32	T34	T35	T38	T50	T62	T68	T70	T100
Mode																
100	153	96.1	102	136	81.9	96.9	58.9	92.3	83.9	67.2	57.2	58.8	61.6	49.4	43.1	45.9
010	128	111	84.1	107	74.0	102	90.6	91.1	114	72.6	80.9	63.4	82.3	63.1	53.1	44.4
001	121	90.4	92.2	94.2	72.5	67.5	56.8	63.3	75.1	52.6	54.5	50.0	44.9	37.8	38.1	31.6
110	162	126	128	118	95.1	96.4	99.6	97.7	105	102	95.1	66.3	67.4	59.4	52.2	41.3
101	223	142	112	140	123	98.8	90.1	107	82.3	110	85.7	73.8	84.4	59.1	80.0	41.9
011	230	157	118	109	96.8	104	77.5	75.5	104	92.5	69.9	64.7	70.7	62.8	50.3	39.7
111	201	119	125	125	92.3	102	67.7	85.3	79.5	88.0	87.3	40.3	66.0	58.1	54.1	29.8

Table A4.4 Car-Model -- Damping Factor (x10³).

Lining >	C00	C13	C18	C26	C33	C36	C41	C47	C53	C61	C64	C70	C76	C100
Mode														
100	11.3	8.5	25.1	27.1	34.1	26.8	66.4	68.2	57.7	48.5	77.7	20.1	49.3	59.4
001	12.5	27.1	23.5	25.1	54.7	35.0	51.3	40.0	36.5	28.8	38.9	62.3	56.3	77.9
010	12.3	20.3	26.6	25.1	29.1	23.8	20.4	35.2	38.4	36.4	35.4	44.8	32.0	40.2
101	9.7	17.8	23.6	20.1	19.8	16.0	60.6	39.8	45.7	39.4	46.5	82.3	78.1	82.3
200	9.9	13.1	7.8	23.5	31.4	22.2	28.7	37.9	29.2	38.9	43.0	47.2	65.8	71.6
011	16.7	16.3	18.5	25.9	21.9	31.6	22.4	66.1	60.5	64.5	53.0	63.0	60.8	59.5
201	6.2	11.2	16.1	16.8	22.2	21.0	32.9	54.9	36.6	58.2	48.8	50.5	58.2	117.6
110	5.9	11.8	15.6	29.9	17.1	37.9	30.6	37.8	35.3	28.3	35.8	53.2	50.3	75.3
002	4.8	16.2	12.6	13.5	33.9	18.2	44.8	64.4	38.6	53.4	52.3	76.9	50.6	79.1
102	4.9	21.6	14.6	24.6	36.3	25.9	65.3	45.0	44.4	41.5	59.9	70.4	70.6	56.7
111	3.4	10.7	16.4	23.3	22.0	37.3	29.1	34.0	30.4	47.5	63.5	57.5	57.9	56.8
020	3.3	12.5	25.6	23.1	30.6	24.9	28.9	78.8	40.0	61.9	45.7	61.9	70.4	80.1
Averages														
Axial	12.0	18.6	25.1	25.8	39.3	28.5	46.0	47.8	44.2	37.9	50.7	42.4	45.9	59.2
Tang.	10.8	15.3	19.2	25.3	19.6	28.5	37.9	47.9	47.1	44.1	45.1	66.2	63.1	72.4
Overall	10.3	16.1	21.3	25.2	28.4	29.8	40.1	45.9	43.5	41.9	50.1	54.8	55.0	64.5
(Fund.) Non-Fund.	5.8	14.9	15.3	20.3	30.9	22.4	40.1	56.2	37.8	50.8	49.9	61.4	63.1	81.0

Table A4.5 Car-Model -- Frequency Shift (%).

Lining >	C00	C13	C18	C26	C33	C36	C41	C47	C53	C61	C64	C70	C76	C100
Mode														
100	154.6	3.6	2.1	2.1	4.1	4.1	6.0	7.0	6.5	11.1	8.0	13.2	13.5	13.5
001	168.2	1.9	1.0	2.6	3.8	1.4	5.5	4.0	5.7	5.0	6.9	7.8	7.1	10.7
010	220.2	1.3	2.9	2.9	1.6	3.6	3.1	5.8	4.2	7.1	4.4	7.8	7.6	7.4
101	226.6	1.6	3.2	3.0	4.1	4.9	9.9	6.0	7.8	8.6	10.8	12.0	12.7	17.1
200	251.0	3.8	3.2	3.2	7.5	6.9	7.6	8.6	7.8	8.8	10.2	14.5	16.1	16.3
011	281.8	4.0	2.8	4.8	0.9	7.0	5.1	8.5	7.4	7.0	6.7	12.9	10.6	10.8
201	301.8	3.8	5.3	4.4	1.6	8.5	8.9	11.3	8.6	12.6	15.5	17.0	16.8	25.0
110	312.2	0.4	2.6	5.4	2.4	4.2	4.2	5.6	6.1	8.5	6.9	8.7	9.9	12.4
002	323.8	3.6	2.7	2.7	10.3	3.5	6.7	13.5	11.5	10 9	13.2	11.5	8.2	14.1
102	355.4	1.5	2.8	3.2	6.9	3.7	10.1	1.9	10.4	6.8	10.5	12.7	9.1	13.4
111	366.6	3.7	5.6	7.8	5.3	8.3	8.1	7.4	9.3	13.0	3.4	14.4	12.4	16.7
020	378.2	2.5	3.6	5.6	6.8	6.1	7.1	5.7	8.7	1.6	9.7	12.5	5.6	16.2
Averages														
Axial		2.3	2.0	2.5	3.2	3.0	4.9	5.6	5.5	7.7	6.4	9.6	9.4	10.5
Tang.		2.0	2.9	4.4	2.5	5.4	6.4	6.7	7.1	8.0	8.1	11.2	11.1	13.4
Overall		2.3	2.9	4.1	3.2	4.8	6.0	6.3	6.7	8.6	6.7	11.0	10.6	12.6
(Fund.)														
Non-Fund.		3.0	3.1	3.8	6.6	5.7	8.1	8.2	9.4	8.1	11.8	13.6	11.4	17.0

Table A4.6 Car-Model -- Resonant Amplitude (mV).

Lining >	C00	C13	C18	C26	C33	C36	C41	C47	C53	C61	C64	C70	C76	C100
Mode														
100	180	404	230	151	228	313	161	157	148	137	145	68.5	193	27.0
001	228	209	188	172	135	149	118	150	138	135	111	109	117	28.8
010	310	149	188	106	108	149	143	127	143	47.2	79.6	63.3	56.3	29.4
101	229	223	151	147	96.5	214	120	118	125	107	94.1	109	124	31.7
200	239	120	161	141	90.2	121	52.6	61.9	88.6	87.9	52.9	20.6	69.2	15.4
011	212	119	143	138	96.5	101	132	72.3	67.9	82.5	50.3	31.2	60.3	18.7
201	223	143	182	153	94.6	121	48.4	59.0	102	60.5	43.3	17.6	40.9	7.0
110	300	140	142	84.4	86.0	53.9	71.8	49.6	73.1	34.5	48.4	19.4	40.7	11.7
002	143	92.2	128	67.1	104	82.5	45.2	40.5	36.3	19.4	25.5	23.3	46.9	1.9
102	222	98.4	106	95.6	42.6	98.5	24.9	41.6	48.6	48.7	31.4	22.7	43.0	5.1
111	146	113	102	96.5	60.8	68.6	60.4	55.0	70.8	34.1	31.8	23.5	27.0	21.8
020	215	79.1	66.6	50.1	36.7	53.1	42.3	30.8	36.4	17.0	35.7	21.7	24.1	18.5